Development and application of comparative Diffusion Tensor Imaging (DTI) to examine cross-species differences in the hemispheric asymmetry and age-related decline of brain white matter

A Dissertation
Presented to
The Academic Faculty

by

Bhargav K. Errangi

In Partial Fulfillment
of the Requirements for the Degree
Doctor of Philosophy in the
School of Bio-Medical Engineering

Georgia Institute of Technology
August 2011

Development and application of comparative Diffusion Tensor Imaging (DTI) to examine cross-species differences in the hemispheric asymmetry and age-related decline of brain white matter

Approved by:

Dr. James K. Rilling, Advisor
Department of Anthropology
Emory University

Dr. John Oshinski
School of Bio-Medical Engineering
Georgia Institute of Technology

Dr. Xiaoping Hu
School of Bio-Medical Engineering
Georgia Institute of Technology

Dr. Shella Keilholz
School of Bio-Medical Engineering
Georgia Institute of Technology

Dr. Todd M. Preuss
Center for Translational Social Neuroscience *Emory University*

Date Approved: July 7, 2011

ACKNOWLEDGEMENTS

I am grateful for the support and help from my advisor, Professor Jim Rilling. His consistent academic guidance, financial support, and encouragement make me accomplish this dissertation. Five years studying under his direction is an enjoyable and invaluable experience that will benefit me throughout my life and career. In every sense, none of this work would have been possible without him. I also want to thank Professor Todd Preuss and Professor Xiaoping Hu for their valuable suggestions and insights that helped me a lot in understanding my work better. It is my fortune to have Professor John Oshinski and Professor Shella Keilholz on my thesis committee. I am very grateful for their instructive comments and suggestions.

Far too many people to mention individually have assisted in so many ways during my work at Emory and Georgia Tech. In particular, I would like to thank Dr. Longchuan Li and Matt Glasser without whom this dissertation would not have been possible. A special thanks to Ashley, Patrick, Jenny, and other past and current members of laboratory of Darwinian neuroscience for their constant encouragement and support. Also, I would like to thank Dr. Jim Herndon and other principal investigators of the PO1 grant for the financial support and valuable research guidance. Many thanks to Dr. Govind, Dr. Fawn Stroud, Wendy, and Dr. Xiaodong for their assistance in setting up the non-human primate scan. Finally, a huge thank you to my wonderful parents and loving friends for always being there when I needed them most, they deserve more credit than I can ever give them.

TABLE OF CONTENTS

LIST OF TABLES

LIST OF FIGURES

SUMMARY

A complete scientific understanding of human nature requires delineation of the neurobiological characteristics underlying the unique features of the human mind. This effort can be facilitated by comparing the human brain with the brains of other living primate species. Humans are more susceptible to neurodegenerative diseases than other primate species, including our closest living primate relatives, the chimpanzees. Comparing age-related changes in brain structure between humans and non-human primates could, therefore, potentially shed light on the neurological basis of this human vulnerability. Further, human brains are lateralized with specialized cognitive and behavioral functions. Comparing the magnitude of hemispheric asymmetries in brain structure between humans and non-human primates can probe insights into this human specific capability and learn more about human evolution. Diffusion weighted MRI protocols were developed for different species, taking into account their neuroanatomical differences. For Chimpanzees, a multi-shot DWI sequence was developed and compared with a single-shot DWI sequence to determine which provided a better quality diffusion data free of acquisition related artifacts. Different simulation techniques were used to evaluate the effect of segmentation-related motion artifact (ghosting) on the multi-shot DTI data. Although both protocols generated high-resolution diffusion MRI data with correctable susceptibility-induced distortions, the single-shot protocol enables the acquisition of the high-resolution diffusion MRI data freed of ghosting and with twice the signal-to-noise ratio (SNR), for the same scan duration. The acquired chimpanzee and macaque diffusion data were used to compare the magnitude of microstructural

asymmetries and age-related decline of brain white matter with those in humans. Hemispheric asymmetry results show a pattern of strong leftward asymmetry in human DTI indices that differs markedly from the chimpanzee (multi-shot data) and the rhesus macaque patterns involving both rightward and leftward asymmetries. The magnitude of leftward asymmetry increased for chimpanzees scanned with single-shot DTI sequence. Region of interest analyses within the corpus callosum revealed a significant age-related increase in fractional anisotropy (FA) in the genu for chimpanzees (multi-shot data) and no significant change in any region for macaques. Additionally, voxel-wise analysis using Tract Based Spatial Statistics (TBSS) revealed widespread age-related FA increases for chimpanzees (multi-shot data) and weak age-related decreases in FA for macaques across most white matter tracts. Overall, results from these multi-shot data analyses suggest that rhesus monkeys show age-related decreases in white matter integrity that parallel changes found in humans, whereas chimpanzees show age-related increases in white matter integrity. On the contrary, the single-shot data results for chimpanzees revealed no significant relationship between age and the different DTI indices. These noteworthy species differences may help to explain the unique features of the human mind and why humans are more susceptible to neurodegenerative diseases. Furthermore, these studies demonstrate the need for complementary histological studies of white matter microstructure in humans, chimpanzees and macaques to clarify the cellular and molecular basis of these findings.

CHAPTER 1

INTRODUCTION

1.1 Brief Introduction to Diffusion Imaging

Magnetic Resonance Imaging (MRI) is a widely used, non-invasive medical imaging technique that provides high quality images of biological tissues. MRI is based on the principles of Nuclear Magnetic Resonance (NMR) and offers good contrast between different soft tissues of the body compared to other imaging modalities. This makes it especially useful in imaging the brain, muscles, the spine, and tumors. Over the years, many developments have been made in the field of MRI to provide an in-depth understanding of human anatomy and function. These developments are related to different contrast mechanisms making use of the magnetic properties of tissues. One such development is Diffusion Tensor Imaging (DTI), the main technique used for this thesis project.

1.2. Diffusion Tensor Imaging (DTI)

Diffusion tensor magnetic resonance imaging (DT-MRI) measures the diffusion of water molecules in biological tissues. By characterizing the diffusion of water molecules (Basser, Mattiello et al. 1994), DTI can be used to detect changes in the tissue microstructure. Diffusion is a physical process that involves the translational movement of molecules via thermally driven random motions, called Brownian motion. When there are no hindrances to diffusion, the amount of diffusion is same in all the directions and is termed as isotropic diffusion. However, if there are barriers to diffusion, such as white matter axons, diffusion will be preferred in some directions over others; this is termed

anisotropic diffusion. Diffusion weighting can be achieved by applying a pair of strong diffusion gradients (diffusion sensitization or diffusion weighting gradient). Figure 1.2 shows a spin echo pulse sequence with the diffusion gradient applied in z-direction.

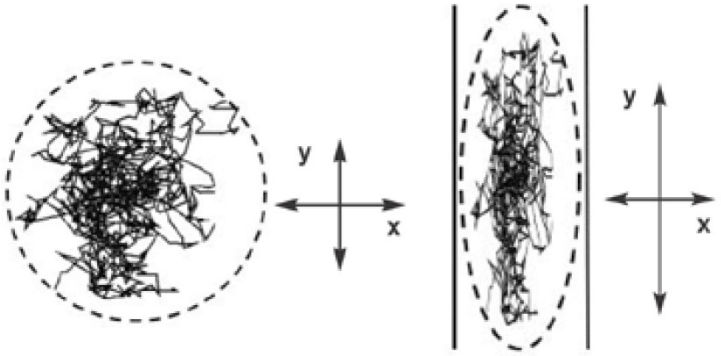

Figure 1.1: Figure showing the molecular displacements in isotropic (left) and anisotropic (right) media. Displacements are random for an isotropic sample and oriented more along the principal axis in an anisotropic sample

Magnetic resonance measurements of diffusion are sensitive to the displacement of the molecules along the axis that diffusion-sensitizing gradients are applied. Therefore, diffusion along different directions can be readily measured by changing the direction of the diffusion sensitizing gradients. The degree of the diffusion weighting is described by

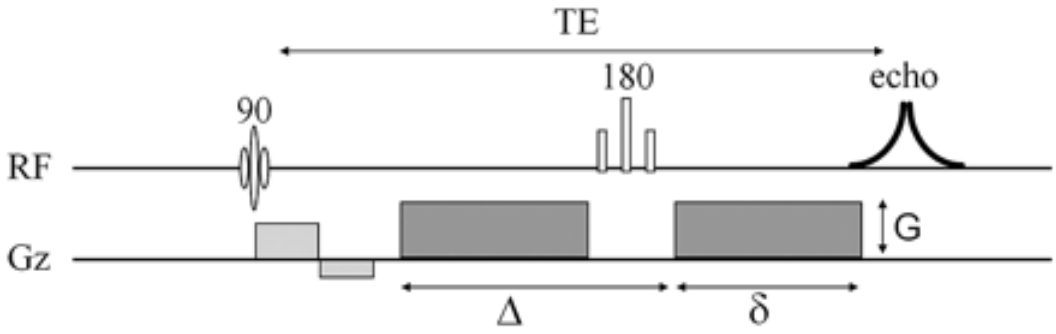

Figure 1.2: Illustration of spin echo sequence with diffusion weighting gradient

a parameter called b value, which depends on the amplitude of the diffusion gradient (G), the duration of each diffusion gradient (δ), and the interval between the onset of the diffusion gradient before the refocusing pulse and that following the refocusing pulse(Δ). This relationship is given by,

$$b = \gamma^2 G^2 \delta^2 (\Delta - \delta / 3) \quad (1)$$

Where, γ is the gyromagnetic ratio. In an isotropic case, diffusion can be fully characterized by a scalar called the diffusion coefficient (D). D is calculated from the attenuation of the diffusion weighted signal intensity compared to the one without any diffusion gradient at the same voxel. The attenuated signal in the presence of the diffusion weighted gradient is given by,

$$S = S_0 / e^{-bd} \quad (2)$$

Where, S_0 is the signal intensity when no diffusion gradient is applied. The contrast in diffusion-weighted images is dependent on the diffusive mobility of the tissue under study. For the same degree of diffusion weighting, the signal from free water or cerebrospinal fluid (CSF) will be highly attenuated compared to the signal from the restricted water in the tissue compartments. In the presence of anisotropy, diffusion can no longer be characterized by a single scalar coefficient but requires a tensor, <D>, which fully describes molecular mobility along each direction and the correlation between these directions. The diffusion tensor (<D>) is symmetric and is given by,

$$\langle \mathbf{D} \rangle = \begin{matrix} \mathbf{D_{XX}} & \mathbf{D_{XY}} & \mathbf{D_{XZ}} \\ \mathbf{D_{YX}} & \mathbf{D_{YY}} & \mathbf{D_{YZ}} \\ \mathbf{D_{ZX}} & \mathbf{D_{ZY}} & \mathbf{D_{ZZ}} \end{matrix} \quad (3)$$

Signal attenuation not only depends on the diffusion effects measured along one direction of the diffusion sensitizing gradient pulse, but may also include the contributions from the other directions. So in order to determine the diffusion tensor accurately, diffusion-weighted images have to be collected along several gradient directions. As the diffusion tensor is symmetric, measurements along at least six directions are necessary. In any anisotropic media, the diffusion tensor, its constituent principal diffusion directions, and principal diffusivities are estimated at each voxel. The former are mutually perpendicular, preferred directions along which molecular displacements of the molecules are uncorrelated, while the later are the diffusivities along these directions. These measures are also called Eigen values, λ_1, λ_2, λ_3 (principal diffusivities) and Eigen vectors V_1, V_2, V_3 (principal directions). The largest Eigen vector of the tensor corresponds to the principal diffusion direction within a voxel. Once the diffusion tensor and constituents are estimated, the amount of restriction to diffusion in an anisotropic media can be typically expressed as Fractional Anisotropy (FA) (Pierpaoli, Jezzard et al. 1996).

$$\mathbf{FA} = \sqrt{3}\,[(\lambda_1 - \lambda)^2 + (\lambda_2 - \lambda)^2 + (\lambda_3 - \lambda)^2] \Big/ \sqrt{2}[(\lambda_1)^2 + (\lambda_2)^2 + (\lambda_3)^2] \quad (4)$$

FA is rotationally invariant and is a measure of orientation coherence. FA is calculated from the Eigen values as given below, where $\lambda = (\lambda_1 + \lambda_2 + \lambda_3)/3$, and is defined as the apparent diffusion coefficient (ADC) and mean diffusivity (MD). ADC is a quantitative metric of water motility (independent of the orientation) in a voxel and is commonly but not necessarily negatively correlated with FA. The values of FA range from 0 to 1. In white matter, the FA values are closer to 1 since the water diffusion is restricted by its fiber constituents, which are arranged in parallel. On the other hand, FA is near 0 in ventricular cerebrospinal fluid, where diffusion is isotropic. Examples of FA, ADC and color-coded FA maps measured on voxel-by-voxel basis are shown in Figure 2.3.

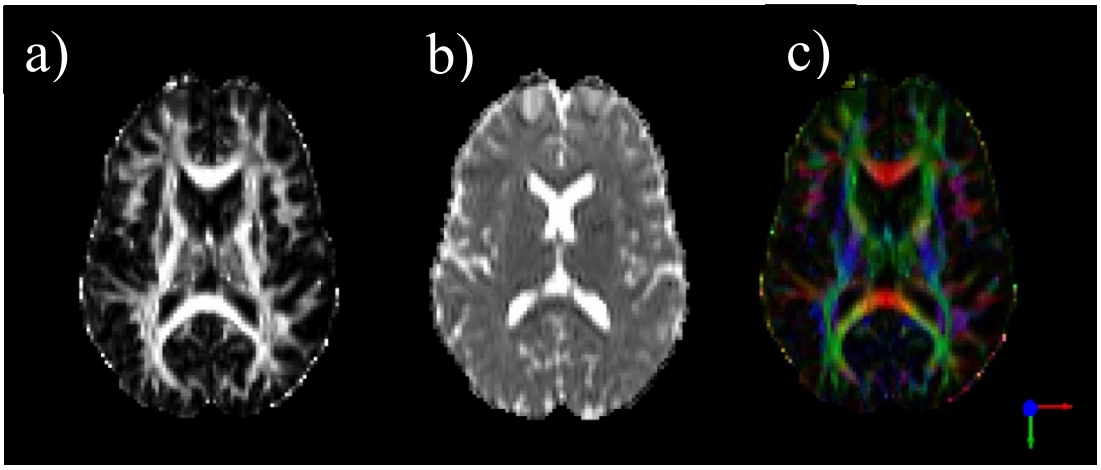

Figure 1.3: Illustration of different diffusion tensor derived indices. a) FA map gives the degree of anisotropy at each voxel. White matter has the highest anisotropy, whereas CSF has the least anisotropy; in between there is a continuum. b) Average diffusivity at each voxel is given by the ADC map. CSF has high intensity due to free water in that region. c) Different fiber orientations given by the principal diffusion direction are shown in the color-coded FA map. Blue: superior to inferior; red: medial to lateral; green: anterior to posterior

1.3 Diffusion Tensor Tractography

The white matter fiber structure can be visualized and reconstructed by tracing the principal eigen vector, which corresponds to the largest eigen value in a voxel. This method is called tractography and is an effective technique for visualizing the white matter connectivity patterns in the human brain (Johansen-Berg and Behrens 2006). The fiber tracts can be reconstructed using a deterministic or a probabilistic approach (Ciccarelli, Behrens et al. 2006; Behrens, Berg et al. 2007).

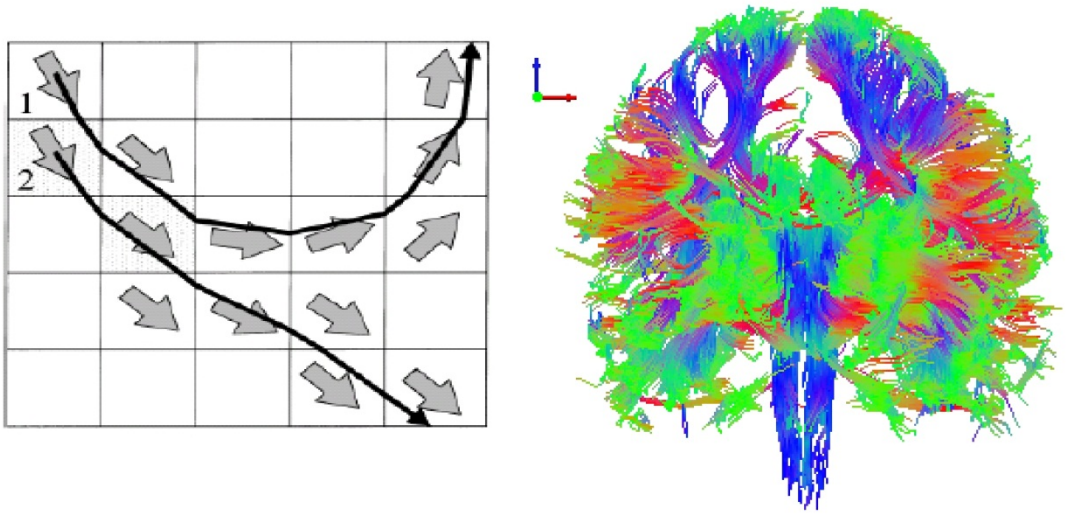

Figure 1.4: Schematic shows the basic idea of fiber tractography and an example of fiber tractography

Chapter 2

Literature Review

2.1. Brain Aging

Human Brain Aging: The effects of aging on gross anatomical structure have been well-studied in humans. There is a gradual decline in brain size from young adulthood to approximately age 50, at which time the slope steepens (Raz and Rodrigue 2006). Many studies have investigated whether these decreases in brain size are driven by changes in gray matter, white matter or both. Studies consistently show age-related declines in gray matter (GM) volume, although the cellular changes responsible for this effect remain uncertain (Blatter, Bigler et al. 1995; Raz, Gunning et al. 1997; Salat, Kaye et al. 1999; Bartzokis, Beckson et al. 2001; Sullivan, Rosenbloom et al. 2004). GM decline does not appear to reflect loss of a large number of neurons; there may only be a 10 percent loss between ages20-90 years old (Pakkenberg, Pelvig et al. 2003). On the other hand, no consistent pattern has been observed for age-related changes in white matter (WM) volume. Some studies show age-related declines in WM volume (Guttmann, Jolesz et al. 1998; Jernigan, Archibald et al. 2001; Bartzokis, Cummings et al. 2003; Allen, Bruss et al. 2005), whereas others show no significant volume loss until the seventies (Salat, Kaye et al. 1999; Raz, Lindenberger et al. 2005), raising a controversy as to whether the decline begins in mid-life or late-life.

These age-related changes in the brain have functional consequences. For example, age-related declines in both GM and WM volume, especially in the anterior regions, are linked to decreased performance on attention and executive function tasks (Zimmerman, Brickman et al. 2006; Brickman, Habeck et al. 2007)

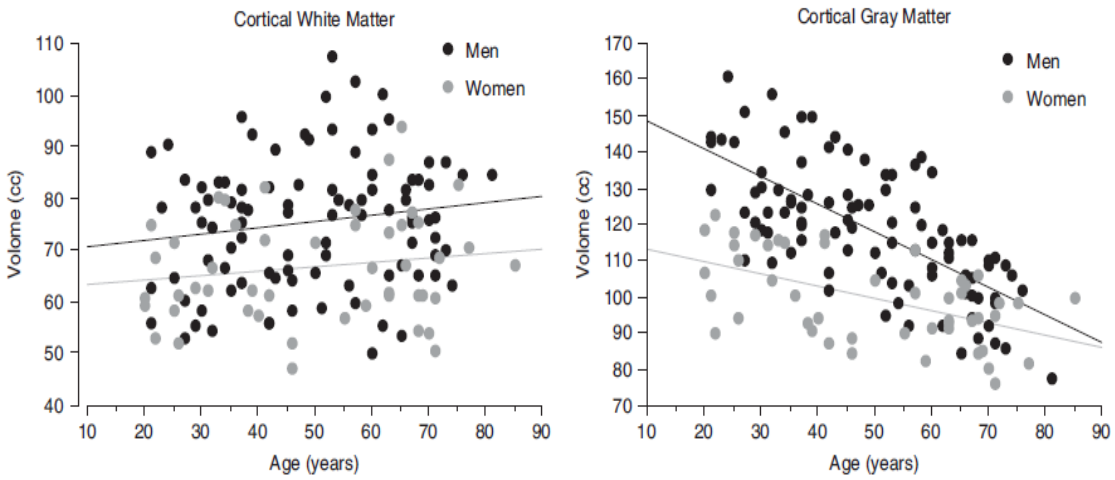

Figure 2.1: A cross-sectional study showing age-related decline in cortical gray but not white matter volume in healthy adults (95 men and 48 women) (Sullivan, Rosenbloom et al. 2004)

The studies discussed above have focused on changes in gross structure volume. However, diffusion-weighted imaging can be used to additionally probe changes in white matter microstructure. Fractional anisotropy (FA) characterizes the degree of anisotropic water diffusion at a voxel (Basser, Mattiello et al. 1994; Pierpaoli, Jezzard et al. 1996) and is thought to reflect microstructural features of white matter such as fiber density, reflecting the total number of fibers per unit area, axon diameter, fiber coherence, and myelination (Pfefferbaum and Sullivan 2003; Buchel, Raedler et al. 2004). FA is highly variable within white matter. FA values are typically high in regions with highly ordered

parallel fibers and low in regions with less coherent fiber orientations or where fiber bundles cross. Significant decreases in white matter FA are associated with certain disease states like Alzheimer`s Disease, Parkinson`s Disease and multiple sclerosis (Rose, Chen et al. 2000; Filippi, Cercignani et al. 2001; Horsfield and Jones 2002; Matsui, Nishinaka et al. 2007; Hess 2009) and with normal, physiological aging in humans.(Peters 2002; Pfefferbaum and Sullivan 2003; Peters and Sethares 2004; Sullivan and Pfefferbaum 2006) Similar to gray and white matter volume changes, FA in the frontal white matter is more susceptible to aging effects than more posterior regions (Salat, Buckner et al. 2004; Salat, Tuch et al. 2005; Sullivan and Pfefferbaum 2006).

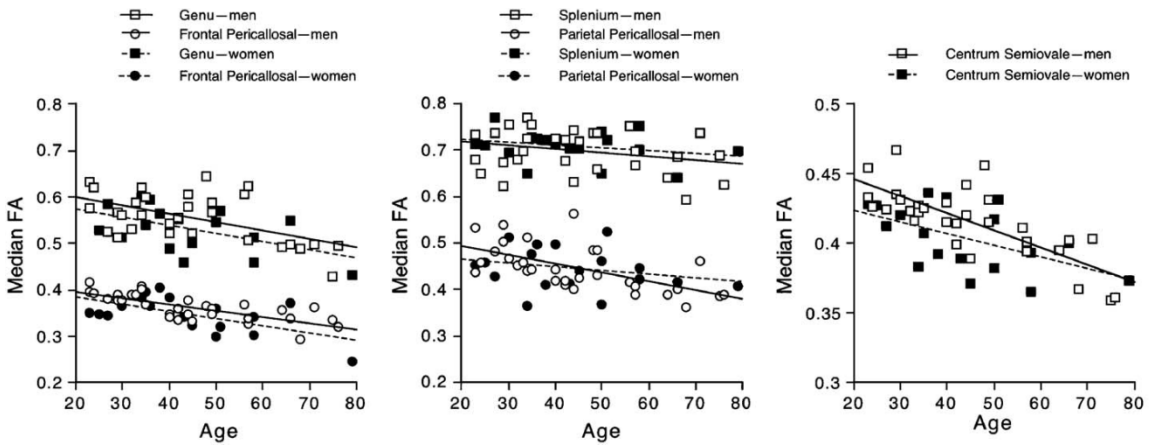

Figure 2.2: Healthy men and women showed equivalent and significant decreases in FA with advancing age, which was greater in the genu than the splenium and greatest in the centrum semiovale (Pfefferbaum and Sullivan 2003)

Several studies have also examined age-related changes in other DTI indices such as axial diffusivity (AD) and radial diffusivity (RD), which refer to the magnitude of diffusion along, and perpendicular to, the principal axis of the axon. RD changes are thought to be associated with changes in myelination, (Song, Sun et al. 2002; Tyszka, Readhead et al. 2006), whereas AD changes are thought to be related to changes in fiber

density (Song, Sun et al. 2003; Tyszka, Readhead et al. 2006). Previous studies revealed two prominent patterns of age-related changes in these diffusivity indices. The first involves age-related declines in FA that are associated with increases in RD only (Bhagat and Beaulieu 2004; Zhang, Du et al. 2008; Madden, Bennett et al. 2009), whereas the second involves age-related declines in FA that are associated with increases in both AD and RD values (Zahr, Rohlfing et al. 2009; Sullivan, Rohlfing et al. 2010). More recently, one study has reported a third pattern involving increases in RD and decreases in AD in certain regions (Bennett, Madden et al. 2010). Age-related changes of these DTI indices have been correlated with decrements in working memory, inter-hemispheric transfer, balance, attention shifting, and reaction time (Janowsky, Carper et al. 1996; Sullivan, Adalsteinsson et al. 2001; Madden, Whiting et al. 2004; Bucur, Madden et al. 2008; Charlton, Landau et al. 2008; Madden, Bennett et al. 2009; Sullivan, Rohlfing et al. 2010).

Non-human primate brain aging: There have been relatively few studies of age-related changes in gross brain structure in non-human primates. In contrast to humans, there is no age-related decline in postmortem brain weight in macaques and only a slight decline in chimpanzees (Herndon, Tigges et al. 1998; Herndon, Tigges et al. 1999), but, like humans, reductions in specific regional volumes, like the basal ganglia, have been observed in rhesus macaques. Although gray matter generally decreases with age in non-human primates, in contrast to humans, white matter has been found to increase with age (Andersen, Zhang et al. 1999; Lyons, Yang et al. 2004; Lacreuse, Diehl et al. 2005; Pierre, Hopkins et al. 2008). Despite the increasing volume of white matter with age,

white matter FA has been reported to decrease with age in rhesus monkeys, particularly within anterior regions and along cortico-cortical association tracts like the superior longitudinal fasciculus and anterior cingulum bundle (Makris, Papadimitriou et al. 2007). In parallel with these changes in FA, histological studies have demonstrated local splitting of myelin and spherical cytoplasmic cavities or balloons within the myelin sheaths of elderly macaques (Feldman and Peters 1998; Peters, Moss et al. 2000; Peters 2002).

There are no published studies examining age-related changes in the WM microstructure in our closest living primate relative, the chimpanzee. Here, for the first time, DTI data were acquired from chimpanzees, and age-related changes in several DTI indices, including FA, ADC, AD and RD, were measured and compared between both chimpanzees and macaques and contrasted with published data from humans.

2.2 Brain Asymmetries

At least three major differences between human and other primate brains are likely relevant to explaining human cognitive and behavioral specializations. First, humans have the largest brains of all living primates. For example, the human brain is at least three times larger than the chimpanzee brain, even after controlling for differences in body size (Stephan, Frahm et al. 1981; Holloway 2000). Second, compared with other primates, association cortices occupy a larger proportion of the brain in humans (Preuss 2004; Rilling 2006). This is true for prefrontal (Passingham 1973; Deacon 1997; Preuss 2004), temporal (Semendeferi and Damasio 2000; Rilling and Seligman 2002) and

probably parietal cortex (Holloway, Broadfield et al. 2003; Orban, Claeys et al. 2006; Bruner 2010), as well as for the white matter underlying these regions (Rilling and Seligman 2002; Schenker, Desgouttes et al. 2005). Third, the human brain is thought to have both greater hemispheric asymmetry and correspondingly greater hemispheric lateralization of function than other primate brains (Corballis 1991; Crow 2002; Toga and Thompson 2003)

Human brain asymmetries have been described in terms of overall hemispheric shape, central sulcus morphology, and various measures in classic language areas like Broca's and Wernicke's areas. With respect to overall hemispheric shape, the human brain often exhibits a pattern of asymmetry in which the right frontal lobe extends beyond the left anteriorly, and the left occipital lobe beyond right posteriorly (LeMay 1976; Holloway and De La Costelareymondie 1982; Lancaster, Kochunov et al. 2003).These protrusions, known as petalias, sometimes leave impressions on the inner surface of the skull that can be detected in endocasts of fossilized skulls (Holloway, Sherwood et al. 2008; Sherwood, Subiaul et al. 2008). Right frontal, left occipital petalias are usually more pronounced in right-handed individuals (Kertesz, Black et al. 1986). Some studies have found a human-like petalia pattern in great apes (Hopkins and Marino 2000; Pilcher, Hammock et al. 2001), whereas others report that the right-frontal, left-occipital petalia asymmetry is unique to humans(Crow 2004; Sherwood, Subiaul et al. 2008) Thus, the existence of human-like cerebral petalia patterns in great apes is still unclear. This human petalia pattern first appears in the hominin fossil record approximately 1.8 mya (Holloway,

Sherwood et al. 2008), suggesting that it may indeed be related to the evolution of unique features of the human mind.

Asymmetries have also been examined in more specific brain regions linked with known lateralized functions, such as handedness and language. The central sulcus includes the primary motor cortex and may relate to handedness. In humans, it is deeper and larger in terms of area in the contra lateral hemisphere to the dominant hand (Davatzikos and Bryan 2002). A similar relationship has been found in chimpanzees(Li, Preuss et al. 2010).

The planum temporale is an auditory processing region located in the posterior temporal lobe that has been linked with handedness and language laterality. The human planum temporale (PT) shows an asymmetry in both volume and surface area, which is strongly correlated with the degree of right-handedness (Foundas, Leonard et al. 1995; Habib, Robichon et al. 1995). Also, a left ward asymmetry in the planum temporale (PT) is reported in the subjects who had language lateralized to the left hemisphere (Geschwind and Levitsky 1968; Foundas, Leonard et al. 1994). However, as with the central sulcus asymmetry, this leftward asymmetry in the planum temporale is also present in chimpanzees (Gannon, Holloway et al. 1998; Hopkins, Marino et al. 1998), and chimpanzees that gesture with the right hand show significantly greater leftward PT asymmetries than those that gesture with their left? hand (Hopkins and Nir 2010). A histological study that examined inter-hemispheric asymmetry in area Tpt, a component of Wernicke's area, similarly found a significant leftward asymmetry in the total neuron

number in both humans and chimpanzees(Sherwood, Subiaul et al. 2008). Nevertheless, (Buxhoeveden, Switala et al. 2001) identified a microstructural asymmetry in the human PT that is absent in both chimpanzees and rhesus macaques. Specifically, humans possess a leftward asymmetry in the width of the minicolumns and neuropil space in the PT. This specialized microstructural asymmetry is not limited to the PT, having also been reported in the left hemisphere of Broca's area (Brodmann areas 44 and 45)(Amunts, Schleicher et al. 1999; Amunts, Schleicher et al. 2003) , primary motor cortex hand area (Amunts, Schlaug et al. 1996; Amunts, Schlaug et al. 1997) as well as primary visual cortex and extrastriate areas (Amunts, Armstrong et al. 2007). Such interhemispheric differences in the amount of neuropil space were not found in chimpanzees (reviewed in(Sherwood, Subiaul et al. 2008)). Indeed, it may be a generalized feature of human cerebral cortical organization.

In humans, Broca's area is leftwardly asymmetric in volume, neuron size and number, gray level index and fiber complexity (Keller, Roberts et al. 2009; Schenker, Hopkins et al. 2010), findings which might plausibly support lateralization of language to the left hemisphere. In contrast, (Schenker, Hopkins et al. 2010) no significant inter-hemispheric differences were found in chimpanzees in the volume, neuronal density and the total neuron number of the cytoarchitechtonically defined Brodmann's areas 44 and 45 (Schenker, Hopkins et al. 2010). These data suggest that Broca's area in the left hemisphere was uniquely modified during human evolution, and perhaps explain its specialization for language.

Most MRI studies investigating white matter asymmetries in the human brain have been conducted on T1-weighted images (Good, Johnsrude et al. 2001; Watkins, Paus et al. 2001). Diffusion MRI provides access to the diffusion characteristics of water *in vivo,* making possible to study the brain anatomical circuitry noninvasively (Mori and Barker 1999; Behrens, Johansen-Berg et al. 2003). Diffusion tensor imaging derived metrices like FA, AD and RD provide more subtle information about the white matter microstructure (Basser 1995) compared to the signal intensity on the T1-weighted images. Microstructural asymmetries in humans have been explored analyzing mainly by analyzing FA. Left greater than right asymmetries were found in uncinate fasciculus (Kubicki, Westin et al. 2002), cingulum bundle (Gong, Jiang et al. 2005), sub insular regions(Rodrigo, Naggara et al. 2007), and in classic language areas(Powell, Parker et al. 2006). Asymmetries were also found in the size of white matter pathways, specifically language regions, explored by DTI (Powell, Parker et al. 2006; Glasser and Rilling 2008). Until now, no studies have compared white matter microstructural asymmetries in humans, chimpanzees, and macaques. Here, for the first time, diffusion MRI data on chimpanzees was acquired and used to compare the magnitude of white matter microstructural asymmetries across the species.

Chapter 3

Subjects and Image Acquisition

3.1 Subjects

30 human males (mean=20.1 years, range= 18-21), 36 female chimpanzees (mean=27.1 years, range=11-54 years) and 24 female macaques (mean=15.8 years, range=6-27 years) were imaged for this study. Of the 36 chimpanzees, thirty (mean=28.4 years, range=11-56 years) were scanned twice in two separate sessions, using two different DTI protocols (Multi-shot DTI, Single-shot DTI) with the inter-session interval ranging from 10 to 14 months. Chimpanzees and macaques were housed at Yerkes National Primate Research Center (YNPRC) in Atlanta, Georgia. All procedures were carried out in accordance with protocols approved by the YNPRC and the Emory University Institutional Animal Care and Use Committee (IACUC, approval number: 194-2009Y).

3.2 Procedure and Image acquisition

Chimpanzees and macaques were immobilized with ketamine injections (2-6 mg/kg, i.m.) prior to being anesthetized with an intravenous propofol drip (10 mg/kg/hour). Subjects were under constant observation by veterinary staff before, during, and after the scan. Diffusion weighted images were acquired on a Siemens 3T Trio scanner (Siemens Medical System, Malvern, PA) with a standard birdcage coil for chimpanzees, a knee coil for macaques, and a standard parallel imaging coil for humans. Head motion was minimized by stabilizing with foam cushions and elastic straps.

3.3 Sequence parameters

Humans: A single shot, echo planar imaging sequence was used to acquire diffusion MRI data for humans. Diffusion-weighting gradients were applied in 64 directions with a b value of 1000 sec/mm^2; repetition time/echo time of 8700/93 msec, field of view of 256×256 mm^2, matrix size of 128×128, resolution of 2×2×2 mm^3, and 64 slices with no gap, covering the whole brain. Two sets of diffusion weighted images with phase encoding directions of opposite polarity were acquired to allow for correction of susceptibility distortion using the method of (Andersson, Skare et al. 2003).Total scan time was approximately 20 minutes. High-resolution T1-weighted images were also acquired using a 3D magnetization-prepared rapid gradient-echo (MPRAGE) sequence. The acquisition parameters were as follows: repetition time of 2600 msec, inversion time of 900 msec, echo time of 3.02 msec, a flip angle of 8°, a volume of view of 256×256×191 mm, a matrix of 256×256×191, and resolution of 1×1×1 mm^3, with one average. Total scan time was approximately 8 minutes.

Chimpanzees: A multi-shot (four segments) spin-echo, echo planar imaging sequence (MS-EPI) and a single-shot (one segment) spin-echo, echo planar imaging sequence (SS-EPI) were used to acquire the diffusion MRI data from chimpanzees. A dual spin-echo technique combined with bipolar gradients was used to minimize eddy current artifacts (Alexander, Tsuruda et al. 1997). For multi-shot EPI, Diffusion-weighting gradients were applied in 60 directions with a b value of 1000 sec/mm^2, repetition time/echo time of 5740/91 msec, field of view of 230×230 mm^2, matrix size of 128×128, resolution of 1.8×1.8×1.8 mm^3, and 41 slices with no gap, covering the whole brain. Two sets of

diffusion weighted images with phase encoding directions of opposite polarity were acquired to correct for susceptibility distortion (Andersson, Skare et al. 2003). For each average of diffusion-weighted images, five images without diffusion weighting (b=0 sec/mm^2) were also acquired with matching imaging parameters. Total scan time was approximately 51 minutes.

Table 3.1: Comparison of multi-shot EPI (MS-EPI) and single-shot EPI (SS-EPI) imaging parameters for chimpanzees

Sequence Parameters	Multi-shot EPI (n=36)	Single-shot EPI (n=30)
FOV (mm^2)	**230*230**	**130*230**
FOV (%)	**100 %**	**56.30 %**
Matrix Size	**128*128**	**72*128**
Partial Fourier Factor	**n/a**	**6/8**
Phase Encoding Steps	**128**	**54**
NEX (dwi)	**2**	**8**
NEX (b0)	**10**	**10**
TE(ms)	**91**	**84**
Scan Time (min)	**51**	**54**

For single-shot EPI, Diffusion-weighting gradients were applied in 60 directions with a b value of 1000 sec/mm^2, repetition time/echo time of 5740/84 msec, field of view of

130×230 mm^2, matrix size of 72×128, resolution of 1.8×1.8×1.8 mm^3, partial fourier factor of 6/8 and 41 slices with no gap, covering the whole brain. Eight averages of diffusion weighted images with phase encoding directions of opposite polarity (4 averages per each direction) were acquired to correct for susceptibility distortion (Andersson, Skare et al. 2003). For each polarity of diffusion-weighted images, five images without diffusion weighting (b=0 sec/mm^2) were also acquired with matching imaging parameters. Total scan time was approximately 54 minutes. High-resolution T1-weighted images were also acquired using a 3D magnetization-prepared rapid gradient-echo (MPRAGE) sequence. The acquisition parameters were as follows: repetition time of 2400 msec, inversion time of 1100 msec, echo time of 4.13 msec, a flip angle of 8°, a volume of view of 256×256×154 mm, a matrix of 256×256×192, and resolution of 0.8×0.8×0.8 mm^3, with 2 averages. Total scan time was approximately 21 minutes.

Macaques: A multi-shot (three segments) spin-echo, echo planar imaging sequence was used to acquire the diffusion MRI data from macaques. A dual spin-echo technique combined with bipolar gradients was used to minimize eddy current artifacts (Alexander, Tsuruda et al. 1997). Diffusion-weighting gradients were applied in 60 directions with a b value of 1000 sec/mm^2; repetition time/echo time of 6970/104 msec, field of view of 141×141 mm^2, matrix size of 128×128, resolution of 1.1×1.1×1.1 mm, 41 slices with no gap, covering the whole brain. Averages of four averages of diffusion-weighted images with phase-encoding directions of opposite polarity (two averages per each direction) were acquired to correct for susceptibility distortion (Andersson, Skare et al. 2003). For each average of diffusion-weighted images, five images without diffusion weighting (b=0

sec/mm^2) were also acquired with matching imaging parameters. The total diffusion MRI scan time was approximately 90 minutes. High-resolution T1-weighted images were also acquired using a 3D magnetization-prepared rapid gradient-echo (MPRAGE) sequence. The acquisition parameters were as follows: a repetition time/inversion time/echo time of 2500/950/3.49 msec, a flip angle of 8°, a volume of view of 128×128×96 mm, a matrix of 256×256×192, and resolution of 0.5×0.5×0.5 mm^3, with 3 averages. Total T1 scan time was approximately 33 minutes.

3.4 Image Analysis Tools

DTI Image processing was carried out using tools from the Oxford Center for Functional Magnetic Resonance Imaging of the Brain's software library (http://www.fmrib.ox.ac.uk/fsl/). Eddy current distortion and susceptibility distortion (discussed in detail in the next chapter) were corrected using the method proposed by (Andersson, Skare et al. 2003). Matlab (Matlab 7, Mathworks) codes incorporated in SPM5 were used for the Eddy current distortion correction. DTI-fit within the FMRIB`s diffusion tool box (http://www.fmrib.ox.ac.uk/fsl/fdt) was used to independently fit diffusion tensors to each voxel. Maps of Fractional Anisotropy (FA), Mean Diffusivity (MD) and the three Eigen values (L_1, L_2, L_3) reflecting the primary, secondary, and tertiary values of diffusion were calculated using DTI-fit. Axial Diffusivity (L_1) and Radial Diffusivity (average of L_2 and L_3) images were also calculated for each subject.

Chapter 4

DTI Protocol Development and Artifacts

4. 1 Background

One important factor that affects the comparability of results across species is the difference in brain and head sizes. Chimpanzee heads are as large as or larger than human heads, but their brains are about one-third the volume of humans. Macaque heads and brains are even smaller than chimpanzees. Human female brains average approximately 1200 cc; chimpanzees about 320 cc; rhesus macaques about 90 cc (Herndon, Tigges et al. 1998; Herndon, Tigges et al. 1999; Rilling 2006). These differences in brain size affect results through differences in signal-to-noise ratios (SNR) and partial voluming. If humans and non-human primates are scanned with the same voxel size, the size of the voxel will be larger relative to actual anatomical size in non-human primates, simply because non-human brain structures are smaller than their human homologues. This will lead to partial voluming (i.e., worse anatomical resolution) and erroneous misclassification of the data. In other words, voxels along the edges of ROIs will contain more unwanted tissue in small brains than in large brains.

Several steps have been taken to address these issues. First, in order to obtain comparable anatomic resolution in all three species, chimpanzees and macaques were scanned at higher resolution (decreased voxel size) compared with humans. Voxel sizes were scaled to the brain size of each species. For example, to match partial voluming for data acquired with 2 mm isotropic voxel size in humans, 1.3mm isotropic and 0.3 mm

isotropic voxel sizes are needed for chimpanzees and macaques respectively. This will markedly decrease the signal to noise ratio of the images. Moreover, increased spatial resolution demands a larger acquisition matrix, which increases the echo time (TE) and repetition time (TR). The lengthened TE and large acquisition matrix can lead to severe signal loss, motion artifacts, and artifacts that evolve with increase in TE like susceptibility-related distortions. Along with these technical limitations, there is a practical limitation on the maximum amount of time that an animal can safely be inside the scanner under anesthesia. Due to the above mentioned reasons, scaling might not be exactly based on the ratio of their brain sizes. Table below contains the final DTI voxel sizes developed considering the factors mentioned above.

Table 4.1: Table showing the scaled voxel sizes and the number of averages for different species

Species	DTI Voxel Size	Number of Averages
Humans	2 mm (Isotropic)	2
Chimpanzees	1.8 mm (Isotropic)	2
Macaques	1.1 mm (Isotropic)	4

Second, in order to compensate for reduced signal to noise ratio due to smaller voxel sizes, more averages of each scan were collected for non-human primates compared to humans. For example, the voxel size for macaques is almost half of humans, in order to compensate for that 2 additional averages are acquired for macaques, by which the SNR is increased by a factor of $\sqrt{2}$. Diffusion weighted sequences and T1-weighted sequences were acquired keeping these factors in mind.

4.2 Echo Planar Imaging (EPI)

Echo Planar Imaging (EPI) is one of the most commonly used magnetic resonance imaging sequences for acquiring diffusion weighted images. Diffusion is the random thermal motion of molecules through a tissue compartment. The signal intensity of Magnetic Resonance Imaging is dependent on water motion, among other factors, which intrinsically produces contrast. In diffusion-weighted echo-planar imaging, image acquisition is sensitized to the diffusion of water molecules by inserting very strong motion-sensitizing gradient pulses into the echo-planar imaging pulse sequence.

Principle: In Echo Planar Imaging (EPI), all the k-space lines are acquired within a single repetition i.e. the complete image is acquired from one single free induction decay signal around 40 to 100 ms in duration of a gradient echo or spin echo sequence. Similar to a conventional Spin Echo sequence, a Spin Echo based echo planar imaging sequence begins with 90 and 180 RF pulses. However, after the 180 RF pulse, the frequency-encoding gradient oscillates rapidly from a positive to negative amplitude, forming a train of echoes. Since the complete image is acquired within a single repetition it is called as a single-shot sequence. On the other hand, if all the data points required to make-up an image are acquired in several free induction decays, it is called a multi-shot EPI or interleaved EPI. This technique is sometimes referred to as segmented EPI, since the data points are acquired by dividing the k-space into two or more segments.

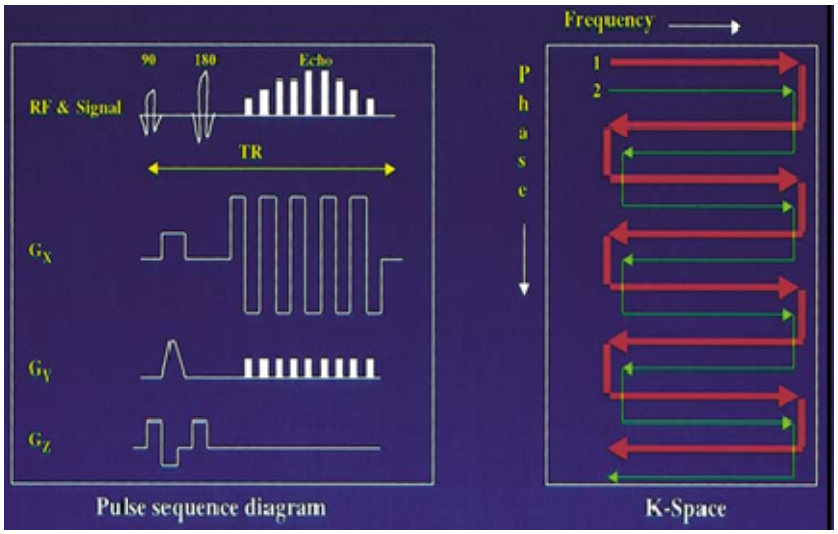

Figure 4.1: Pulse sequence diagram and k-space traversal of a single shot EPI sequence (Haacke et al Magnetic Resonance Imaging: Physical Principles and Sequence Design)

For example, in a two shot EPI, the first interleave covers the whole of k-space in alternate lines, and then the second pass fills in the lines between (Figure 5.2). The same principle is extended to any number of interleaves.

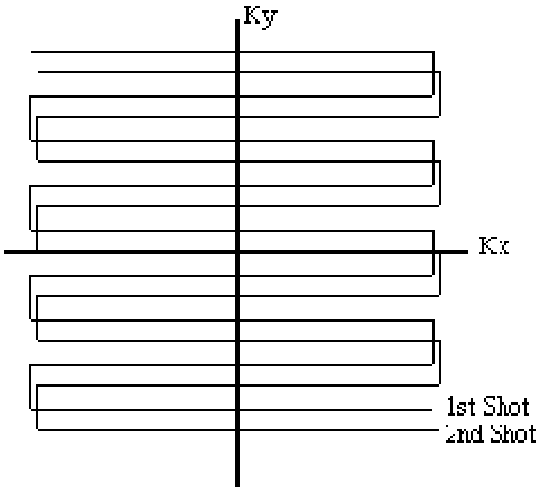

Figure 4.2: K-space traversal in a two-shot Echo planar Imaging. The first interleave covers the whole of k-space in alternate lines, and then the second pass fills in the lines between

.

4.3. Technical Challenges and Artifacts

There are several practical and technical challenges involved in acquiring diffusion weighted images from chimpanzees using EPI. Currently, Echo planar imaging-(EPI) based sequences are the only realistic option compared to conventional spin-echo (SE) and gradient-echo (GE) sequences for acquiring diffusion data in living chimpanzees because of scan time considerations. Unfortunately, these sequences are prone to susceptibility-induced distortion. In Single Shot EPI only one excitation is necessary to acquire an image and hence, the DWI images become less sensitive to subject motion compared to multi-shot sequence, but extremely sensitive to small deviations in the magnetic field. One of the most serious problems of EPI is caused by field inhomogeneity. Field inhomogeneities can be caused by imperfections within the magnet, eddy-current induced local gradients, and magnetic susceptibility effects caused by the sample, especially near the air-tissue interfaces. The variations in the field cause the signals to resonate at different frequencies. The effects are less severe along the readout direction in EPI due to the usage of large gradients. However, along the phase encode direction, the off-resonance effects are more severe, resulting in a considerable shift in pixel position. This, in turn, causes spatial distortion of the images. Spatial distortion can also be caused if the external shim coils are not optimally set or if there is poor bandwidth in the phase encoding direction (Jezzard and Balaban 1995). These effects are exaggerated at higher field strengths.

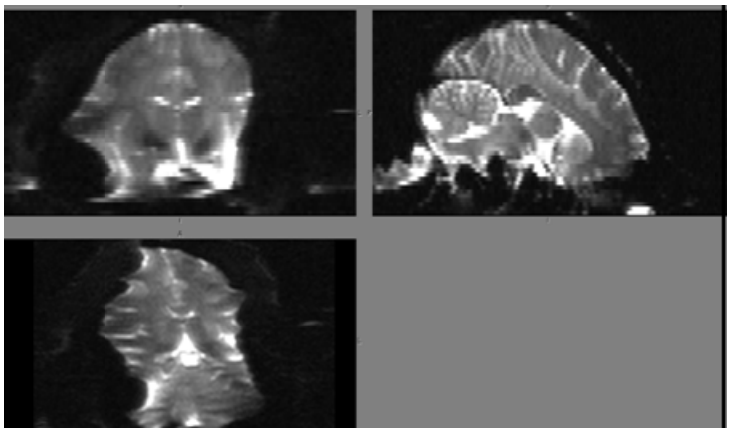

Figure 4.3: Large Geometric distortions caused by the magnetic susceptibility artifact at the air-tissue interfaces using single-shot EPI sequence in chimpanzees

In chimpanzees, due to complicated sinus anatomy and large air-tissue interfaces, the spatial distortion caused by magnetic susceptibilities is severe. In addition to the complicated anatomy, increased resolution to avoid partial voluming in chimpanzees demands a larger acquisition matrix, which increases the echo time (TE) and repetition time (TR). This will increase the severity of susceptibility induced distortion due to increase in TE. Moving from single shot imaging to multi-shot EPI imaging reduces the extent of spatial distortion due to increases in the number of excitations (reduced TE) needed to acquire the information from one slice.

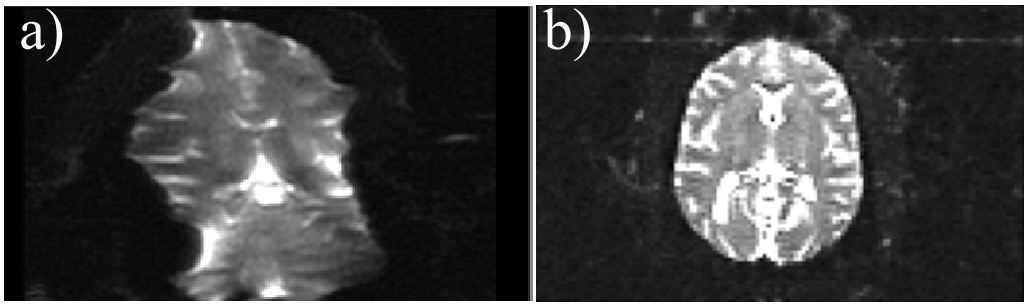

Figure 4.4: Illustration of geometric distortions caused by the magnetic susceptibility artifact in a) single-shot EPI sequence and b) multi-shot EPI sequence. A b0 image is shown for comparison

Therefore, the off-resonance errors, resulting from field inhomogeneity and susceptibility, which evolve constantly with time, are significantly reduced.

4.4 Distortion correction scheme

Any residual distortion due to magnetic susceptibility can be corrected using the method proposed by (Andersson, Skare et al. 2003). This method uses two diffusion weighted averages: one with bottom-up and the other with top-down traversal of k-space in the phase-encode direction (Morgan, Bowtell et al. 2004).

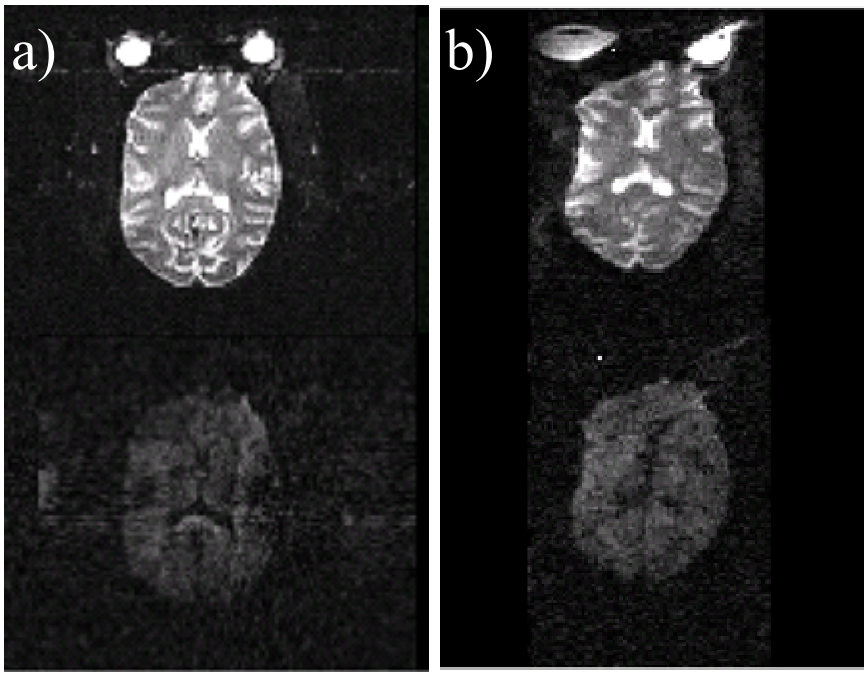

Figure 4.5: Significantly reduced geometric distortions using segmented EPI sequence (a) compared to single shot EPI (b) in chimpanzees. One of the diffusion weighted volumes is shown in the figure after using the correction scheme mentioned above. A single average of b0s (upper row) and diffusion weighted images (lower row) of the data are shown

This results in two images with identical magnitude distortions in opposing directions. A displacement field is estimated from these two distorted images. This displacement field contains information about the signal, which differs in the two acquisitions only with respect to the effects of susceptibility of the induced field inhomogenities. This displacement field is applied for each diffusion direction to restore the images to their undistorted state using a least squares approach. These can be combined for each acquisition and the two acquisitions are averaged to yield an undistorted, averaged diffusion weighted image.

Based on the facts mentioned above, a multi-shot sequence may therefore be used to alleviate the susceptibility-induced distortion and signal loss. However, a potential drawback of multi-shot EPI is that it increases the scan time by n fold, where n is the number of shots or segments used in the sequence. It also increases the susceptibility to brain motion. Phase mismatch due to segmented acquisition makes it vulnerable to physiologically-associated motion artifacts. Gated multi-shot sequences can reduce the motion artifacts significantly, but will at least double the scanning duration, and are therefore impractical given the time limits of scanning living chimpanzees.

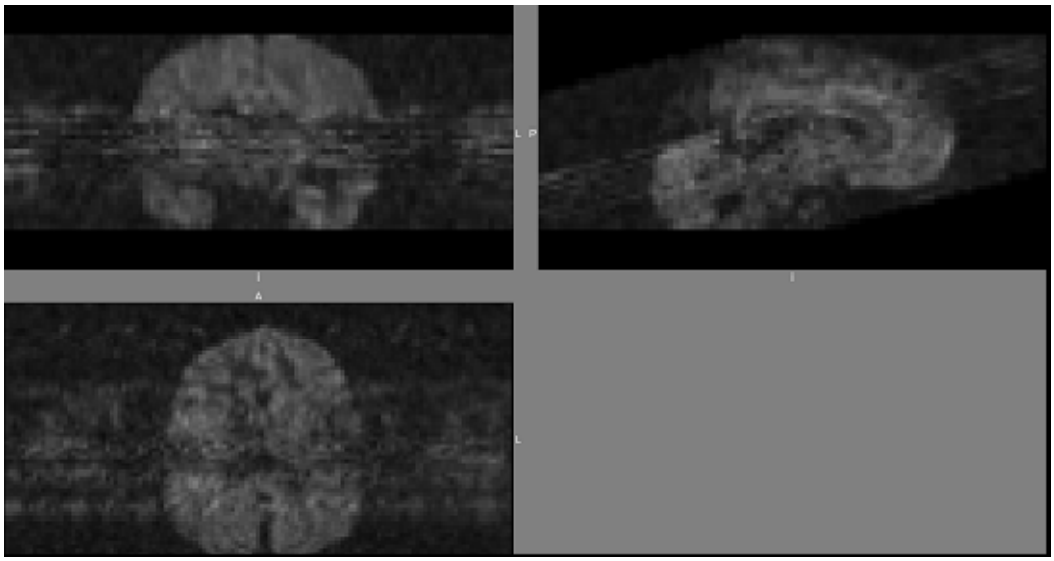

Figure 4.6: Figure shows increased motion artifact in chimpanzees using segmented EPI. Ghosts appear in the image as streak of lines covering a range of slices

4.5 Ghosting and Its Effect on Chimpanzees DTI Data

Subject motion in segmented EPI causes small incoherent phase changes between the segments, leading to severe image artifacts. These artifacts are often referred to as image ghosts. The main source of motion that gives rise to ghosting is thought to be cardiac pulsation with occasional involuntary movement of the subject. This is one of the potential problems of segmented EPI acquisition. Even the use of cardiac gating to synchronize the data acquisitions in combination with simple readout navigator echo approach cannot suppress all motion-related phase errors. As a result, residual artifacts are often found in the corrected images. Ghosting not only causes signal to appear outside the brain (a well-known ghosting pattern), but also a loss of signal from within the brain, leading to worse SNR within the brain. Poor SNR has a significant effect on the DTI metrics. When true FA is close to zero, (i.e. in CSF) noise will cause the FA values to deviate from zero in the positive direction, i.e overestimate FA. On the other hand, when

true FA is closer to 1, noise will cause the values to deviate from 1 in the negative direction, i.e underestimate FA. Between these two extremes, there is a continuum for different values of FA.

In our sample of chimpanzees, ghosting is negatively correlated with age (r=-.81, p=0.001) and weight (r=-.63, p=0.01). In macaques, there is a trend for a negative correlation between age and ghosting (r=-.23, p=0.09). These correlations may result from differences in motion-related ghosting associated with cardiac pulsations as a function of age and weight. Young chimps are thought to beat their hearts forcefully and hence leading to higher pulsatile motion.

a)

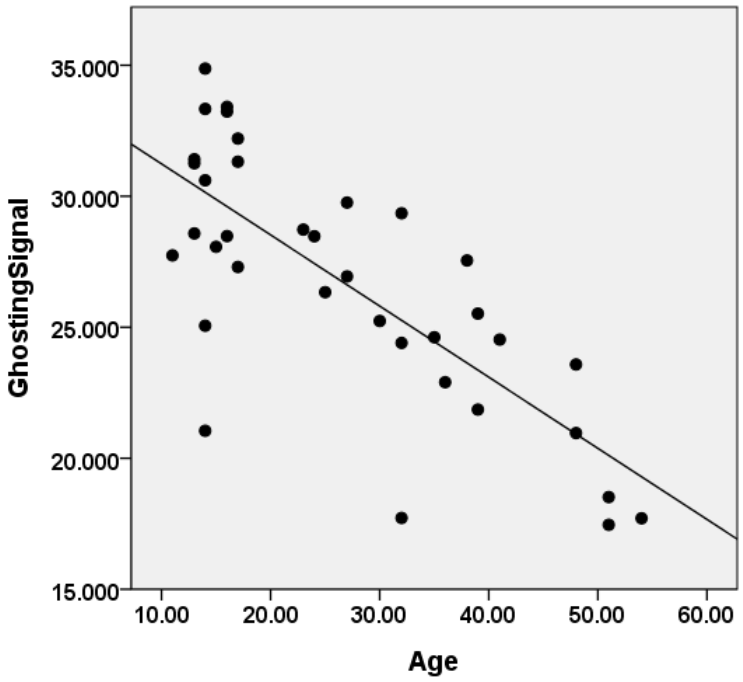

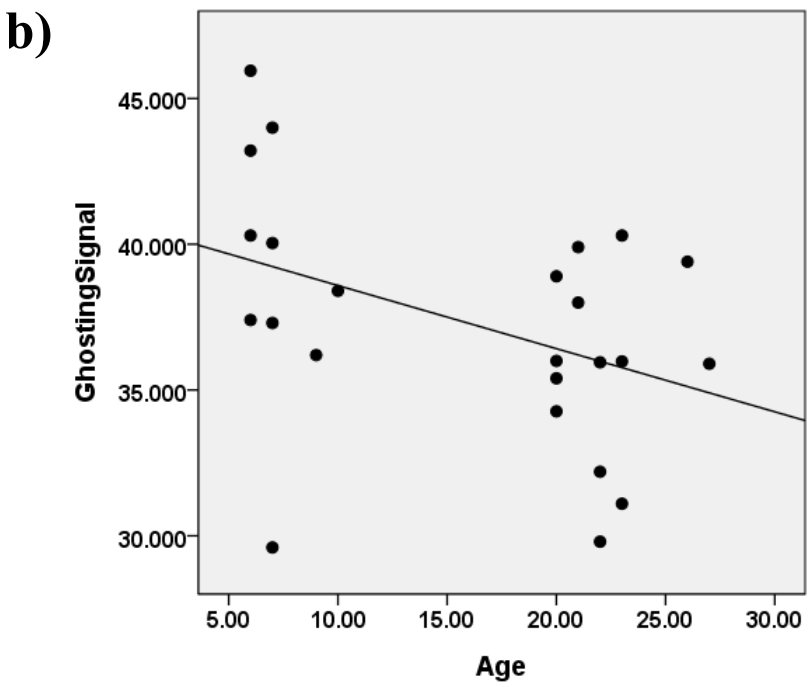

Figure 4.7: Correlation between signal loss due to ghosting and age in a) chimpanzees(r=-.81, p=0.001) and b) macaques (r=-.23, p=0.09)

In order to evaluate the influence of ghosting on the DTI metrics, three different simulation techniques were conducted and compared.

Method 1: A measure of ghosting signal from the DTI images was estimated by drawing an ROI outside and 8mm below the brain's gravity center, near the temporal lobe, where ghosting is observed to be maximal across the group. A true measure of ghosting signal is estimated by subtracting the measured signal in the ghosting ROI from the signal in the background ROI.

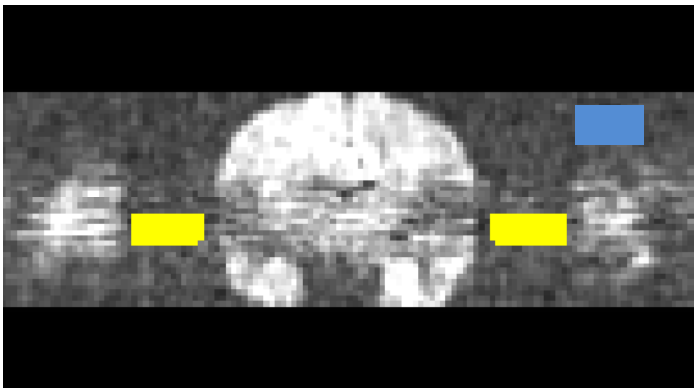

Figure 4.8: ROI drawn to measure the signal due to ghosting where it is observed to be maximal across the group. ROI (yellow) is drawn outside and 8mm below the gravity center of the brain. Background ROI (Blue) is also shown in the figure

Mean and standard deviation of this difference signal are measured for all 60 diffusion directions and provided as input for the simulation. The simulations were carried out, independently accounting for the effects of the ghosting signal for each of the diffusion weighted directions.

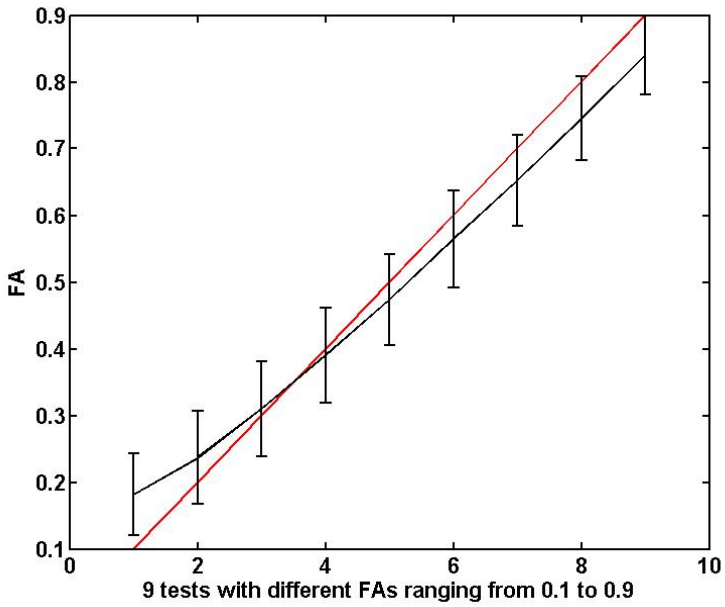

Figure 4.9.A: FA simulation results for Lulu with ghosting modeled as mu (mean) of 17.8 and sigma of 0.74 (standard deviation)

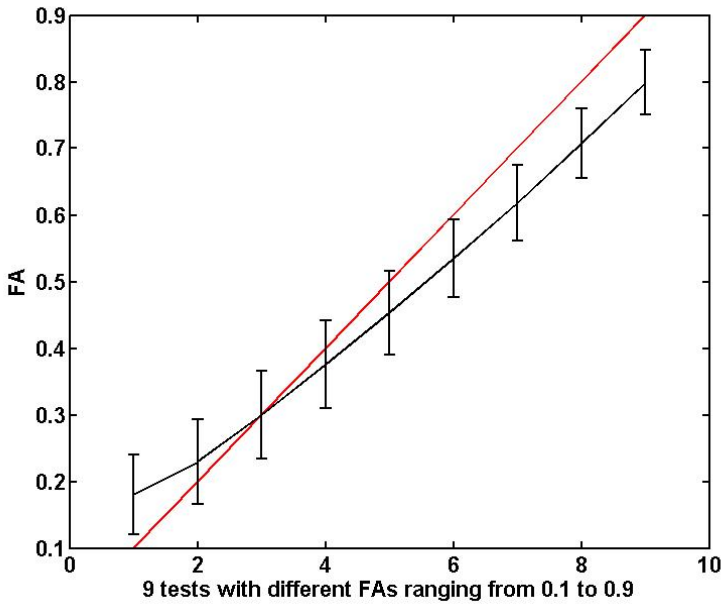

Figure 4.9.B: FA simulation results for Callie with ghosting modeled as mu (mean) of 32.3 and sigma of 4.7 (standard deviation)

The simulated FA values for an old chimpanzee (51 years) (Figure 5.9.A) and a young chimpanzee (17 years) (Figure 5.9.B) are compared above. The red line indicates the standard FA values ranging from 0.1 to 1. The black line indicates the simulated FA under the influence of ghosting noise.

Method 2: In method 2, simulations of the FA values were performed using the method proposed by (Koay and Basser 2006). Instead of just subtracting the background ROI signal from the ghost ROI signal in method 1, the measure of ghosting signal was estimated using the relationship:

$$\mathbf{M} = \sqrt{\mathbf{A}^2+\Delta^2} \quad \text{(Gudbjartsson and Patz 1995)} \qquad (5)$$

where A is the ghosting signal free from background noise, M is the measured signal (ghosting signal +background noise), and Δ is the standard deviation of the original complex image (equal to the standard deviation of the measured signal when the signal is dominant). Δ can be estimated from the mean of background noise based on the

relationship: mean of background noise (no signal) = 1:25*Δ (Appendix B, relationship B.21, Haacke et al Magnetic Resonance Imaging: Physical Principles and Sequence Design). The ghosting signal free of background noise was measured for all 60 directions and used as an input for simulation. The direction-dependent noise variance was taken into account in the diffusion tensor estimation. The simulation results for Lulu and Callie using method 2 are presented below.

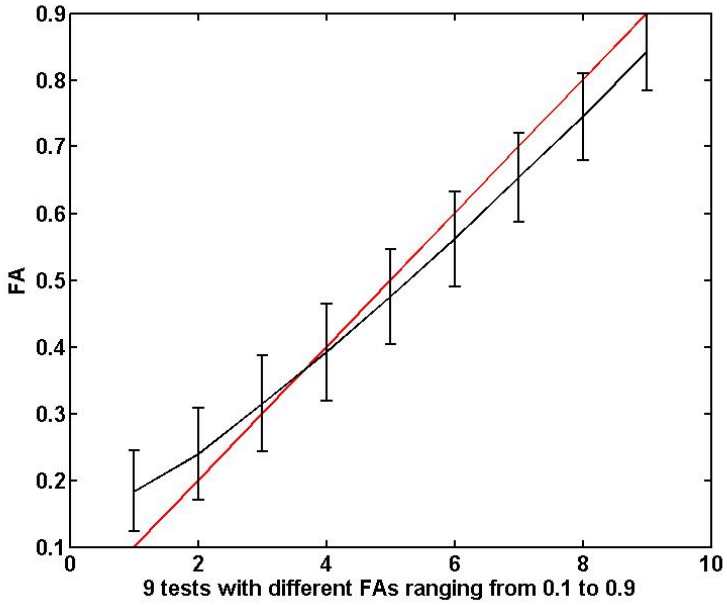

Figure 4.10.A: FA simulation results for Lulu using the corrected scheme proposed in method 2

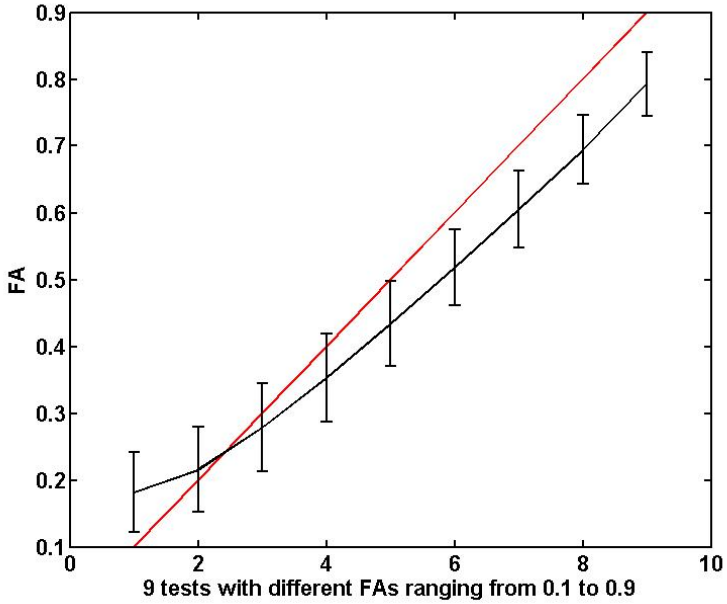

Figure 4.10.B: FA simulation results for Callie using the corrected scheme proposed in method 2

Method 3: In method 3, ghosting is assumed to be a measure that is directly proportional to the total brain signal, instead of calculating the signal from an ROI outside the brain where ghosting is maximal. In other words, the input signal for the simulation is the total brain signal, measured from the brain mask for all the diffusion directions. Steps involved in the estimation of ghosting signal, free from background noise, using the standard deviation of the complex images (Method 2) were used in this method. Results indicate that the direction of FA change as well as the magnitude of overestimation/underestimation of FA is very similar between method 2 and method 3.

Methodologically, method 2 is the more accurate way of estimating the ghosting signal from the standard complex images. Results show that the influence of ghosting on FA is more pronounced in method 2, especially for the younger subjects, where ghosting appears to be predominant. Method 2 and Method 3 are similar in principle, but the

source of ghosting signal is different. Results show that the trend and the magnitude of FA change under the influence of ghosting is very similar between method 2 and method 3. The simulation results from method 2 indicate that the magnitude of FA overestimation for lower FA regions and underestimation for higher FA regions under the influence of ghosting is significantly different between the older and the younger subjects ($t=-3.41$, $p = 0.021$). More validation tests assessing the influence of ghosting on DTI metrics are presented in the next chapter.

Based on the above discussion, there is no current single-shot EPI or multi-shot EPI protocols optimized for humans that can be readily used for acquiring the diffusion MRI data in chimpanzees. In order to acquire relatively high-resolution, high SNR *in vivo* diffusion MRI data in chimpanzees with correctable susceptibility-induced distortion within a limited time frame, several protocols have been tested on the chimpanzees.

The first protocol was a multi-shot EPI sequence (4 segments) that had the advantages of reduced susceptibility distortion and signal loss compared to that of the corresponding single–shot sequence. However, long scan time per average and segmentation-related artifacts like physiologically-induced motion leading to ghosting were the major disadvantages with this protocol. The second protocol was a cardiac-gated multi-shot EPI sequence. This protocol significantly reduced the amount of ghosting at the expense of a very long scan time. The third protocol was a modified single-shot EPI sequence with reduced field-of-view (FOV) in the phase encoding direction.

Sequence	Advantages	Disadvantages
Single-shot EPI	Fast	Large spatial distortion
Multi-shot EPI (4 segments)	Less Distortion	Movement artifact i.e. ghosting
Cardiac-gated EPI	Less ghosting	Time consuming
Single-shot EPI with reduced FOV	Less ghosting and distortion	Low SNR
Single-shot EPI with reduced FOV and partial Fourier reconstruction	Less ghosting, less distortion, and better SNR	

Figure 4.11: DTI protocol development in chimpanzees

Reducing FOV in the phase-encoding directing will significantly decrease the TE and hence the susceptibility-induced distortion. The only disadvantage with this is a lower SNR due to reduced FOV. This is compensated for in the final protocol by using partial Fourier imaging technique. Partial Fourier technique reduced the susceptibility-induced distortion proportional to the portion of the k-space sampled (i.e., shorter readout window). The most obvious advantage of this final single-shot protocol compared to the multi-shot one is the absence of the segmentation-related artifacts and its high sampling efficiency. However, there will be a large susceptibility distortion and an advanced post-processing algorithm is required to correct it. Based on the comparison of different

diffusion sequences, it can be concluded that the single-shot sequence with reduced FOV and partial Fourier reconstruction is the superior method for acquiring quantitative in vivo diffusion data in chimpanzees.

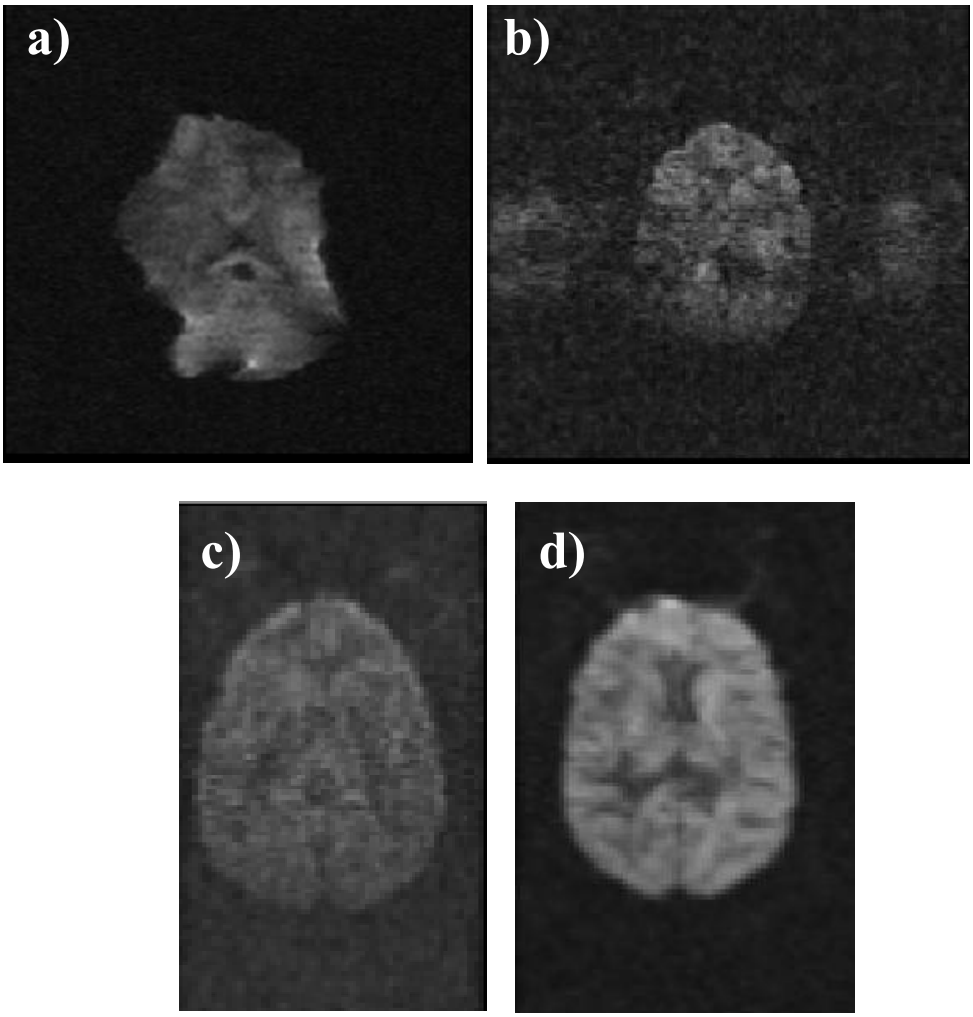

Figure 4.12: Figure comparing different diffusion weighted sequences a) single-shot, b) multi-shot, c) single-shot with reduced FOV, and d) single-shot with reduced FOV and partial Fourier used for chimpanzees. A diffusion weighted volume is shown for comparison

4.6 Phantom Tests

Phantom tests were conducted to evaluate the following:

1. The possible presence of any obvious artifacts affecting the measured FA and ADC values in the single-shot sequence with partial Fourier.
2. The differences in the measured FA/ADC values between the data with and without partial Fourier in order to determine the effects of using partial Fourier on the measured DTI indices.
3. Evaluate the differences in the measured FA/ADC values between single-shot and multi-shot sequences.

Phantom data for the single-shot sequence were acquired with and without use of partial Fourier acquisitions. Multi-shot phantom data acquired previously was used for comparisons. The phantom data acquired using the partial Fourier and no-partial Fourier techniques were devoid of any obvious artifacts and the average ADC values calculated from the phantom data is close to the ADC of pure water at 20 degree C (0.002 mm^2/s). The figure below compares the b0 and diffusion weighted images for multi-shot, single-shot (no PF), and single-shot (with PF). The multi-shot phantom data is disturbed by ghosting and other artifacts, whereas the single-shot data appears to be unobstructed by any artifacts.

.

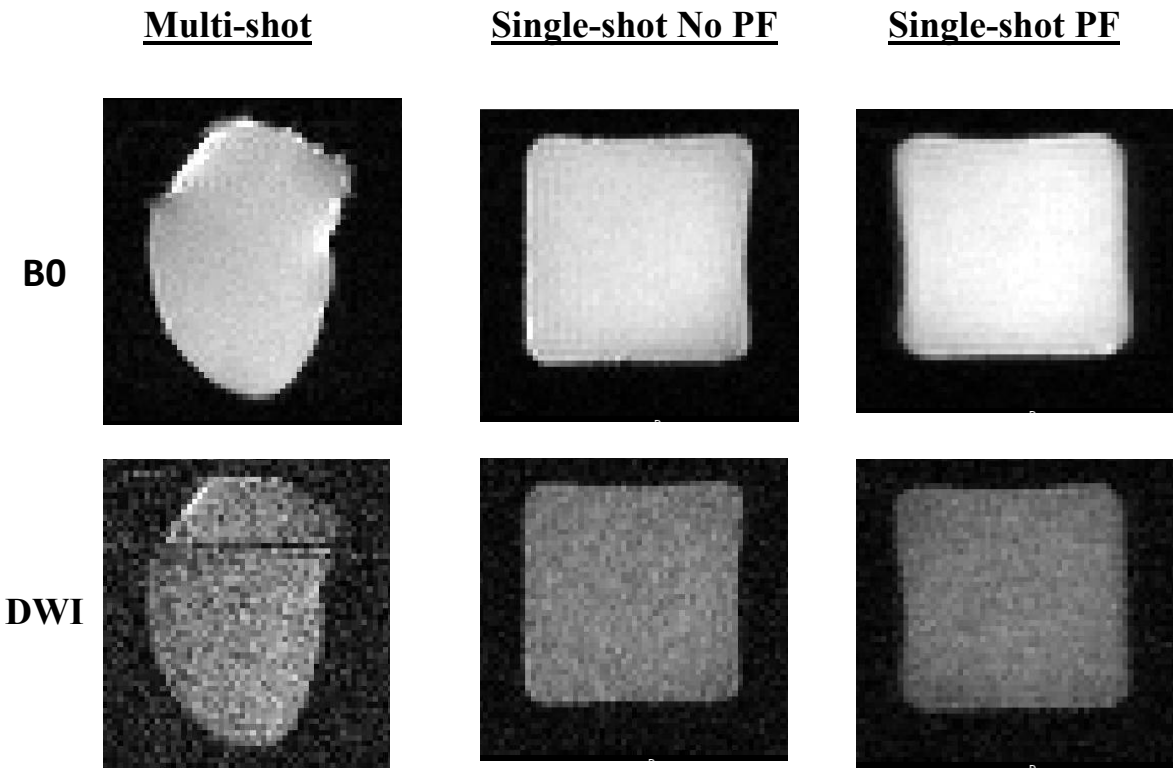

Figure 4.13: The b0 and diffusion weighted images from the phantom tests using multi-shot, single-shot no partial Fourier and single-shot with partial Fourier are shown respectively. The intensity ranges are identical for all three sets of images (0-500).

Mean FA and mean ADC values are measured and compared for the three sequences with the following two objectives in mind: the first is to determine if there is any effect of using partial Fourier on the measured DTI indices, and the second is to test for the differences in multi-shot and single-shot sequences. There is no difference in the FA/ADC values between the single-shot sequence with partial Fourier and without partial Fourier indicating no effect of partial Fourier on the measured DTI metrics. However, there is a difference in the measured FA/ADC between the single-shot and multi-shot sequences. We should expect an FA value close to zero and an ADC value close to the

ADC of water if everything goes right with the sequence, but there is some residual FA present in the phantom data acquired using the multi-shot sequence. Also, there are a lot of additional factors like ghosting affecting the FA values in the multi-shot sequences. These reasons could possibly explain why we see a difference in FA between multi-shot and single-shot and make us feel more confident about the single-shot results.

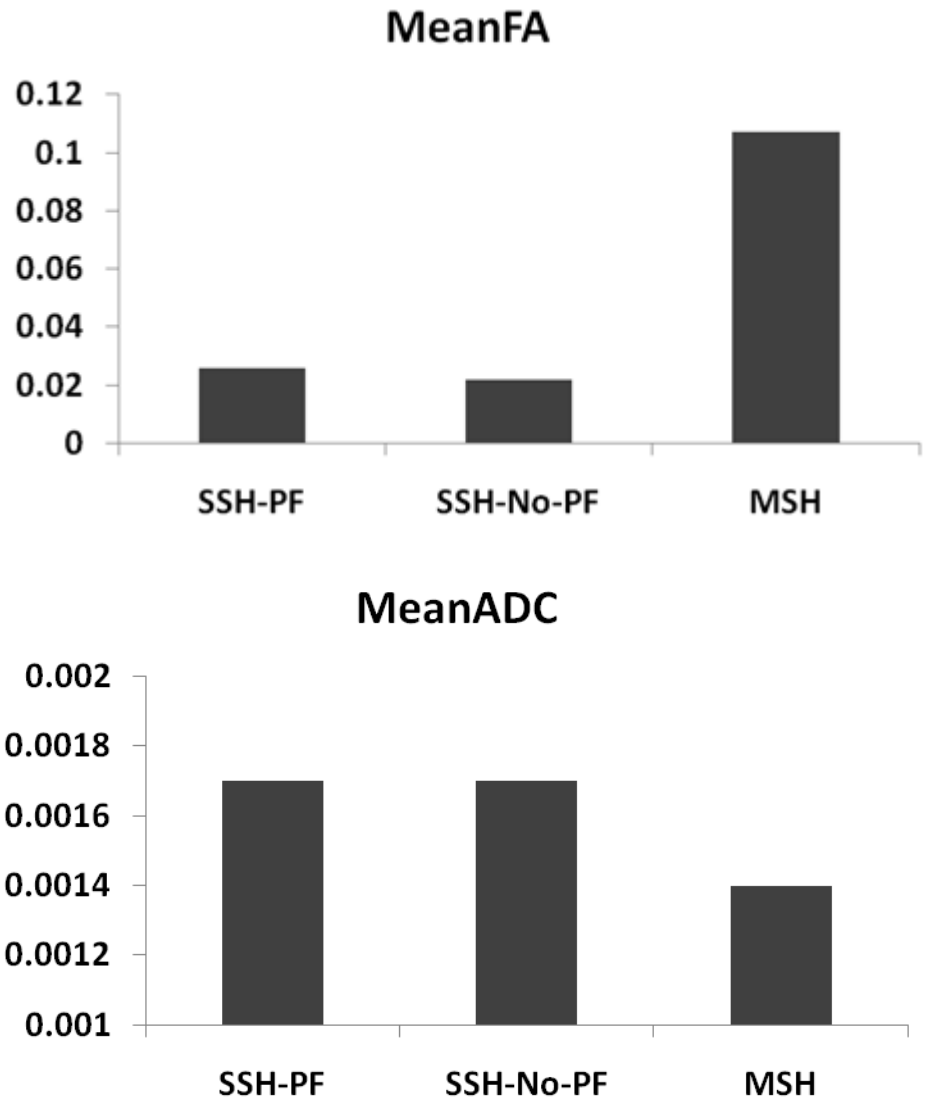

Figure 4.14: Mean FA and Mean ADC were measured and compared across all the three sequences

Chapter 5

DTI and Comparative Aging of White Microstructure

5.1 Outline

DTI data were acquired from chimpanzees and macaque monkeys, and age-related changes in several DTI indices, including fractional anisotropy (FA), apparent diffusion coefficient (ADC), axial diffusivity (AD) and radial diffusivity (RD), were measured and compared between chimpanzees and macaques and contrasted with published data from humans. Region of interest analysis and tract based spatial statistics (TBSS) analysis were used to describe the age-related changes in non-human primates. Results from both the multi-shot and single-shot data for chimpanzees are presented and discussed.

5.2 Corpus Callosum (CC) ROI Analysis

The corpus callosum can be divided into six different segments based on Witelson`s procedure (Witelson 1989). The six different segments are (from anterior to posterior) genu, rostral body, anterior mid body, posterior mid body, isthmus and splenium. Using Witelson`s procedure, the six different segments were defined along the horizontal line joining the farthest ends of corpus callosum. For example, the splenium is defined as one-fifth of the total distance along the horizontal line from the posterior end of the corpus callosum to the anterior end. ROIs based on the Witelson procedure were defined on mid sagittal slices of the T1-weighted images. T1-weighted images provide good contrast between the white matter and gray matter within the brain and are very useful in defining the anatomical regions of interest. In most of the cases, the longest line joining both the

ends of corpus callosum is not horizontal in the mid-sagittal plane due to inaccuracy in aligning the slices parallel to the corpus callosum during acquisition. Hence, we need to rotate the mid-sagittal images in order to follow Witelson`s convention. The structural images are rotated using NUDGE (FMRIB`S rotation tool). The rotation and translation parameters provided to the Nudge are based on different trials and visual inspection of the alignment.

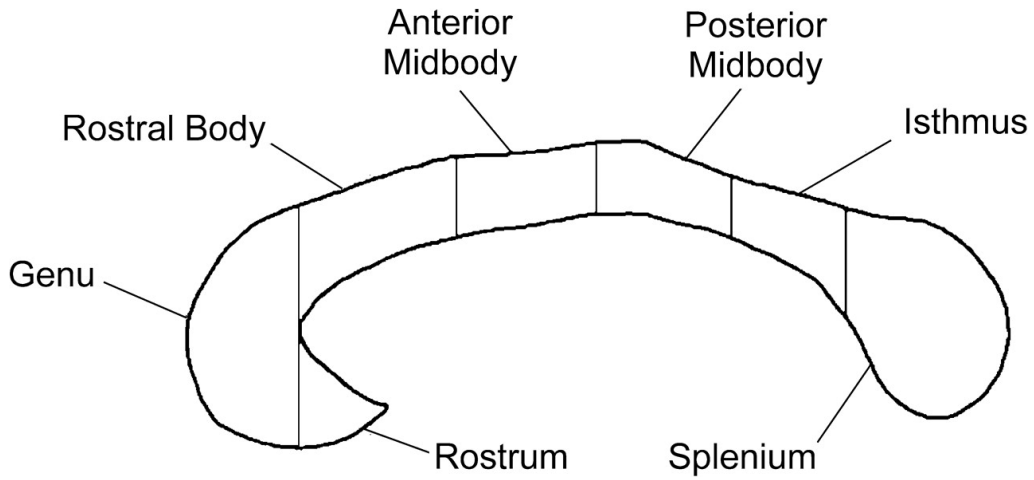

Figure 5.1: Witelson`s convention of drawing the ROIs in the corpus callosum

In the next step, partial volume maps based on the percentage of white matter, gray matter and CSF within each voxel were obtained from the structural images using FAST, FMRIB`S automated segmentation tool (http://www.fmrib.ox.ac.uk/fsl/fast4/) (Zhang, Brady et al. 2001). Next, the white matter partial volume map was transformed into the FA space using FLIRT, FMRIB`S automated registration tool (http://www.fmrib.ox.ac.uk/analysis/research/irt/) (Jenkinson and Smith 2001).

Different image registration methods were compared to determine the best registration method. The four different registration methods tested were:

1. FA to T1 co-registration with sinc interpolation
2. FA to T1 co-registration with sinc interpolation and using a Corpus Callosum box to limit the cost function. This box limits the registration parameters to the region of interest i.e. corpus callosum in this case.
3. T1 to FA co-registration with sinc interpolation
4. T1 to FA co-registration with sinc interpolation and using a Corpus Callosum box to limit the cost function

Registration accuracy was measured as the degree of misalignment after co-registration. Once the ROI is moved from one space to the other, the numbers of voxels that do not match between the native ROI and the transformed ROI were measured by subtracting the ROIs after co-registration. These numbers are normalized to accommodate for the difference in voxel sizes between the structural space and the diffusion space. In other words, the number of misaligned voxels when a structural ROI is moved to diffusion space is normalized by dividing by the number of CC voxels in diffusion space (reference space). These normalized numbers were measured for the four different registration methods for a group 12 chimps. Analysis of variance (ANOVA) was used to test for the differences between the different registration methods.

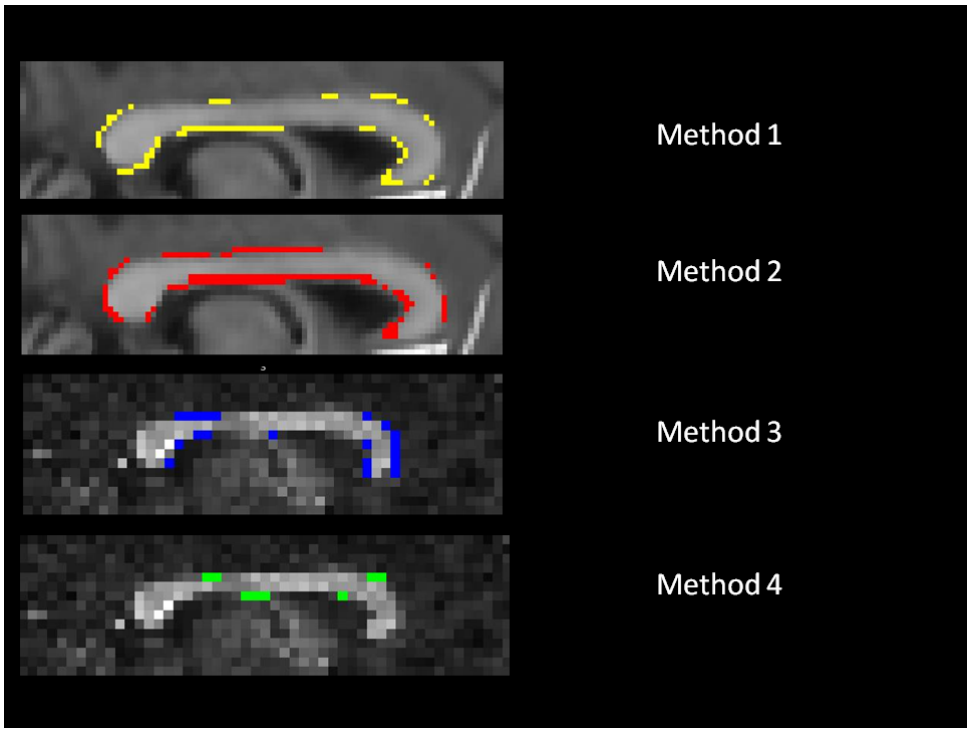

Figure 5.2: Qualitative representation of the degree of misalignment. Voxels colored in yellow, red, blue and green indicate the number of voxels that are misaligned for the four different registration methods respectively for subject Callie

Figure 5.2 shows the representation of the degree of misalignment for different registration methods. Qualitatively, method 4 has less misalignment compared to other methods. Figure 5.3 below confirm quantitatively that the mean of misalignment factor for method 4 is about 0.11 and significantly lower compared to other methods.

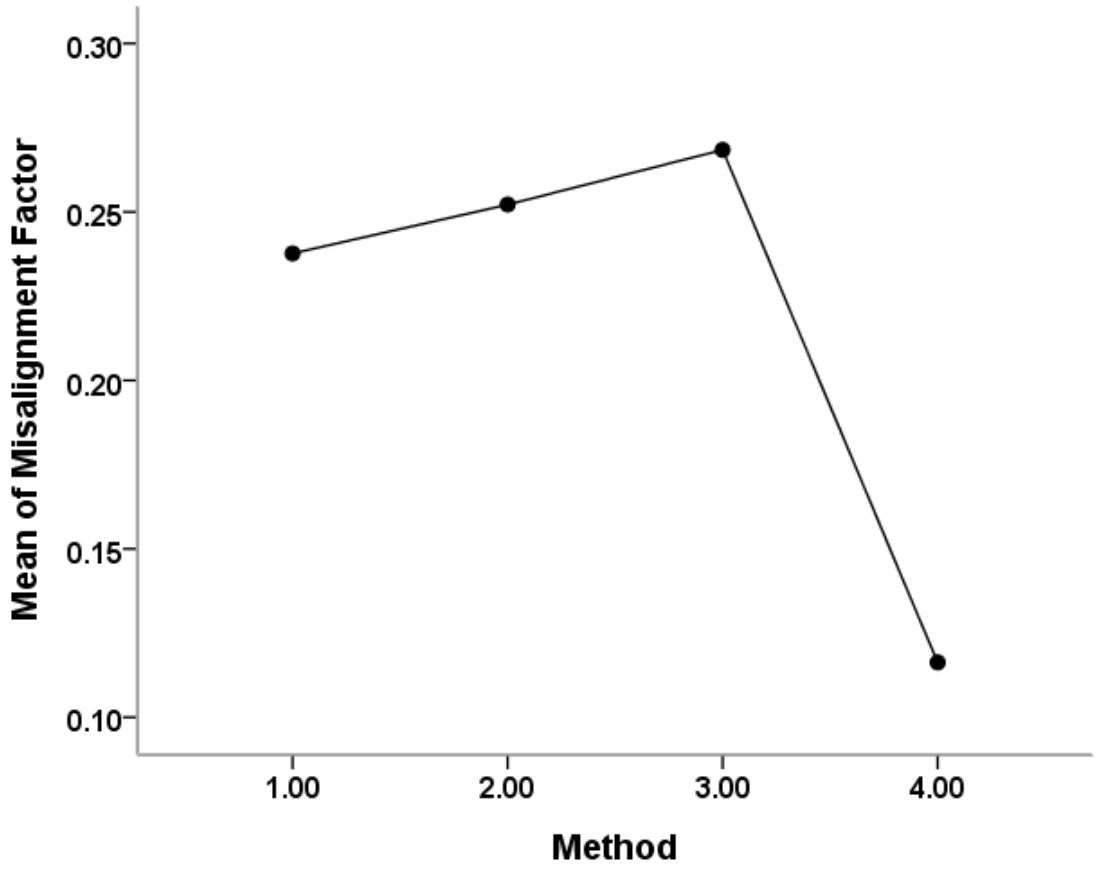

Figure 5.3: Mean of misalignment factor for the four methods. Method 4 has the least misalignment compared to other methods

Analysis of Variance (ANOVA) was conducted to test for the differences in the misalignment factor across the four different registration methods. The ANOVA result table below indicates that there is a significant difference between the four groups at $p<0.001$. Based on the qualitative and quantitative comparisons of different registration methods within a group of 12 subjects, method 4 was chosen as the registration method for the analysis. A mask encompassing the CC was drawn and used as an input weight image to confine the registration parameters to that region for all the subjects. The white matter partial volume map in FA space was thresholded using a white matter percentage of 50 percent to avoid partial voluming. The ROIs defined on the structural images were

then transformed into the DTI space and multiplied by the white matter partial volume map in the diffusion space to ensure that the ROIs were located within the white matter of the diffusion anisotropy image. DTI metrics (FA, MD, AD and RD) were calculated from the six different segments of the corpus callosum. Bivariate linear correlations (Two-tailed, $p<0.05$) between age and the mean DTI indices were conducted using SPSS (http://www.spss.com/).

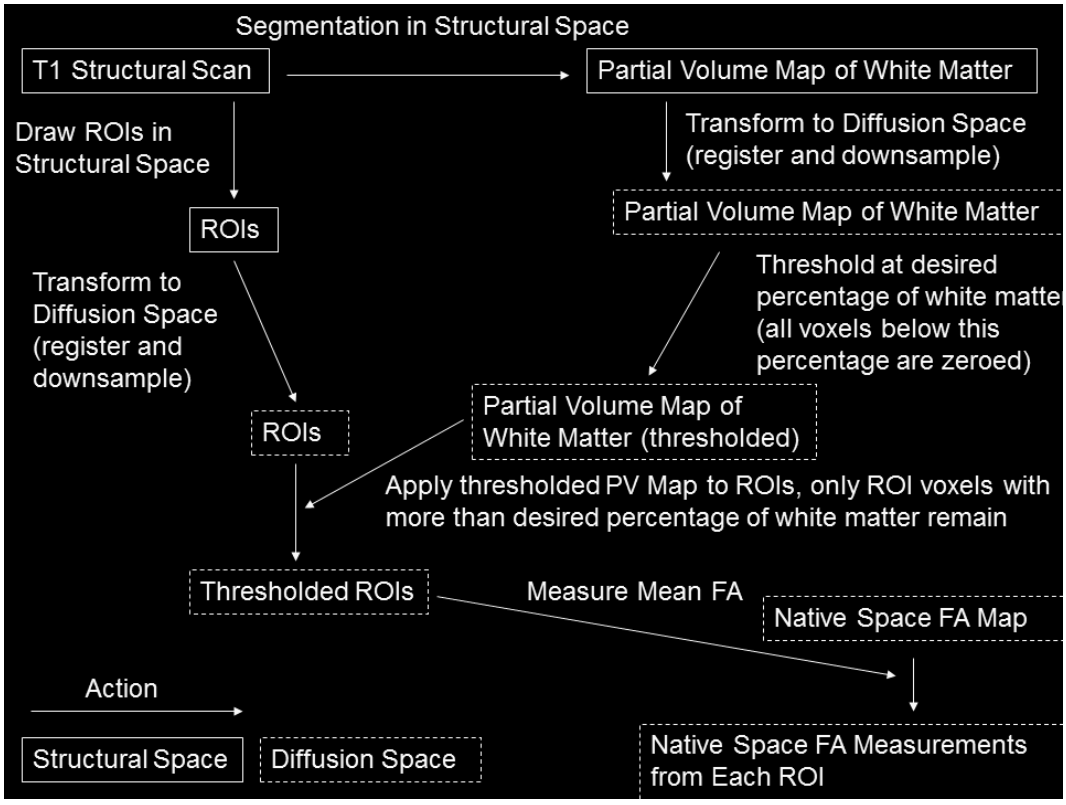

Figure 5.4: Flow chart illustrating different steps used in the ROI method

5.2.1 Results

Chimpanzee multi-shot data results: Correlations between age and the mean diffusion metrics for the six different segments of the corpus callosum are summarized in Figure 6.6. Mean FA increased with age in all segments except for the anterior mid-body, however this increase was only statistically significant for the genu (r=0.36, p=0.03). Age-related increases in FA were accompanied by decreases in ADC, AD and RD. Mean ADC values decreased with age for all segments, reaching significance in three segments: the genu (r=-0.39, p=0.01), isthmus(r=-0.33,p=0.04) and splenium (r=-0.36,p=0.027). Although not significant, mean AD values decreased with age for all segments. Finally, significant negative correlations between RD and age were seen in the genu (r=-0.39, p=0.01) and isthmus (r=-0.35, p=0.03).

Region	FA	ADC	AD	RD
(1)Genu	r=.36*	r=-.39*	r=-.24	r=-.39*
(2)Rostral body	r=.04	r=-.24	r=-.21	r=-.21
(3)Anterior mid body	r=-.05	r=-.11	r=-.18	r=-.04
(4)Posterior mid body	r=.14	r=-.25	r=-.08	r=-.30
(5)Isthmus	r=.22	r=-.33*	r=-.13	r=-.35*
(6)Splenium	r=.16	r=-.36*	r=-.32	r=-.28

Figure 5.5: Relationship between age and the mean DTI metrics for the six segments of the corpus callosum using multi-shot sequence. Correlation coefficients for age vs. DTI metrics for all six ROIs. * = $p < 0.05$

a)

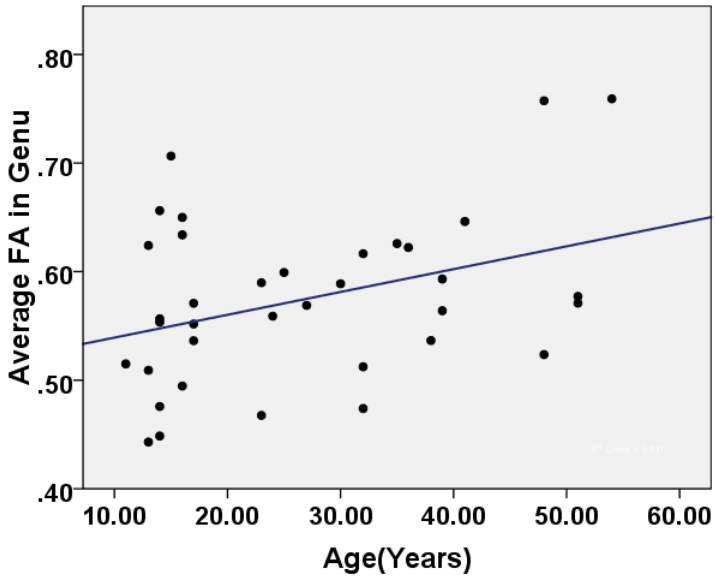
Average FA in Genu
.80
.70
.60
.50
.40
10.00
20.00
30.00
40.00
50.00
60.00
Age(Years)

b)

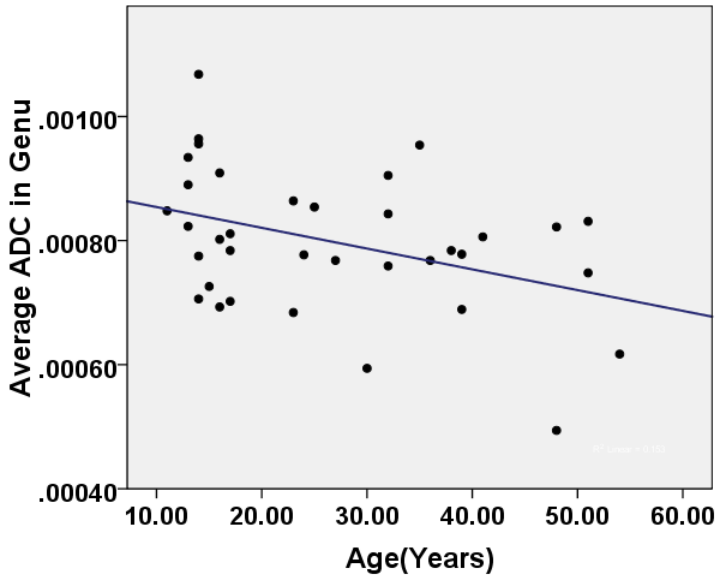
Average ADC in Genu
.00100
.00080
.00060
.00040
10.00
20.00
30.00
40.00
50.00
60.00
Age(Years)

c)

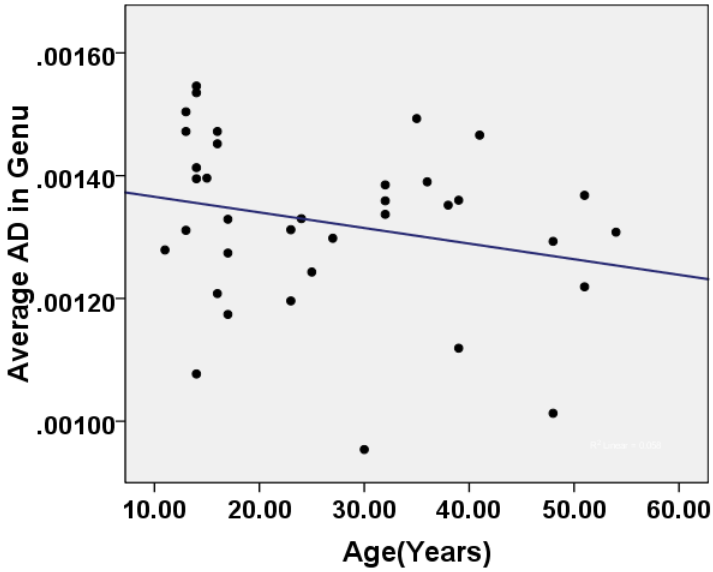

d)

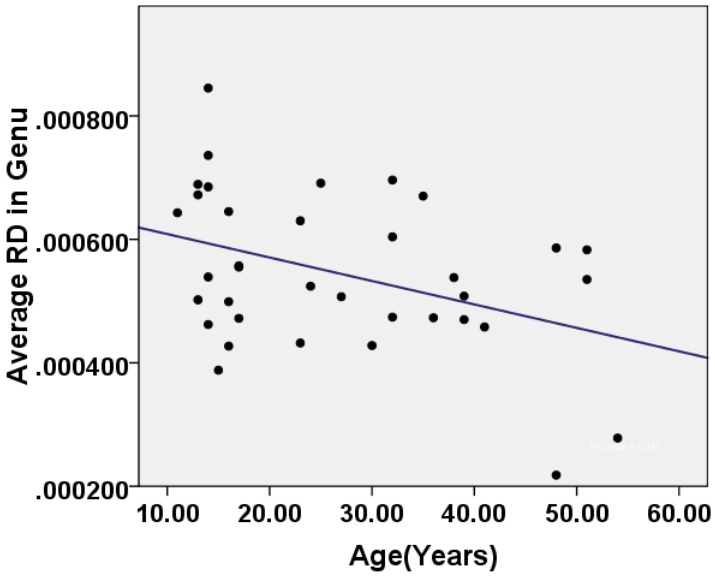

Figure 5.6: Age-related changes in DTI metrics in the genu of the corpus callosum for chimpanzees. Age vs. a) FA, b) ADC, c) AD and d) RD. Correlations were significant in a) r=0.36, b) r=-0.39, and d) r=-0.39

Chimpanzee single-shot data results: Correlations between age and the mean diffusion metrics for the six different segments of the corpus callosum are summarized in Figure 5.7. Mean FA increased with age in all segments except for the anterior midbody, however this increase was not statistically significant for any region. Age-related increases in FA were accompanied by decreases in ADC, AD and RD. Mean ADC, Mean AD, and Mean RD values decreased with age for all segments except for posterior midbody, with only isthmus ADC (r=-0.59, p=0.05) and AD (r=-0.65, p=0.02) reaching significance.

Region	FA	ADC	AD	RD
(1)Genu	r=.21	r=-.17	r=.10	r=-.24
(2)Rostral body	r=.08	r=-.26	r=-.08	r=-.28
(3)Anterior mid body	r=-.14	r=-.10	r=-.19	r=-.05
(4)Posterior mid body	r=.04	r=.23	r=.27	r=.19
(5)Isthmus	r=.21	r=-.59*	r=-.65**	r=-.49
(6)Splenium	r=.21	r=-.20	r=-.43	r=-.07

Figure 5.7: Relationship between age and the mean DTI metrics for the six segments of the corpus callosum using single-shot sequence. Correlation coefficients for age vs. DTI metrics for all six regions of corpus callosum. * = $p < 0.05$ and ** = $p < 0.01$.

With respect to FA, results from single-shot CC ROI analysis showed a similar trend compared to multi-shot results, except that genu showed a significant positive correlation with age using multi-shot data.

Macaques: No region in the corpus callosum showed significant age-related changes in FA. Although not significant, mean FA values decreased with age for anterior midbody, posterior midbody, isthmus and splenium. On the other hand, significant negative correlations were observed between AD and age in the anterior midbody (r=-.50, p=0.01), posterior mid body(r=-.53, p=0.01), isthmus (r=-.68, p=0.004) and splenium (r=-.57, p=0.009). A significant negative correlation was also observed between ADC and age in the isthmus(r=-.40, p=0.01) and splenium (r=-.39, p=0.01).

a)

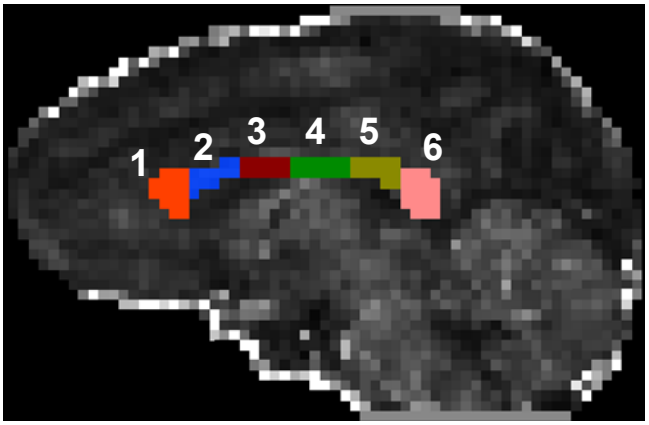

b)

Region	FA	ADC	AD	RD
(1)Genu	r=.05	r=-.19	r=-.18	r=-.19
(2)Rostral body	r=.07	r=-.20	r=-.17	r=-.18
(3)Anterior mid body	r=-.24	r=-.23	r=-.50*	r=-.01
(4)Posterior mid body	r=-.04	r=-.33	r=-.53*	r=-.17
(5)Isthmus	r=-.24	r=-.40*	r=-.68*	r=-.13
(6)Splenium	r=-.15	r=-.39*	r=-.57*	r=-.07

Figure 5.8: Relationship between age and the mean DTI metrics for the six segments of the corpus callosum for macaques. a) Definition of six corpus callosum ROIs, b) correlation coefficients for age vs. DTI metrics for all six ROIs. * = $p < 0.05$ and ** = $p < 0.01$ from 1 to 6 are shown on a subject`s FA image

5.3 Voxel-Wise Analysis

Voxel wise statistics were carried out using Tract Based Spatial Statistics (TBSS) implemented in FSL 4.1 (FMRIB, Oxford. http://www.fmrib.ox.ac.uk/fsl/). TBSS is an observer-independent sensitive tool for the voxel-wise analysis of white matter microstructure (Smith, Jenkinson et al. 2006). Compared to other voxel-based morphometry (VBM) style approaches(Good, Johnsrude et al. 2001), TBSS has the advantage of reducing the misalignment between the subjects as well as avoiding the use of arbitrary smoothing kernels for generating statistics. First, all subjects' FA images were non-linearly registered to a population-specific FA template. This is done in two steps: first, deriving a minimal deformation target (MDT) and normalizing all the subject's FA images to this MDT, and second, registering MDT to the cohort-specific template using affine registration. The cohort-specific template was derived from the same group of subjects using the following series of registrations. First, a template FA image selected from a randomly chosen subject was aligned so that the sagittal plane was parallel to the interhemispheric fissure of the brain, and the axial plane was perpendicular to the sagittal plane and parallel to the bicommissural line (the line connecting the anterior and posterior commissures). The origin of the space was defined as the center of the anterior commissure. Then each subject`s FA image is registered to this template using rigid body registration and averaged. This step creates a rigid body registration template for the group of subjects. In the next step, each subject`s FA image is registered to the rigid body template using affine registration and averaged. This step creates an affine registration template. In the last step, each subject`s FA image is registered to the affine registration template using non-linear registration and averaged to create a cohort-

specific symmetrical template. Non-linear registration is required to ensure accurate registration between different brains, and is implemented using FNIRT in the FSL package. Second, all the registered images were averaged to create a mean FA image and subsequently a mean FA skeleton, which is an average representation of centers of all the common tracts. Next, all the subjects' FA images were projected onto the mean FA skeleton by filling the skeleton with FA values from the nearest relevant tract center. For individual images, FA values are analyzed along the normal projection for each point of the skeleton image and a peak value is assigned to the skeleton. The FA values vary rapidly perpendicular to the tract direction, but change slowly along the tract direction. By assigning the peak value to the skeleton, this procedure effectively lines up the center of individual white matter tracts. This step effectively corrects for misalignment of individual fiber tracts. The projection operation is performed under two conditions: A distance map is created from the skeleton mask to establish search borders for individual tracts. The borders are created by equally dividing the distance between two nearby tracts. Secondly, a multiplicative 20-mm full width at half-max Gaussian weighting is applied during the search to limit the maximum projection distance from the skeleton. Lastly, the skeletonized FA images were used in the covariate analysis with age as a covariate and tested for significance with a p-value < 0.05, corrected for multiple comparisons, unless otherwise specified. Five thousand random permutations were used for generating the statistics using the randomize tool, implemented in FSL. TBSS was also applied to the non-FA images (AD and RD) generated from the diffusion tensor. First, the non-linear transformations derived by registering the FA images to the template were applied to the non-FA images. Next, the transformed non-FA images were projected

onto the mean FA skeleton used in the FA analysis using the same skeleton projection vectors. The resulting skeletonized non-FA images were used for the voxel-wise statistics.

5. 3. 1 Results

Chimpanzee multi-shot results: Results for the voxel-wise correlations between age and FA from multi-shot data are presented in Figure 5.10 (a). Significant positive correlations are seen in most of the major white matter tracts. Consistent with the ROI results of the corpus callosum, there are no regions with significant negative correlations with age. Results for the voxel-wise correlations between age and the three diffusivity measures (ADC, AD and RD) are presented in Figures5.10 (b), 5.10 (c) and 5.10 (d) respectively. Results indicate significant negative correlations with age for all the three diffusivity measures corrected for multiple comparisons at $p < 0.05$.

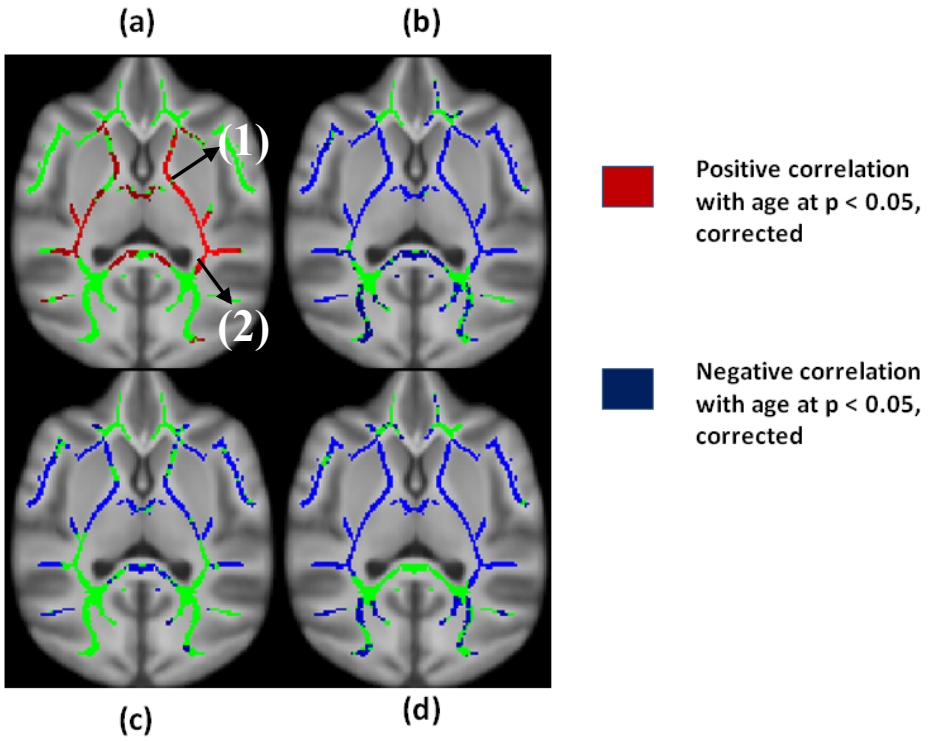

Figure 5.9: Voxel wise correlations between age and a) FA, b) ADC, c) AD and d) RD for chimpanzees. Voxels colored red show positive correlations with age and voxels colored blue show negative correlations with age. Example regions showing the two different patterns from table 1 are labeled as (1) and (2)

Age-related increases in FA were accompanied by two distinct patterns of decreases in diffusivity measures. First, decreases in both RD and AD, but greater decreases in RD. Second, decreases in RD with no change in AD. The first was by far the most common. Fiber tracts showing each of these two patterns are labeled (1) and (2) respectively in Figure 5.10.

Whole brain mean FA vs. Age: Whole brain mean FA is calculated from the skeletonized tracts of all the chimps and correlated with their respective ages. Results

show a significant positive correlation between whole brain FA and age using linear regression (r=.447, p=0.006).

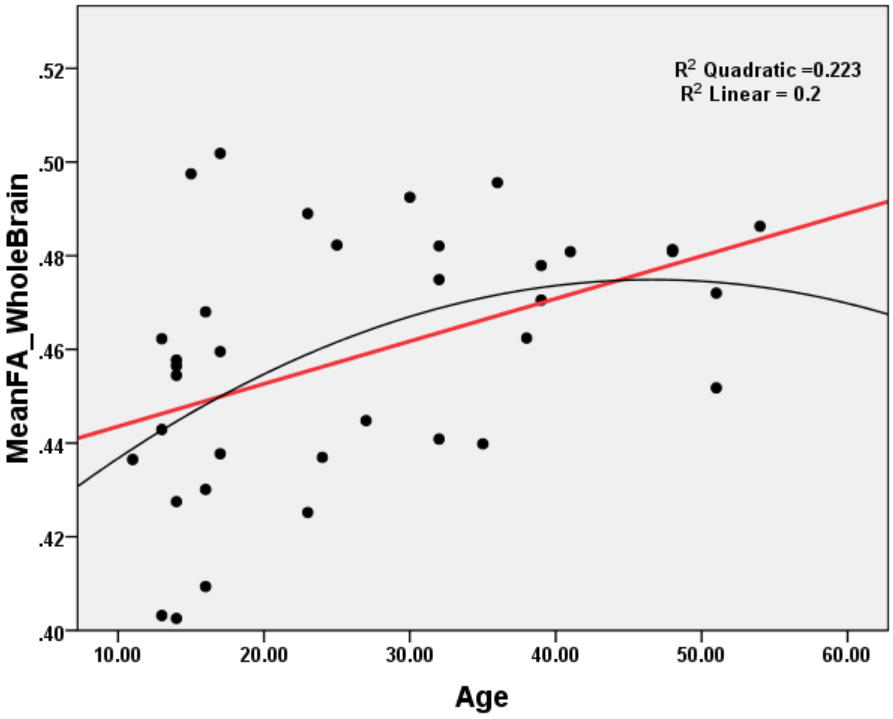

Figure 5.10: Correlations between age and whole brain skeletonized FA for chimpanzees. Red line indicated linear fitting and black line indicated curvilinear fitting. Curvilinear regression better fits the data compared to linear regression (r^2= 0.223, p= 0.04)

TBSS ROI Analysis: TBSS based corpus callosum ROI analysis is conducted to evaluate the correlation between FA and age at the skeleton level. The reasons for employing the skeleton-based ROI method are twofold: first, voxelwise whole-brain analysis involves multiple voxels (order of 10^6 in the current study) and stringent corrections for multiple comparisons are required for identifying significant effects. The ROI method, on the other hand, does not require such a correction and should therefore be more sensitive for detecting differences within selected ROIs. Second, partial

voluming is considerable, even in our diffusion MRI data with the resolution of 1.8 mm^3 isotropic, likely due to chimpanzee's smaller brain volume compared to humans. Comparing only the maximal FA values projected onto the white-matter skeleton within the ROIs (i.e., the skeleton-based ROIs) could minimize the partial volume issue. Corpus callosum ROIs are defined on the TBSS skeleton for all the subjects using Witelson's approach. Mean FA values increased with age for all segments, reaching significance in two segments: the posterior midbody (r=0.395, p=0.04) and isthmus (r=.506, p=0.022).

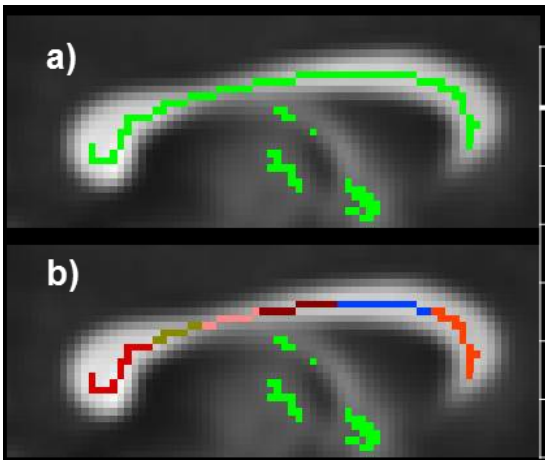

c)

Region	FA vs. Age (r)
GENU	.224
Rostral Body	.041
Anterior mid body	.185
Posterior mid body	.395*
Isthmus	.506*
Splenium	.230

Figure 5.11: Relationship between age and the mean FA for the six segments of the corpus callosum for chimpanzees using TBSS skeleton-based ROI approach. a) mid-sagittal section through TBSS skeleton image of one chimpanzee, b) definition of six corpus callosum ROIs, c) correlation coefficients for age vs. mean FA for all six ROIs. * = $p < 0.05$

Chimpanzee single-shot results:

Results for the voxel-wise correlations between age and FA from single-shot data (n=30) are presented in Figure 5.13 (a). There are no significant correlations between FA and age at a corrected threshold. However, non-significant negative correlations are seen in most

of the major white matter tracts. Consistent with the ROI results of the corpus callosum, there are no regions with significant positive or negative correlations with age.

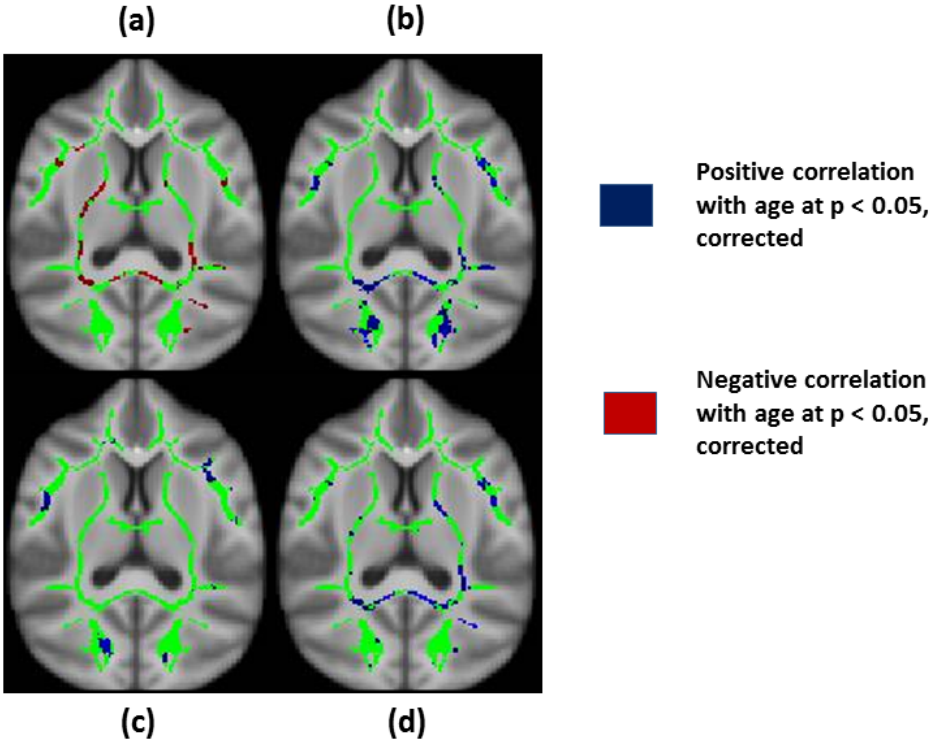

Figure 5.12: Voxel wise correlations between age and a) FA, b) ADC, c) AD and d) RD using single-shot data (n=30) for chimpanzees. Voxels colored red show non-significant negative correlations with age and voxels colored blue show non-significant positive correlations with age

This is in contrast to the multi-shot results (n=36) described above, where there were widespread significant positive correlations and no negative correlations between FA and age after correction. Results for the voxel-wise correlations between age and the three diffusivity measures (ADC, AD and RD) are presented in Figures 5.13 (b), 5.13 (c) and 5.13 (d) respectively. Results indicate non- significant negative correlations with age for all the three diffusivity measures at $p < 0.05$.

Whole brain mean FA vs. Age: Whole brain mean FA is calculated from the skeletonized tracts of all the single-shot chimps and correlated with their respective ages. Results show a non-significant negative correlation between whole brain FA and age using linear regression (r=-.14, p=0.453).

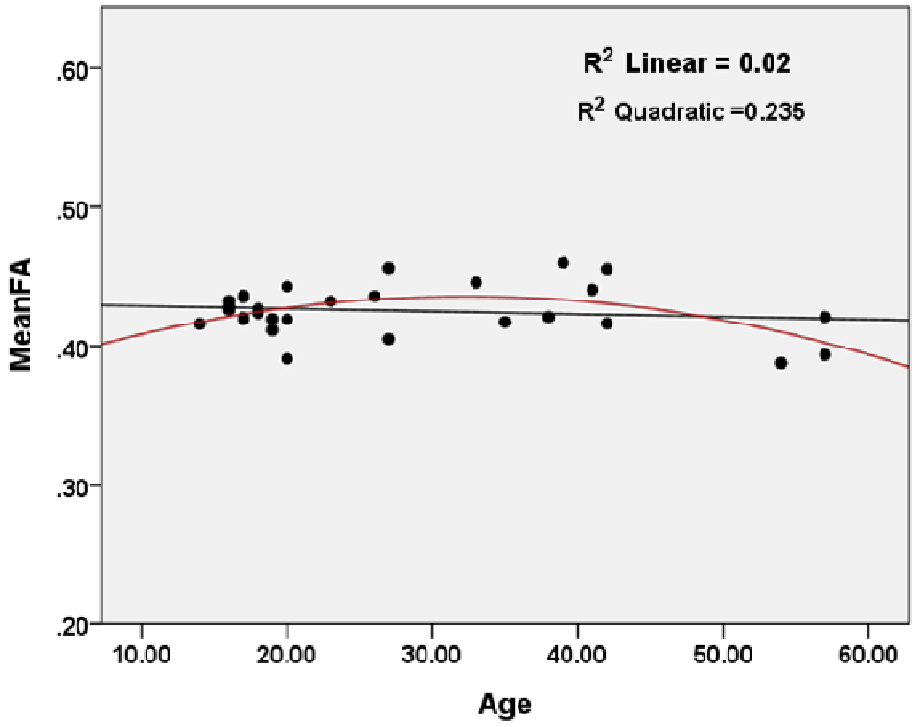

Figure 5.13: Correlations between age and whole brain skeletonized FA for single-shot chimpanzees. Red line indicated linear fitting and black line indicated curvilinear fitting. Curvilinear regression better fits the data compared to linear regression (r^2= 0.235, p= 0.067)

Skeleton-based ROI analysis results are as follows: genu and splenium FA show a non-significant negative correlation with age, whereas rostral body, anterior mid body and posterior mid body shows a non-significant positive correlation with age. Isthmus is the only region that showed a significant positive correlation with age. These results are in contrast to the overall TBSS results and also to the results from the multi-shot data, in which there were only positive correlations with age.

Macaques: The voxel-wise correlations for macaques showed no significant correlations at a corrected threshold. However, when thresholded very liberally at $p<0.05$ uncorrected for multiple comparisons, widespread negative correlations were found between age and FA. Consistent with the corpus callosum ROI analysis, only AD showed significant age related decreases within most of the major white matter tracts. An example of the fiber tract showing this pattern is labeled in figure 5.15. No significant positive correlations with age were observed for any of the DTI indices.

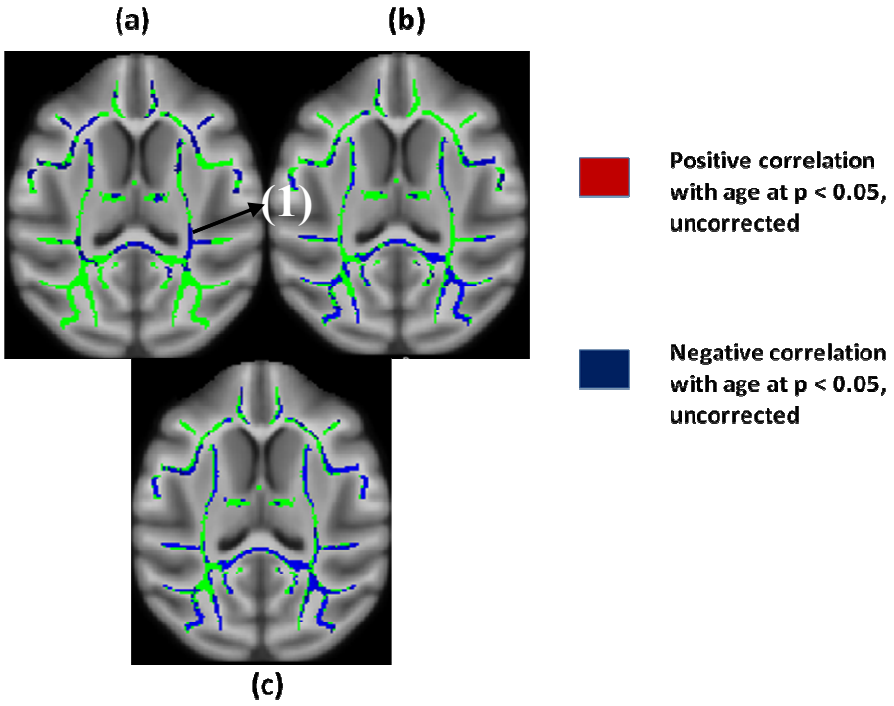

Figure 5.14: Voxel wise correlations between age and a) FA, b) ADC, and c) AD for macaques. Voxels colored red show positive correlations with age and voxels colored blue show negative correlations with age. Pattern of age-associated decrease in AD is labeled as (1)

5.4 Discussion

Results from the above section will be discussed in two parts: First, the multi-shot results for chimpanzees will be discussed and compared with humans and macaques results. Different possible neurobiological interpretations based on those results will be presented. Second, the differences in single-shot and multi-shot results for chimpanzees will be discussed and future directions will be proposed.

Multi-shot results: Age-related changes in white matter microstructure in chimpanzees and macaques using DTI are measured using different methods, and compared with previous findings in humans. The main finding is that, in stark contrast to humans, who exhibit marked age-related FA decreases and ADC increases, white matter FA did not decrease, and in many regions increased or did not change, with age in chimpanzees. The diffusivity measures (AD and RD) either decreased or did not change with age. Also, macaques did not show significant age-related changes in DTI metrics at standard statistical thresholds, although when liberal statistical thresholds were adopted, age-related decreases in white matter FA were observed and these were accompanied by decreases in AD.

Human aging involves both macrostructural and microstructural white matter changes. Most studies show that declines in gray and white matter volume begin in early adulthood (Blatter, Bigler et al. 1995; Raz, Gunning et al. 1997; Salat, Kaye et al. 1999; Bartzokis, Beckson et al. 2001; Sullivan, Rosenbloom et al. 2004), whereas a few others suggest that white matter volume is relatively stable until age 70 and rapidly declines thereafter (Salat,

Kaye et al. 1999; Raz, Lindenberger et al. 2005). White matter FA is relatively stable until about age 30 and then decreases (Peters 2002; Pfefferbaum and Sullivan 2003; Peters and Sethares 2004; Sullivan and Pfefferbaum 2006; Westlye, Walhovd et al. 2010). Age-related changes in FA are often attributed to changes in microstructural features such as fiber density (Pierpaoli, Jezzard et al. 1996; Beaulieu 2002; Shenkin, Bastin et al. 2003) and myelination (Pfefferbaum and Sullivan 2003; Buchel, Raedler et al. 2004). In humans, decreases in FA are accompanied by increases in RD. Age-related changes in AD have also been reported, though the direction of these changes varies across pathways and the magnitude is smaller than for RD (Bhagat and Beaulieu 2004; Sullivan and Pfefferbaum 2006; Zhang, Du et al. 2008; Madden, Bennett et al. 2009; Zahr, Rohlfing et al. 2009; Bennett, Madden et al. 2010).

White Matter Tract	FA	ADC	AD	RD
Cortico- Spinal System (L,R)	↑	↓	↓	↓
Anterior and Posterior limbs of Internal Capsule (L,R)	↑	↓	↓	↓
Genu of Corpus Callosum	↑	↓	↓	↓
Uncinate Fasciculus(L,R)	↑	↓	↓	↓
Extreme Capsule(L,R)	↑	↓	↓	↓
Arcuate Fasciculus(L,R)	↑	↓	↓	↓
Splenium of Corpus Callosum	↑	↓	↓	↓
Anterior Pericallosal white matter(L,R)	↑	↓	—	↓
Inferior Longitudinal Fasciculus(L,R)	↑	↓	—	↓

Table 5.1: Age-related increases in FA were associated with one of the two patterns of decreases in diffusivity measures for different white matter tracts of chimpanzees. ↑, ↓ indicates an age-related increase and decrease respectively. L, R indicates that the correlation is significant in both the left and right hemispheres of the brain for that specific tract

Animal studies suggest that increases in RD are due to de-myelination (Song, Sun et al. 2002; Nair, Tanahashi et al. 2005), whereas decreases in AD are related to decreases in fiber density (Song, Sun et al. 2003). In contrast to what has been observed in humans, we find here that chimpanzees show age-related increases in FA and associated decreases in ADC, RD, and AD in most of the major white matter tracts (Table 5.1).

Although imaging results alone cannot definitively establish the microstructural basis of these age-related changes in diffusion, the combination of decreases in both RD and AD raises the possibility that although fiber density decreases with age, chimpanzees continue to accumulate myelin into old age. Indeed, continued myelin production is observed in some older monkeys (Peters, Moss et al. 2001), which may be a compensatory mechanism for myelin degeneration. Based on the multi-shot results, it might be that myelination outpaces degeneration in chimpanzees, whereas the opposite is true of humans and macaques.

On current evidence, major age-related neurodegenerative diseases like Alzheimer's disease and Parkinson`s disease appear to be largely or exclusively human-specific (Gerlach and Riederer 1996; Nelson, Stefansson et al. 1996; Cork and Walker 1999). Non-human primates show some aspects of these diseases (Cork, Walker et al. 1989; Schultz, Dehghani et al. 2000), but do not readily develop the full neuropathological, behavioral or clinical phenotypes seen in humans (Walker and Cork 1999). Neurofibrillary tangles and some beta amyloid accumulation have been described in an aged chimpanzee and tangles were indistinguishable at the ultrastructural level from

those occurring in humans with Alzheimer`s disease (Rosen, Farberg et al. 2008), but this animal had a tauopathy rather than Alzheimer's; no cases of Alzheimer's in chimpanzees have been reported so far. Rhesus macaques develop beta amyloid plaques liked aged humans (Gearing, Tigges et al. 1996), but neurofibrillary tangles, a very common Alzheimer`s pathology, are not present (Nelson, Stefansson et al. 1996).

In humans, several studies have shown a significant correlation between cognitive decline and decreases in white matter microstructural integrity with age (Sullivan and Pfefferbaum 2006; Madden, Bennett et al. 2009; Zahr, Rohlfing et al. 2009; Sullivan, Rohlfing et al. 2010). Rhesus macaques exhibit age-related cognitive deficits in attention shifting and working memory that are also observed in humans (Herndon, Moss et al. 1997; Moss, Herndon et al. 1998; Voytko 1998; Voytko 2000; Voytko 2002; Moore, Killiany et al. 2003; Voytko and Tinkler 2004; Makris, Papadimitriou et al. 2007). Age-related declines in motor function and activity level (Moscrip, Ingram et al. 2000; Zhang, Andersen et al. 2000; Lacreuse and Herndon 2003) observed in rhesus macaques also mirror human aging. On the other hand, very few studies have looked at the age-related cognitive decline in chimpanzees. While older monkeys suffer performance decrements in the delayed recognition task, older chimpanzees perform at levels comparable to younger adults, suggesting resistance to age-related cognitive decline (Riopelle and Rogers 1969). Thus, at this time, limited evidence suggests that chimpanzees may not suffer cognitive decline with aging to the same extent that monkeys and humans do. If these trends are supported by future studies of cognitive aging in chimpanzees, then our multi-shot data suggest that chimpanzees may avoid cognitive decline by maintaining the

health of their white matter. Chimpanzees might thus serve as a valuable model for understanding healthy brain aging.

Human life expectancy is significantly longer than that of chimpanzees, even in traditional foraging societies that lack the healthcare of modern civilization (Hawkes, O'Connell et al. 1998; Hawkes 2004; Hawkes, Smith et al. 2009; Herndon and Walker 2010). Whereas chimpanzees can live into their 40s in the wild (Thompson, Jones et al. 2007) and up to age 59 in captivity (Herndon, Tigges et al. 1999), humans can live to age 80 in hunter-gatherer societies (Blurton Jones, Hawkes et al. 2002) and in excess of 100 years in industrialized societies. How should we compare the ages of humans and chimpanzees? If we assume—as we have in arguing that chimpanzees preserve white matter health with age—that human lifespan is a stretched-out version of chimpanzee lifespan, we would conclude (following a 6:10 rule, based on the numbers cited above), that a 50-year-old chimpanzee would be approximately equivalent in age to an 83-year-old human. Alternatively, however, one might argue that the appropriate comparison is between chimpanzees and humans of the same absolute age. In that case chimpanzees might fail to show age-related declines in FA similar to humans simply because they do not live long enough (in absolute terms). This is not a plausible explanation for differences in brain aging, however, because age-related decline in human FA values begins at age 30 (Westlye, Walhovd et al. 2010), whereas the old chimpanzees in our sample (ages 40—54) have yet to experience a decline in white matter FA. We cannot currently exclude the possibility that our results are driven by a "cohort" effect that

influences white matter integrity differentially for different age cohorts. Longitudinal studies are planned to distinguish between true biological changes and cohort effects.

Thus, our multi-shot results suggest that chimpanzee white matter ages more slowly, in absolute terms, than human white matter. However, given that chimpanzees die at a younger age than humans, some physiological systems must age more rapidly. This is not the case for the reproductive system, as chimpanzee and human females undergo similar age-related changes in reproductive cycles (Walker and Herndon 2008), ovarian follicle depletion (Jones, Walker et al. 2007), and fertility (Allen, Bruss et al. 2005; Lacreuse, Chennareddi et al. 2008; Herndon 2010). One system that may age more quickly in chimpanzees is the cardiovascular system, since heart disease was found to be the most common cause of death in captive chimpanzees, although the pathogenesis of heart disease appears to be different in chimpanzees and humans (Varki, Anderson et al. 2009).

Both the corpus callosum ROI analysis and the voxel-wise analysis using TBSS showed an age-related increase in FA in chimpanzees and associated decreases in, RD, sometimes accompanied by lesser decreases in AD. These results are different than what has been reported in humans, where FA decreases and diffusivity increases with age. Macaques in our study showed a modest decrease in FA compared to humans. The slope of the FA decrease within the corpus callosum is less steep for macaques (0.6 percent /year) compared to humans (1.7 percent/year). In other words, humans show a significant difference in FA when older individuals are compared to younger ones, which is not true

in macaques. On the other hand, AD decreased with age in macaques, with no change in RD. Also, the sample size of macaques (n=24) is small and not uniformly distributed across different age ranges (young macaques (n=9), old macaques (n=15)) compared to human data in the literature. This could explain the lower level of significance in macaques. The cellular significance of these changes in diffusion metrics with age across species can be interpreted as follows: at the micro-structural level, humans might be demyelinating (increase in RD), resulting in an overall decrease in FA and increase in ADC with age. Changes in AD may be related to changes in fiber density, but the direction of these changes varies across fiber tracts in humans. On the other hand, chimpanzees might be both adding myelin and losing fibers (decreases in both AD and RD, and hence ADC), resulting in no change or an overall increase in FA. Macaques results could reflect a decrease in fiber density (decreases in AD) with no significant change in the myelin content (no change in RD), resulting in a slight or non-significant decline in FA. Across all species, age-related changes in FA were more influenced by changes in RD than AD. These patterns are summarized in Figure 5.16. More generally, the age-related changes in the DTI metrics are different across three species, with humans showing more extreme degenerative changes compared with either chimpanzees or macaques.

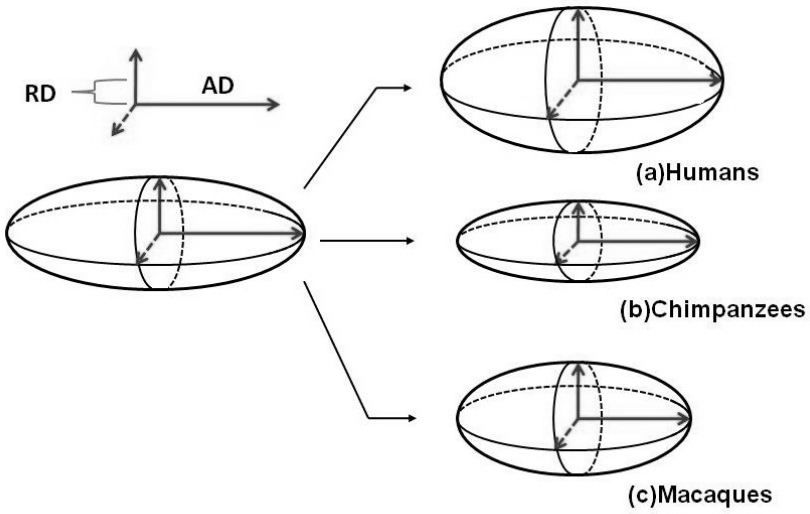

Figure 5.15: Age-related changes in the size of the diffusion ellipsoid associated with the changes in AD and RD for a) humans, b) chimpanzees, and c) macaques

Though speculative, we suggest that these changes in diffusivity may reflect age-related increases in myelination that outpace myelin degeneration in chimpanzees and age-related decreases in axonal fiber density in macaques. This noteworthy species difference may help to explain why humans are more susceptible to neurodegenerative diseases than chimpanzees and macaques, and demonstrates the need for complementary histological studies of white matter microstructure in humans, chimpanzees and macaques to clarify the cellular and molecular bases of our findings.

Multi-shot data vs. Single-shot data validation tests for chimpanzees: Geometric distortion due to magnetic susceptibilities is severe in chimpanzees due to their complicated sinus anatomy and large air-tissue interfaces. In order to reduce the amount of spatial distortion, DWI images were acquired using segmented EPI. However, segmented EPI is sensitive to motion induced ghosting. Motion can arise from bulk head

movements or from involuntary cardiac pulsations and respiratory function (Le and Hu 1996). Segmented ghosting was present in both chimpanzee and macaque DWI images. This ghosting could potentially influence DTI calculations, especially in chimpanzees where the ghosting was more severe. The amount of ghosting was negatively correlated with both age ($r=-.81$, $p=0.001$) and weight ($r=-.63$, $p=0.01$) in chimpanzees. There was also a trend for ghosting to decrease with age in macaques ($r=-.23$, $p=0.09$). Given this age-related pattern, an important point that should be considered before drawing any conclusions is the potential effect of ghosting on the DTI indices and their age-related changes in chimpanzees. Underestimation of FA due to high levels of ghosting in younger chimps could potentially be driving the overall increase in FA with age. FA simulation tests under the influence of ghosting (discussed in chapter 4) were conducted to evaluate ghosting as a potential confound driving age-related increases in FA. Results show a considerable effect of ghosting on FA and suggest that our findings/interpretations based on multi-shot results are more likely to be influenced by ghosting and its effects. The single-shot data acquired on a subset ($n=30$) of chimpanzees from the same group show a different trend compared to the multi-shot results (ROI and TBSS analysis results for the single-shot data are provided in the results section). Single-shot data was tested and is believed to be of superior quality compared to multi-shot data, and most importantly, devoid of ghosting artifact, providing unbiased FA values. A validation test was conducted to see if this age-related decline in FA, which was contrary to what was found with the multi-shot data is cohort-dependent. TBSS age-related analysis was conducted on the multi-shot data of the same set of 30 chimps and compared with the single-shot results.

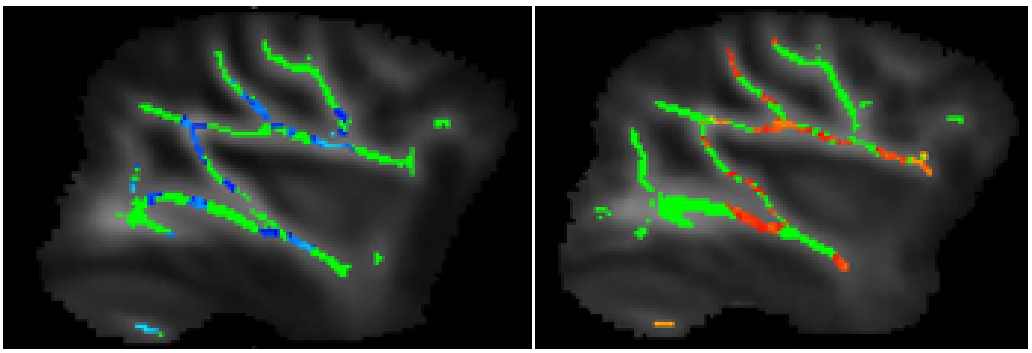

Figure 5:16: TBSS related analysis results for the same set of 30 chimps scanned with multi-shot (left) and single-shot (right) sequences. Voxels colored in blue indicate non-significant positive correlations with age and voxels colored in red indicate non-significant negative correlations with age

There were no significant positive or negative correlations between FA and age at the p=0.05 level, after multiple comparisons correction. In contrast to the multi-shot results, there were negative correlations between FA and age at the p=0.05 level before correction. There were very few significant negative correlations between age and FA before correction. In short, the same set of 30 chimps scanned with the multi-shot sequence and the single-shot sequence showed opposite trends in age-related changes in FA invalidating the multi-shot results. Whole brain voxel-wise comparisons between multi-shot and single-shot data for the same set of 30 chimps were performed to test for differences in the magnitude of FA between the two sequences. A two-sample paired t-test was conducted using TBSS.

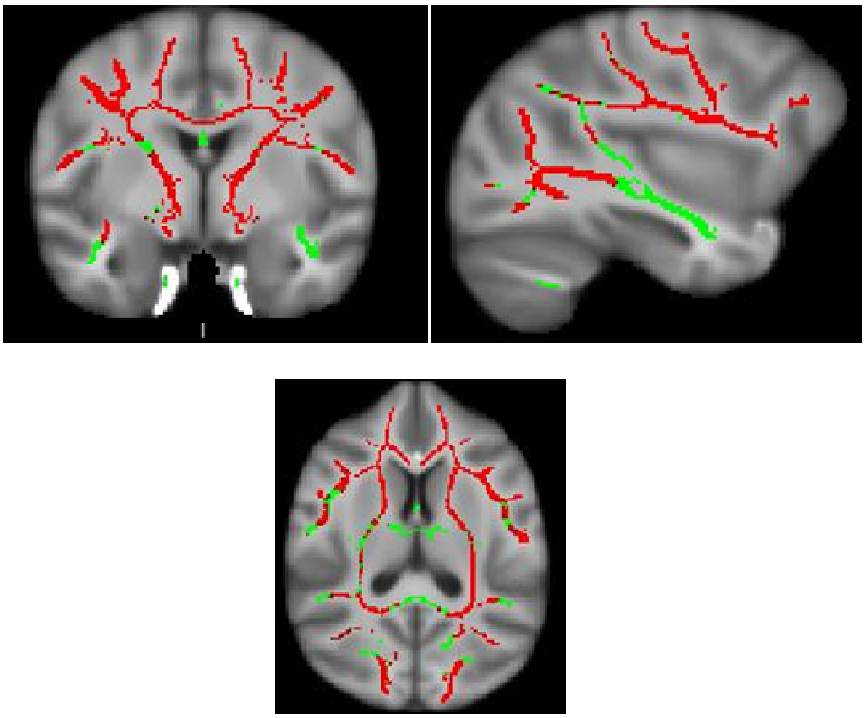

Figure 5.17: Multi-shot vs. single-shot paired t-test analysis using TBSS. Voxels colored in red indicate significant multi-shot FA greater than single-shot FA and voxels colored in blue indicate significant single-shot FA greater than multi-shot FA

There were no voxels showing significant single-shot greater than multi-shot differences, but suprisingly there were many white matter tracts throughout the brain showing higher FA in the multi-shot data. In reality, if there is an effect of ghosting on FA, we would expect to observe the opposite pattern: single-shot FA greater than multi-shot FA. However, the trend here is significantly opposite. An important point to note is that there were very few or no single-shot greater than multi-shot voxels throughout the brain. This can be due the correction employed to remove the effect of ignoring cross-terms in the b-matrix in multi-shot data. If anything, this correction will increase the FA values of the multi-shot data and it is odd that the FA values are increased throughout the brain after correction. Also, there might be an effect of excessive susceptibility-induced distortion correction in single-shot chimps. In general, spatial distortion due to magnetic

susceptibility is large in single-shot data and requires intensive correction to reduce its effect. This step causes additional blurring of the data, which might influence the FA values. The differences in the FA values and the presence of residual FA in the multi-shot phantom data (discussed in chapte 4) can explain this difference. These hypotheses are very preliminary and need to be further explored in the future.

In summary, the results from the single-shot data analyses indicate that there is an opposite trend in the age-related changes of FA compared to the multi-shot results. Further, the magnitude of FA in the single-shot data is significantly lower compared to the multi-shot FA. This should not affect the age-related results, but is an important issue to address accepting the efficacy of the single-shot data. The final conclusion for this section is two-fold: First, since the single-shot data proved to be more accurate and of better quality compared to multi-shot data in this data set, the results from multi-shot data are invalidated. Consequently, the neurobiological interpretations provided in this discussion based on the multi-shot data are subject to change. Second, the accuracy of the single-shot data, more specifically the difference in the magnitude of FA compared to multi-shot data, should be addressed and more validation tests are needed to verify this.

Chapter 6

DTI and Comparative White Matter Hemispheric asymmetries

6.1 Outline

Most MRI studies investigating white matter asymmetries in the human brain have been conducted on T1-weighted images (Good, Johnsrude et al. 2001; Watkins, Paus et al. 2001). Diffusion tensor imaging derived metrics like FA, AD and RD provide more subtle information about the white matter microstructure (Basser 1995) compared to the signal intensity on the T1-weighted images. Diffusion MRI data acquired from chimpanzees were used to compare the magnitude of white matter microstructural asymmetries between humans, chimpanzees, and macaques. First, the multi-shot data of chimpanzees is analyzed and the results are compared with humans and macaques. Second, the single-shot data results for chimpanzees are presented and compared with the multi-shot results.

6.2 Method

TBSS asymmetry analysis: Voxel-wise statistics were carried out using Tract Based Spatial Statistics (TBSS) implemented in FSL 4.1 (FMRIB, Oxford. http://www.fmrib.ox.ac.uk/fsl/). TBSS is considered to be an observer-independent sensitive tool for generating the voxelwise analysis of white matter microstructure (Smith, Jenkinson et al. 2006). Compared to other voxel-based morphometry (VBM) style approaches, TBSS has the advantage of reducing the misalignment between the subjects as well as avoiding the use of arbitrary smoothing kernels when generating the

statistics. The first step in the TBSS analysis was to non-linearly register all the subjects' FA images to a population-specific FA template derived from the same group of subjects. Non-linear registration is required to ensure accurate registration between different brains and their respective hemispheres, and was implemented using FNIRT in the FSL package. Second, all the registered images were averaged to create a mean FA image and a subsequent mean FA skeleton, which is an average representation of the centers of all the common tracts. A symmetrical FA skeleton is created by averaging the skeleton with its mirror image and including overlapping voxels which had one to one correspondence between the left and right sides of the brain, (Smith, Jenkinson et al. 2006). Next, all the subjects' FA images were projected onto the symmetrical mean FA skeleton by filling the skeleton with FA values from the nearest relevant tract center. Lastly, a left-right difference FA image is created for each subject and compared with zero using a permutation based one-sample t-test with a p-value < 0.01, corrected for multiple comparisons. Five thousand random permutations were used for generating the statistics using the randomize tool, implemented in FSL. TBSS was also applied to the non-FA images (AD and RD) generated from the diffusion tensor. First, the non-linear transformations that were derived by registering the FA images to the template were applied to the non-FA images. Next, the transformed non-FA images were projected onto the symmetrical mean FA skeleton used in the FA analysis using the same skeleton projection vectors. The resulting skeletonized non-FA images were used for the voxel-wise statistics.

Voxel-based morphometry (VBM) analysis: White matter volume asymmetry analysis was carried out using VBM analysis implemented in FSL 4.1 (FMRIB, Oxford. http://www.fmrib.ox.ac.uk/fsl/). In the first step, T1-weighted images were segmented to white, gray, and CSF partial volume maps using FAST, FMRIB`S automated segmentation tool (http://www.fmrib.ox.ac.uk/fsl/fast4/) (Zhang, Brady et al. 2001). Next, segmented white matter maps and their left-right flipped versions were used to generate a symmetrical white matter template. Once the symmetrical template was derived, the original white matter maps and their flipped versions were registered to the template using FNIRT, implemented in the FSL package. Last, a permutation-based paired t-test (Corrected for multiple comparisons) was performed on the registered white matter maps to determine left-right differences.

6.3 Results

In humans, TBSS revealed widespread leftward (left>right) asymmetries in white matter FA, with minimal rightward asymmetries. Although patterns of white matter FA asymmetries are very similar in chimpanzees and macaques, both differed from humans. Chimps and macaques had similar amounts of leftward and rightward asymmetries rather than the strong leftward bias found in humans. Results showing the general pattern of asymmetries for humans, chimpanzees, and macaques are presented in figures 6.1(a), 6.1(b) and 6.1(c) respectively. Results are significant at $p < 0.01$ and are corrected for multiple comparisons.

The total number of skeleton voxels that showed significant asymmetry was measured as a percentage of the total number voxels in the skeleton for all species. The results are summarized in the figure below. There is an obvious left-ward bias in humans compared to chimpanzees and macaques. The total percentage of skeleton voxels with asymmetry is lower for humans because the total number of voxels within the skeleton itself is nearly twice as large compared to other species.

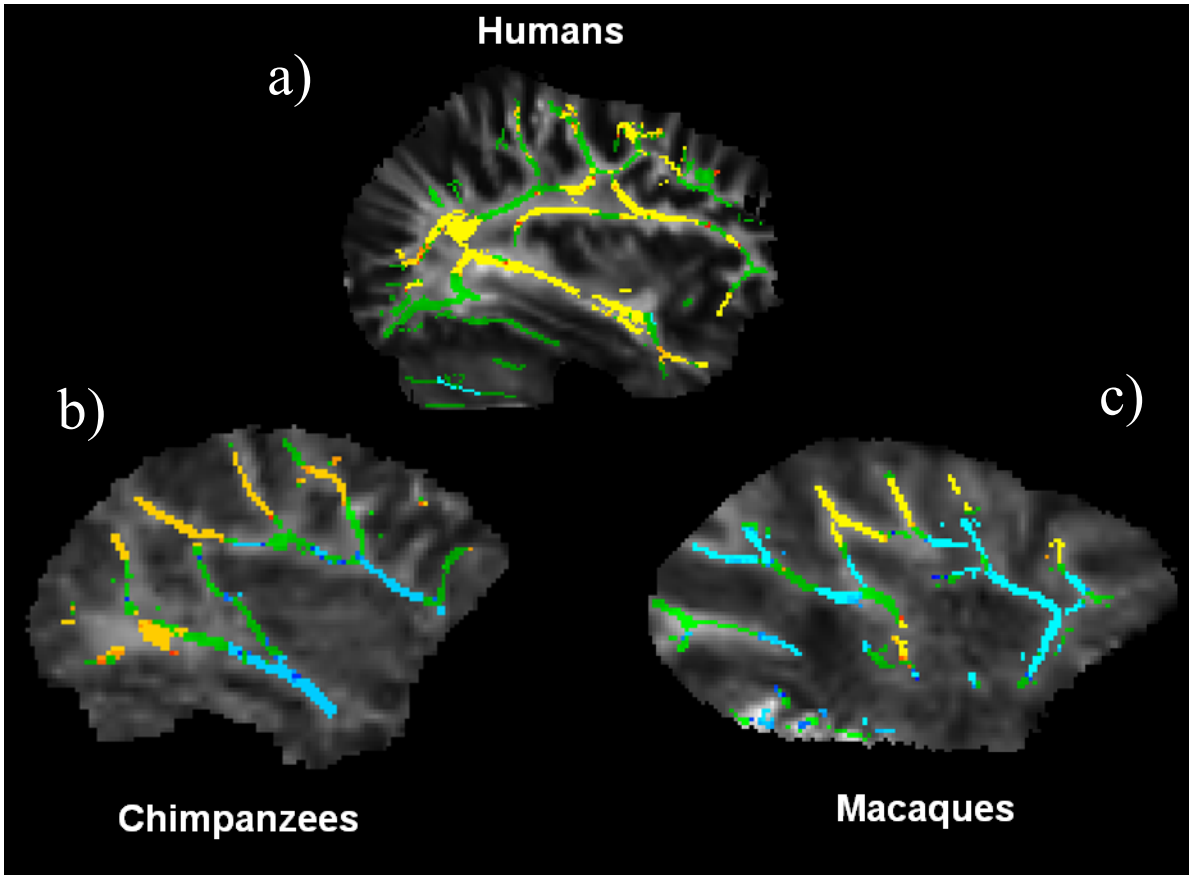

Figure 6.1: Significant L-R differences in FA for a) humans, b) chimpanzees, and c) macaques. Voxels colored yellow show leftward asymmetry and voxels colored blue show rightward asymmetry. Results are significant at $p<0.01$, corrected for multiple comparisons

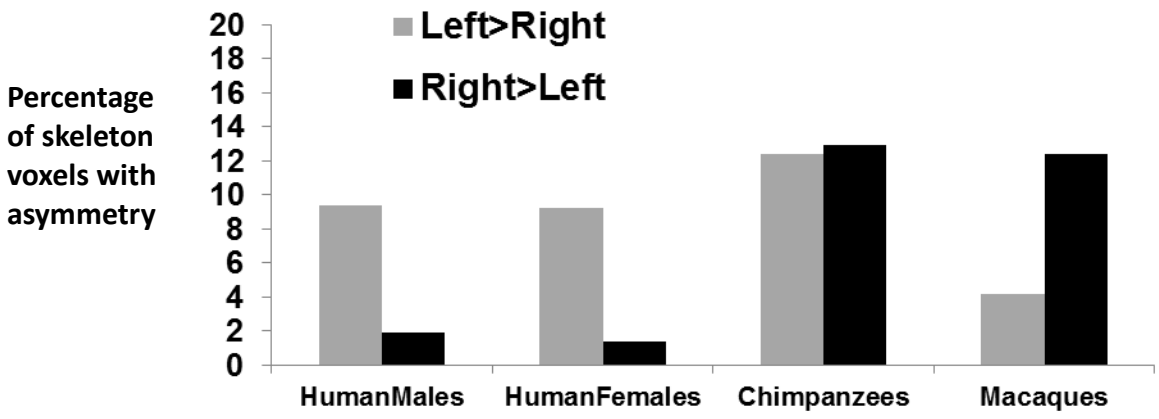

Figure 6.2: Figure illustrating the number of voxels with asymmetry as a percentage of total number of skeleton voxels

Asymmetries across different major white matter tracts: The pattern of asymmetries across different major white matter tracts are summarized in the table below.

Table 6.1: Pattern of asymmetries across some of the major white matter tracts

White matter tract	Humans	Chimpanzees	Macaques
Arcuate fasiculus and SLF	L	Mixed	Mixed
Corticospinal tract system	L	L	L=R
Inf. longitudinal fasciculus	L	R	R
Uncinate fasciculus	Mixed	R	R
Cingulum bundle	L	L	L

Association tracts such as the superior longitudinal fasciculus (SLF), inferior longitudinal fasciculus (ILF), and arcuate fasciculus (AF) show significant leftward asymmetry in humans and mixed/mostly rightward asymmetry in chimpanzees and macaques. The uncinate fasciculus shows a mixed asymmetry in humans and a rightward asymmetry in other species. The cingulum bundle is the only tract that showed leftward bias in FA for all the species. The influence of AD and RD on the FA asymmetry is shown for different tracts in figure 6.3.

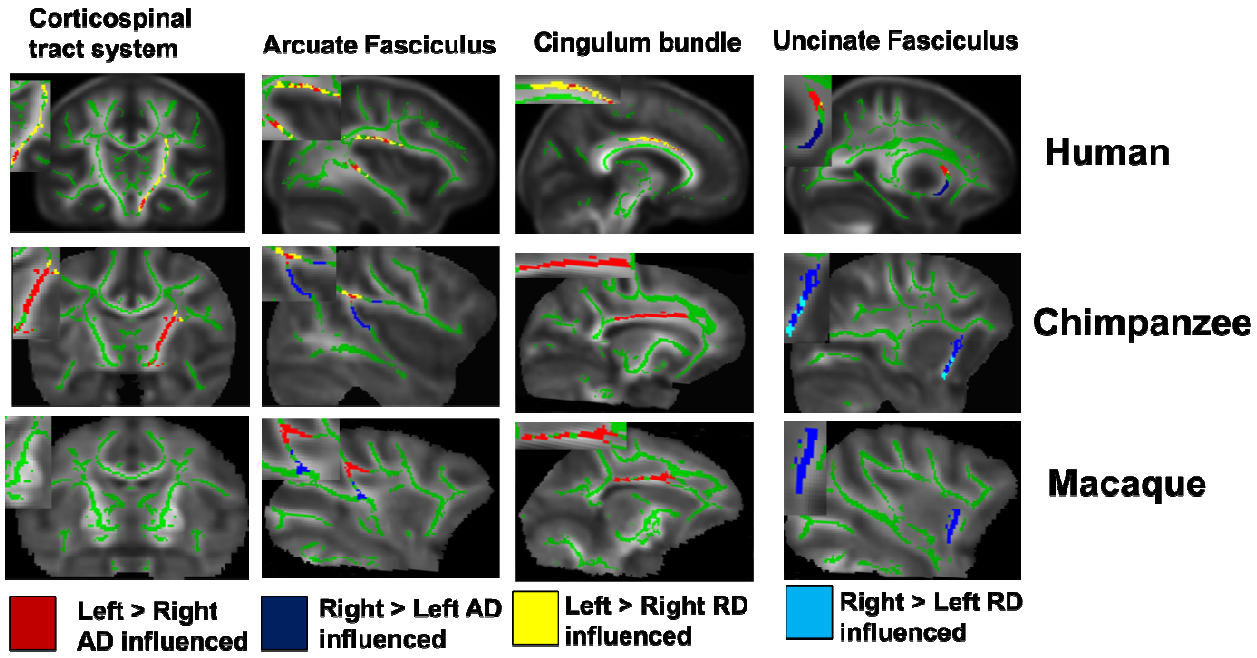

Figure 6.3: Influence of AD and RD on FA asymmetry for different white matter tracts

These maps are derived by masking the AD and RD TBSS voxel-wise results with the FA asymmetry map ($p<0.01$) and in the next step, an AD-RD difference map is created from the masked voxels. If the magnitude of AD-RD map is positive, the FA asymmetry at that particular region of interest is AD driven and vice-versa. For humans, the majority

of the leftward asymmetry in FA is RD driven. For chimpanzees and macaques, the mixed asymmetry in FA is mainly driven by AD.

Chimpanzee single-shot data results: TBSS asymmetry analysis conducted on the chimpanzee single-shot data (n=30) shows a mixed asymmetry similar to the multi-shot results. The percentage of skeleton voxels with asymmetry is compared between the multi-shot and the single-shot results.

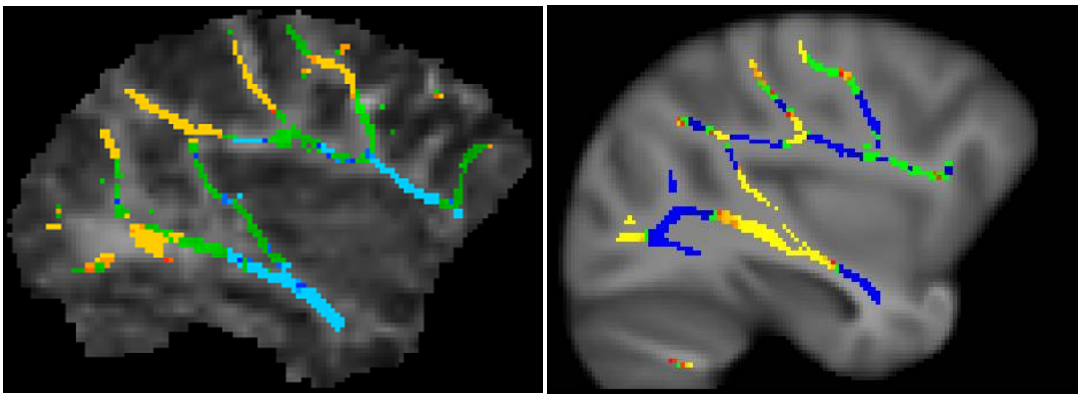

Figure 6.4: TBSS asymmetry results for the 30 chimpanzees acquired using single-shot sequence (right). There is mixed asymmetry in FA similar to the multi-shot results (left). Voxels colored yellow show leftward asymmetry and voxels colored blue show rightward asymmetry. Results are significant at $p<0.01$, corrected for multiple comparisons

The percentage of skeleton voxels with asymmetry is compared between the multi-shot and the single-shot results below. Even though there is similar percentage of mixed asymmetry in the multi-shot results and the single-shot results (n=30), the regions with a specific pattern of asymmetry significantly differed. The pattern of asymmetry in the updated single-shot results differed markedly from the human results

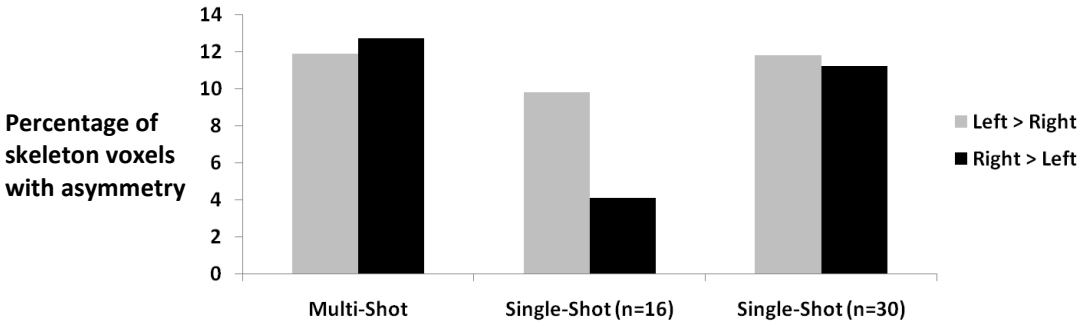

Figure 6.5: Percentage of skeleton voxels with asymmetry between multi-shot (n=36), single-shot (n=16), and single-shot (n=30) results

Voxel-based morphometry (VBM) results: VBM results show a significant left ward asymmetry ($p<0.01$) at the hook of arcuate fasciculus for all three species

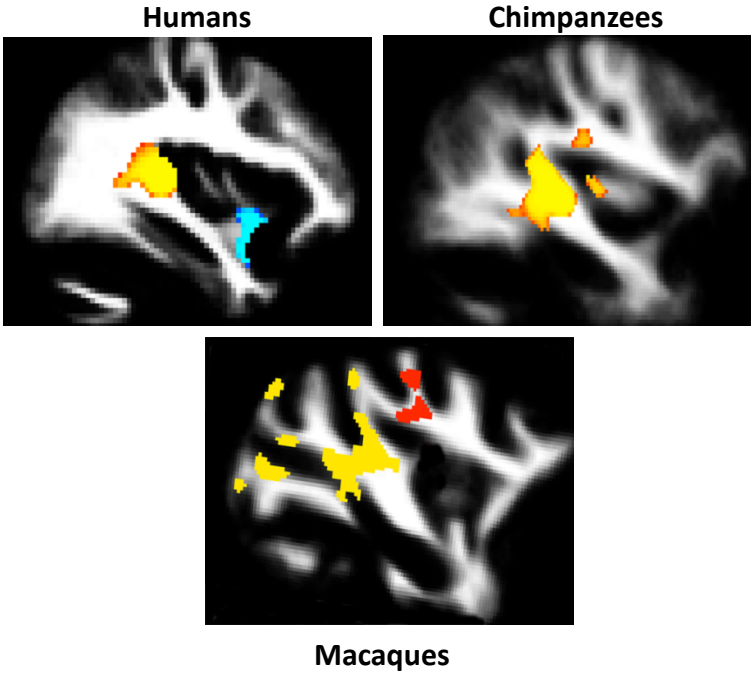

Figure 6.6: White matter volume asymmetry for all three species. Voxels colored in red-yellow indicate leftward asymmetry and voxels colored in blue-light blue indicate rightward asymmetry

In chimpanzees and macaques, leftward volumetric asymmetries are also found in the region of superior longitudinal fasciculus. Significant rightward asymmetries are found in the uncinate region for humans, similar to the TBSS results.

6.4 Discussion

Results from the above section will be discussed in two parts: First, the discussion will be focused on comparing the multi-shot results for chimpanzees with humans and macaques results. Second, the differences in single-shot and multi-shot results for chimpanzees will be discussed and future directions will be proposed.

Multi-shot results: Hemispheric asymmetry in white matter microstructure and white matter volume in humans, chimpanzees, and macaques were measured and compared. The main finding is that humans exhibit marked leftward FA asymmetry, whereas, chimpanzees and macaques show a mixed FA asymmetry. Further, VBM analysis looking at the white matter volumetric asymmetries shows a significant leftward asymmetry for all the species near the hook of arcuate fasciculus.

The human brain has undergone a significant change in size and organization throughout human evolution. Humans have always been thought to exhibit greater hemispheric asymmetry and hence greater lateralization of function, compared to our closest living primate relatives(Sherwood, Subiaul et al. 2008) . Attempts have been made to link the cognitive and behavioral specializations of human brain with its structural hemispheric asymmetries(Geschwind and Levitsky 1968). The human brain displays strong leftward dominance for language functions, and asymmetries have been described and in the two classic language areas: Broca's and Wernicke's areas (Keller, Roberts et al. 2009; Schenker, Hopkins et al. 2010). Some of the cortical areas associated with language function also display asymmetries in great apes. The sulci within the inferior frontal

cortex, which contains the Broca'a area, showed a leftward asymmetry in depth and length in chimpanzees, bonobos, and gorillas (Cantalupo and Hopkins 2001). The location of the Brodmann's areas corresponding to Broca's area vary extensively, relative to the sulcal borders in both humans (Amunts, Schleicher et al. 2003) and chimpanzees (Sherwood, Broadfield et al. 2003). It has also been shown that a population level asymmetry is shared by humans and great apes with respect to planum temporale and area Tpt, two major components of Wernicke`s area. It yet remains to be determined how these gross asymmetries relate to the underlying neural organization of the tissue.

Most of the studies discussed above have compared macrostructural asymmetries between humans and their closest-relative living species, but recently, a human specific microstructural asymmetry has been identified in the PT that is absent in both chimpanzees and rhesus macaques. A similar asymmetry was also observed in Broca's area (Brodmann areas 44 and 45)(Amunts, Schleicher et al. 2003), primary motor cortex hand area (Amunts, Schmidt-Passos et al. 1997), as well as primary visual cortex and extrastriate areas(Amunts, Armstrong et al. 2007). Specifically, humans possess a leftward asymmetry in the width of the minicolumns and neuropil space in these regions. This suggests that the microstructural asymmetries are human specific and possibly relevant in explaining human cognitive specializations.

Results from the voxel-wise analysis showed a marked leftward asymmetry in FA for humans, whereas, chimpanzees and macaques had no distinct bias. On the other hand, volumetric asymmetries are consistently left-ward biased in superior longitudinal

fasciculus, hook of arcuate fasciculus, and middle longitudinal fasciculus across all the species. The white matter volume corresponding to the hook of the arcuate fasciculus is leftward biased for humans, chimpanzees, and macaques. This region is just caudal to the planum temporale, a region widely studied and shown to be leftward asymmetric in terms of volume in both humans and great apes. In contrast to the volumetric asymmetries, TBSS results show a significant leftward asymmetry in this region only for humans. These results suggest that leftward asymmetries in white matter volume are not uniquely human and are therefore not likely relevant to explaining human cognitive specializations. On the other hand, TBSS results show that leftward asymmetries in white matter FA, believed to index myelination or fiber density, are more pronounced in humans and may therefore be more directly relevant to human cognitive specializations.

Multi-shot vs. single-shot analysis in chimpanzees: In order to evaluate the influence of ghosting and its effect on multi-shot data, a validation test was performed by dividing the total number of chimps (n=36) into three equal groups.

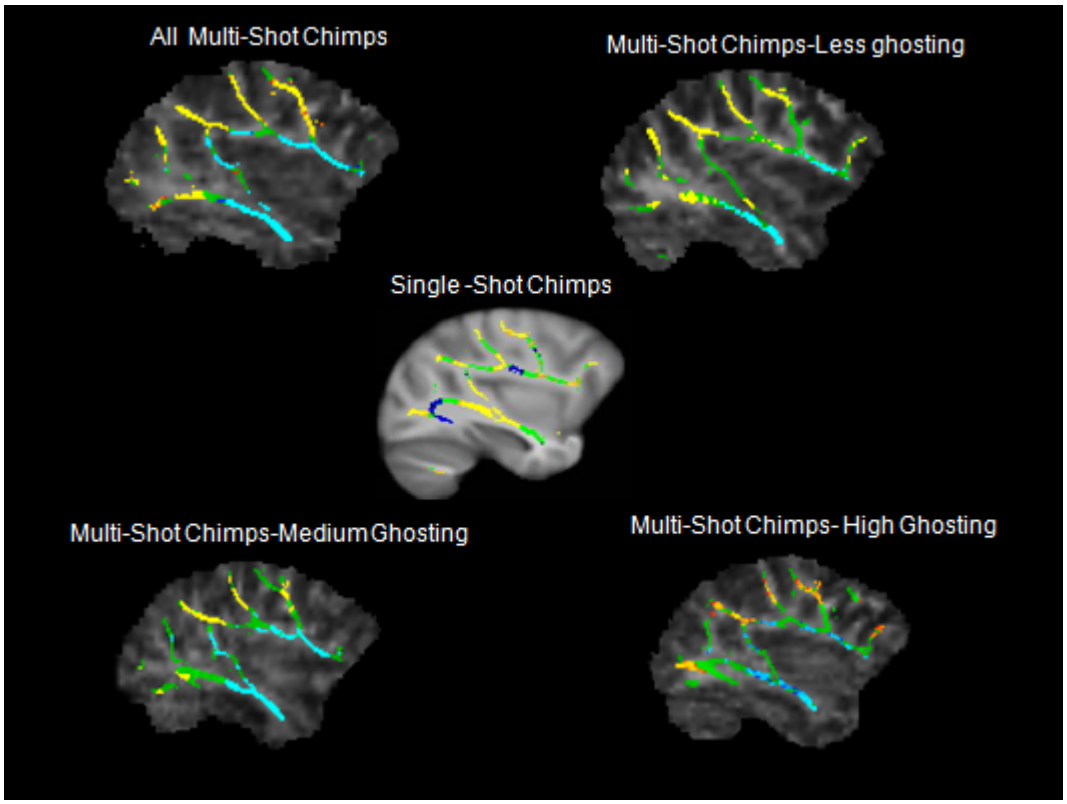

Figure 6.7: TBSS asymmetry results for three groups of chimpanzees divided based on their levels of ghosting. Voxels colored yellow show leftward asymmetry and voxels colored blue show rightward asymmetry. Results are significant at $p<0.01$, corrected for multiple comparisons. Single-shot results were also shown for comparison.

Division was made based on the magnitude of ghosting calculated by the method proposed in the ghosting simulation studies section. TBSS asymmetry results showed a mixed pattern for the groups categorized as medium and high ghosting, but chimps with low ghosting showed a stronger leftward bias compared to the other groups. The regions that showed leftward asymmetry for single-shot chimps and for the chimps with low ghosting levels are very different. White matter corresponding to the pre-central sulcus is the only region that showed significant leftward asymmetry in both the analyses. Also, all the chimps with less ghosting are under the old age group, so there could an effect of aging contributing to this difference.

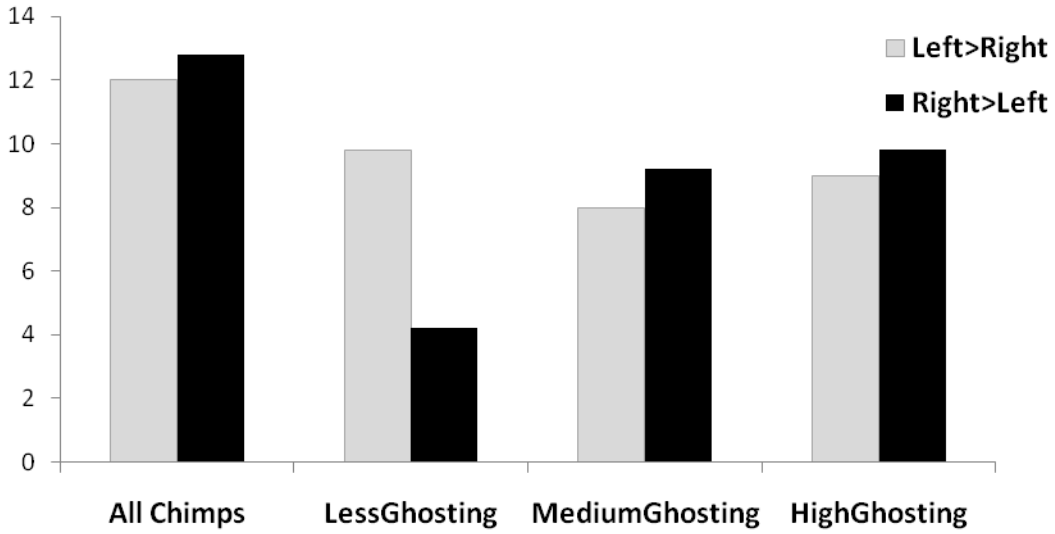

Figure 6.8: Figure illustrating the number of voxels with asymmetry as a percentage of total number of skeleton voxels for different chimps groups divided based on their levels of ghosting. They are also compared to the results for all the multi-shot chimps

In summary, the results from the single-shot data asymmetry analysis indicate a mixed hemispheric asymmetry in chimpanzees, dissimilar to human results. Further, there are a few regions that showed a significant leftward bias in chimpanzees using single-shot data that matched with the human results.

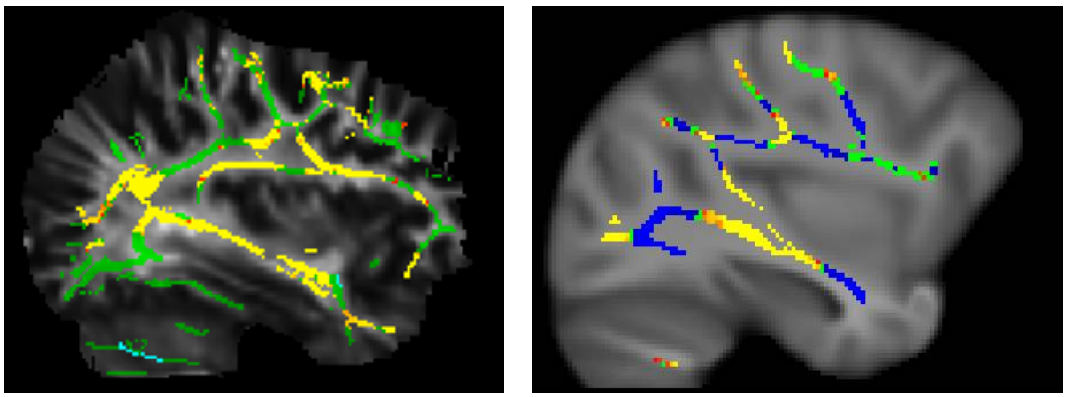

Figure 6.9: TBSS asymmetry results for the 30 chimpanzees acquired using single-shot sequence (right) and humans (left) are shown for comparison

Association tracts such as superior longitudinal fasciculus, middle longitudinal fasciculus, arcuate fasciculus, and white matter corresponding to pre and post central sulci showed significant leftward asymmetry in both the species. There are rightward asymmetries in chimpanzees in visual cortex, inferior temporal lobe, and inferior fronto-orbital regions. The magnitude of leftward asymmetry is definitely higher in humans compared to chimpanzees. Based on the validation test conducted to test the effect of ghosting and the single-shot asymmetry analysis, there seems to be an effect of ghosting on the pattern of hemispheric asymmetries in the multi-shot chimpanzee data, however their actual pattern of their asymmetries is still markedly different from humans based on the single-shot results. Future works include reproducing these results using a larger sample and compare the pattern and magnitude of asymmetries at a tract level.

Chapter 7

Future Directions

The development of the DTI protocol from the multi-shot EPI protocol to the optimized single-shot protocol has been described and each protocol's advantages/disadvantages have been discussed in the DTI protocol development chapter. Compared to the multi-shot protocol, the optimized single-shot protocol is able to acquire diffusion MRI data with double the overall SNR and free of segmentation-related motion artifacts, resulting in better quality results. The susceptibility distortion-related artifacts have proven to be most challenging for *in vivo* chimpanzee being scanned in a 3T human scanner, and using an optimized single-shot protocol, and with effective correction scheme, the effect of this artifact can be greatly reduced. The approach using two averages with two opposite phase polarities seems to work better than the conventional field map approach.

Chimpanzee diffusion MRI data for this study are acquired with a standard CP head volume bird-cage coil. Using a surface coil increases the image sensitivity and hence the SNR compared to a volume coil. However, usage of surface coils is limited due to their restricted coverage and intrinsically inhomogeneous reception profile. This issue can be addressed by extending a single surface coil into a phased array of multiple coils. Optimized phased-array coils coupled with parallel reconstruction techniques improves the image quality with increased SNR and reduced artifacts, especially the geometric distortion due to magnetic susceptibility and other motion artifacts. These coils are already developed for humans and used for acquiring DTI data of superior quality. Complicated head and neck anatomy of chimpanzees prevents the use of standard multi-

channel phase array coils designed for the human head, hence making the option of parallel imaging to reduce susceptibility distortion nonviable. Future work should include developing a custom-made phased array coil for chimpanzees.

In this thesis, different image analysis methods are presented and discussed to examine age-related changes in several DTI indices like FA, MD, AD, and RD. These indices are thought to reflect the different microstructural features of white matter such as fiber density, reflecting the total number of fibers per unit area, axon diameter, fiber coherence, and myelination (Pfefferbaum and Sullivan 2003; Buchel, Raedler et al. 2004).

ROI method analysis looked at the age-related changes in corpus callosum, the largest white matter bundle in the brain. This can be extended to other white matter tracts or regions. Further, age-related changes in GM can also be examined using DTI. More recently, attention has turned to the use of DTI to examine aging effects in gray matter structures (Huang, Zhang et al. 2006; Kochunov, Thompson et al. 2007; Pfefferbaum, Adalsteinsson et al. 2010). The reason behind this is, theoretically, DTI could provide quantitative data about changes in magnitude and orientation of diffusivity resulting from compaction due to local tissue shrinkage or dilation of adjacent CSF-filled spaces, such as sulcal expansion on the cortex or ventricular enlargement on adjacent structures (Pfefferbaum, Adalsteinsson et al. 2010).

The ROI and voxel-wise analysis provide the magnitude of age-related change in FA and

other DTI indices at a particular voxel or a specific region of interest. These methods include white matter from several different projections into the single ROI and therefore are limited when delineation of single tract is required. Also, the ROI method is not always reliable because of the uncertainty of manual specification. DTI tractography (Ito, Mori et al. 2002) will help navigate the white matter fiber connections between different portions of the brain and generate a three-dimensional reconstruction of these fiber tracts(Catani and Thiebaut de Schotten 2008). Tractography will help evaluate the changes in the quantitative properties of the whole tract during the natural aging process. Further, connectivity maps can be derived from the tractography results and relationship between structural brain networks and aging (Gong, He et al. 2009) can be studied. Studying age-related changes in the interregional connections of the brain will help develop a better understanding of brain function (Hagmann, Cammoun et al. 2008) and its decline with age. Integrity of cerebral white matter is very important for efficient cognitive functioning. For example, white matter health is highly correlated with speed-dependent cognitive performance (Oosterman, Sergeant et al. 2004) and executive functioning decline (Gunning-Dixon and Raz 2003). Age-related changes in the white matter structural integrity, reflected by the changes in measured DTI indices, will help explain age differences in cognition. Future directions should include tests that study the relationship between age-related changes in the DTI indices and the results from different age-related cognitive and behavioral performance tasks for non-human primates to see if they follow a similar or different trend compared to humans.

In this thesis, different image analysis methods are presented and discussed to examine brain –hemispheric asymmetries in white matter volume and several DTI indices like FA, MD, AD, and RD. This work can be further extended to looking at gray matter hemispheric asymmetries throughout the brain. Different analyses such as evaluating the tract-level asymmetries using tractography and asymmetries in brain connectivity can be further explored. To determine if the "lateralized hemispheric function is guided by structural asymmetry", the results from different hemispheric structural asymmetry analyses can be compared with the results from different cognitive and behavioral performance tasks.

References

Alexander, A. L., J. S. Tsuruda, et al. (1997). "Elimination of eddy current artifacts in diffusion-weighted echo-planar images: the use of bipolar gradients." Magn Reson Med 38(6): 1016-1021.

Allen, J. S., J. Bruss, et al. (2005). "Normal neuroanatomical variation due to age: the major lobes and a parcellation of the temporal region." Neurobiol Aging 26(9): 1245-1260; discussion 1279-1282.

Allen, J. S., J. Bruss, et al. (2005). "The aging brain: the cognitive reserve hypothesis and hominid evolution." Am J Hum Biol 17(6): 673-689.

Amunts, K., E. Armstrong, et al. (2007). "Gender-specific left-right asymmetries in human visual cortex." J Neurosci 27(6): 1356-1364.

Amunts, K., G. Schlaug, et al. (1997). "Motor cortex and hand motor skills: Structural compliance in the human brain." Hum Brain Mapp 5(3): 206-215.

Amunts, K., G. Schlaug, et al. (1996). "Asymmetry in the human motor cortex and handedness." Neuroimage 4(3 Pt 1): 216-222.

Amunts, K., A. Schleicher, et al. (1999). "Broca's region revisited: cytoarchitecture and intersubject variability." J Comp Neurol 412(2): 319-341.

Amunts, K., A. Schleicher, et al. (2003). "Broca's region: cytoarchitectonic asymmetry and developmental changes." J Comp Neurol 465(1): 72-89.

Amunts, K., F. Schmidt-Passos, et al. (1997). "Postnatal development of interhemispheric asymmetry in the cytoarchitecture of human area 4." Anat Embryol (Berl) 196(5): 393-402.

Andersen, A. H., Z. Zhang, et al. (1999). "Age-associated changes in rhesus CNS composition identified by MRI." Brain Res 829(1-2): 90-98.

Andersson, J. L., S. Skare, et al. (2003). "How to correct susceptibility distortions in spin-echo echo-planar images: application to diffusion tensor imaging." Neuroimage 20(2): 870-888.

Bartzokis, G., M. Beckson, et al. (2001). "Age-related changes in frontal and temporal lobe volumes in men: a magnetic resonance imaging study." Arch Gen Psychiatry 58(5): 461-465.

Bartzokis, G., J. L. Cummings, et al. (2003). "White matter structural integrity in healthy aging adults and patients with Alzheimer disease: a magnetic resonance imaging study." Arch Neurol 60(3): 393-398.

Basser, P. J. (1995). "Inferring microstructural features and the physiological state of tissues from diffusion-weighted images." NMR Biomed 8(7-8): 333-344.

Basser, P. J., J. Mattiello, et al. (1994). "MR diffusion tensor spectroscopy and imaging." Biophys J 66(1): 259-267.

Beaulieu, C. (2002). "The basis of anisotropic water diffusion in the nervous system - a technical review." NMR Biomed 15(7-8): 435-455.

Behrens, T. E., H. J. Berg, et al. (2007). "Probabilistic diffusion tractography with multiple fibre orientations: What can we gain?" Neuroimage 34(1): 144-155.

Behrens, T. E., H. Johansen-Berg, et al. (2003). "Non-invasive mapping of connections between human thalamus and cortex using diffusion imaging." Nat Neurosci 6(7): 750-757.

Bennett, I. J., D. J. Madden, et al. (2010). "Age-related differences in multiple measures of white matter integrity: A diffusion tensor imaging study of healthy aging." Hum Brain Mapp 31(3): 378-390.

Bhagat, Y. A. and C. Beaulieu (2004). "Diffusion anisotropy in subcortical white matter and cortical gray matter: changes with aging and the role of CSF-suppression." J Magn Reson Imaging 20(2): 216-227.

Blatter, D. D., E. D. Bigler, et al. (1995). "Quantitative volumetric analysis of brain MR: normative database spanning 5 decades of life." AJNR Am J Neuroradiol 16(2): 241-251.

Blurton Jones, N. G., K. Hawkes, et al. (2002). "Antiquity of postreproductive life: are there modern impacts on hunter-gatherer postreproductive life spans?" Am J Hum Biol 14(2): 184-205.

Brickman, A. M., C. Habeck, et al. (2007). "Structural MRI covariance patterns associated with normal aging and neuropsychological functioning." Neurobiol Aging 28(2): 284-295.

Bruner, E. (2010). "Morphological Differences in the Parietal Lobes within the Human Genus." Current Anthropology 51.

Buchel, C., T. Raedler, et al. (2004). "White matter asymmetry in the human brain: a diffusion tensor MRI study." Cereb Cortex 14(9): 945-951.

Bucur, B., D. J. Madden, et al. (2008). "Age-related slowing of memory retrieval: contributions of perceptual speed and cerebral white matter integrity." Neurobiol Aging 29(7): 1070-1079.

Buxhoeveden, D. P., A. E. Switala, et al. (2001). "Lateralization of minicolumns in human planum temporale is absent in nonhuman primate cortex." Brain Behav Evol 57(6): 349-358.

Cantalupo, C. and W. D. Hopkins (2001). "Asymmetric Broca's area in great apes." Nature 414(6863): 505.

Catani, M. and M. Thiebaut de Schotten (2008). "A diffusion tensor imaging tractography atlas for virtual in vivo dissections." Cortex 44(8): 1105-1132.

Charlton, R. A., S. Landau, et al. (2008). "A structural equation modeling investigation of age-related variance in executive function and DTI measured white matter damage." Neurobiol Aging 29(10): 1547-1555.

Ciccarelli, O., T. E. Behrens, et al. (2006). "Probabilistic diffusion tractography: a potential tool to assess the rate of disease progression in amyotrophic lateral sclerosis." Brain 129(Pt 7): 1859-1871.

Corballis, M. C. (1991). The lopsided ape: Evolution of the generative mind. New York, NY US, Oxford University Press.

Cork, L. C. and L. C. Walker (1999). "The Neurobiology of Aging in Nonhuman Primates." Alzheimer's Disease(2nd edition): 233-243.

Cork, L. C., L. C. Walker, et al. (1989). "Neurofibrillary Tangles and Senile Plaques in a Cognitively Impaired, Aged Nonhuman Primate." Journal of Neuropathology and Experimental Neurology 48(3): 378-378.

Crow, T. (2004). "Directional asymmetry is the key to the origin of modern Homo sapiens (the Broca-Annett axiom): A reply to Rogers' review of The Speciation of

Modern Homo Sapiens." Laterality: Asymmetries of Body, Brain and Cognition 9(2): 233-242.

Crow, T. J. (2002). "Handedness, language lateralisation and anatomical asymmetry: relevance of protocadherin XY to hominid speciation and the aetiology of psychosis. Point of view." Br J Psychiatry 181: 295-297.

Davatzikos, C. and R. N. Bryan (2002). "Morphometric analysis of cortical sulci using parametric ribbons: a study of the central sulcus." J Comput Assist Tomogr 26(2): 298-307.

Deacon, T. (1997). The Symbolic Species. New York, W.W. Norton.

Feldman, M. L. and A. Peters (1998). "Ballooning of myelin sheaths in normally aged macaques." J Neurocytol 27(8): 605-614.

Filippi, M., M. Cercignani, et al. (2001). "Diffusion tensor magnetic resonance imaging in multiple sclerosis." Neurology 56(3): 304-311.

Foundas, A. L., C. M. Leonard, et al. (1994). "Planum temporale asymmetry and language dominance." Neuropsychologia 32(10): 1225-1231.

Foundas, A. L., C. M. Leonard, et al. (1995). "Morphologic cerebral asymmetries and handedness. The pars triangularis and planum temporale." Arch Neurol 52(5): 501-508.

Gannon, P. J., R. L. Holloway, et al. (1998). "Asymmetry of chimpanzee planum temporale: humanlike pattern of Wernicke's brain language area homolog." Science 279(5348): 220-222.

Gearing, M., J. Tigges, et al. (1996). "A beta40 is a major form of beta-amyloid in nonhuman primates." Neurobiol Aging 17(6): 903-908.

Gerlach, M. and P. Riederer (1996). "Animal models of Parkinson's disease: An empirical comparison with the phenomenology of the disease in man." Journal of Neural Transmission 103(8-9): 987-1041.

Geschwind, N. and W. Levitsky (1968). "Human brain: left-right asymmetries in temporal speech region." Science 161(837): 186-187.

Glasser, M. F. and J. K. Rilling (2008). "DTI tractography of the human brain's language pathways." Cereb Cortex 18(11): 2471-2482.

Gong, G., Y. He, et al. (2009). "Mapping anatomical connectivity patterns of human cerebral cortex using in vivo diffusion tensor imaging tractography." Cereb Cortex 19(3): 524-536.

Gong, G., T. Jiang, et al. (2005). "Asymmetry analysis of cingulum based on scale-invariant parameterization by diffusion tensor imaging." Hum Brain Mapp 24(2): 92-98.

Good, C. D., I. Johnsrude, et al. (2001). "Cerebral asymmetry and the effects of sex and handedness on brain structure: a voxel-based morphometric analysis of 465 normal adult human brains." Neuroimage 14(3): 685-700.

Gudbjartsson, H. and S. Patz (1995). "The Rician distribution of noisy MRI data." Magn Reson Med 34(6): 910-914.

Gunning-Dixon, F. M. and N. Raz (2003). "Neuroanatomical correlates of selected executive functions in middle-aged and older adults: a prospective MRI study." Neuropsychologia 41(14): 1929-1941.

Guttmann, C. R., F. A. Jolesz, et al. (1998). "White matter changes with normal aging." Neurology 50(4): 972-978.

Habib, M., F. Robichon, et al. (1995). "Diverging asymmetries of temporo-parietal cortical areas: a reappraisal of Geschwind/Galaburda theory." Brain Lang 48(2): 238-258.

Hagmann, P., L. Cammoun, et al. (2008). "Mapping the structural core of human cerebral cortex." PLoS Biol 6(7): e159.

Hawkes, K. (2004). "Human longevity: the grandmother effect." Nature 428(6979): 128-129.

Hawkes, K., J. F. O'Connell, et al. (1998). "Grandmothering, menopause, and the evolution of human life histories." Proc Natl Acad Sci U S A 95(3): 1336-1339.

Hawkes, K., K. R. Smith, et al. (2009). "Mortality and fertility rates in humans and chimpanzees: How within-species variation complicates cross-species comparisons." Am J Hum Biol 21(4): 578-586.

Herndon, J. G. (2010). "The grandmother effect: implications for studies on aging and cognition." Gerontology 56(1): 73-79.

Herndon, J. G., M. B. Moss, et al. (1997). "Patterns of cognitive decline in aged rhesus monkeys." Behav Brain Res 87(1): 25-34.

Herndon, J. G., J. Tigges, et al. (1999). "Brain weight throughout the life span of the chimpanzee." J Comp Neurol 409(4): 567-572.

Herndon, J. G., J. Tigges, et al. (1998). "Brain weight does not decrease with age in adult rhesus monkeys." Neurobiol Aging 19(3): 267-272.

Herndon, J. G. and L. C. Walker (2010). "The grandmother effect and the uniqueness of the human aging phenotype." Gerontology 56(2): 217-219.

Hess, C. P. (2009). "Update on diffusion tensor imaging in Alzheimer's disease." Magn Reson Imaging Clin N Am 17(2): 215-224.

Holloway, R. L. (2000). Brain. Encyclopedia of Human Evolution and Prehistory. E. Delson. New York, Garland Publishing: 141-149.

Holloway, R. L., D. C. Broadfield, et al. (2003). "Morphology and histology of chimpanzee primary visual striate cortex indicate that brain reorganization predated brain expansion in early hominid evolution." Anatomical Record 273A(1): 594-602.

Holloway, R. L. and M. C. De La Costelareymondie (1982). "Brain endocast asymmetry in pongids and hominids: some preliminary findings on the paleontology of cerebral dominance." Am J Phys Anthropol 58(1): 101-110.

Holloway, R. L., C. C. Sherwood, et al. (2008). Evolution, of the brain: in humans – paleoneurology. Encyclopedia of Neuroscience. N. H. M.D. Binder, U. Windhorst, M.C. Hirsch, Springer-Verlag.

Hopkins, W. D. and L. Marino (2000). "Asymmetries in cerebral width in nonhuman primate brains as revealed by magnetic resonance imaging (MRI)." Neuropsychologia 38(4): 493-499.

Hopkins, W. D., L. Marino, et al. (1998). "Planum temporale asymmetries in great apes as revealed by magnetic resonance imaging (MRI)." Neuroreport 9(12): 2913-2918.

Hopkins, W. D. and T. M. Nir (2010). "Planum temporale surface area and grey matter asymmetries in chimpanzees (Pan troglodytes): the effect of handedness and comparison with findings in humans." Behav Brain Res 208(2): 436-443.

Horsfield, M. A. and D. K. Jones (2002). "Applications of diffusion-weighted and diffusion tensor MRI to white matter diseases - a review." NMR Biomed 15(7-8): 570-577.

Huang, H., J. Zhang, et al. (2006). "White and gray matter development in human fetal, newborn and pediatric brains." Neuroimage 33(1): 27-38.

Ito, R., S. Mori, et al. (2002). "Diffusion tensor brain imaging and tractography." Neuroimaging Clin N Am 12(1): 1-19.

Janowsky, J. S., R. A. Carper, et al. (1996). "Asymmetrical memory decline in normal aging and dementia." Neuropsychologia 34(6): 527-535.

Jenkinson, M. and S. Smith (2001). "A global optimisation method for robust affine registration of brain images." Med Image Anal 5(2): 143-156.

Jernigan, T. L., S. L. Archibald, et al. (2001). "Effects of age on tissues and regions of the cerebrum and cerebellum." Neurobiol Aging 22(4): 581-594.

Jezzard, P. and R. S. Balaban (1995). "Correction for geometric distortion in echo planar images from B0 field variations." Magn Reson Med 34(1): 65-73.

Johansen-Berg, H. and T. E. Behrens (2006). "Just pretty pictures? What diffusion tractography can add in clinical neuroscience." Curr Opin Neurol 19(4): 379-385.

Jones, K. P., L. C. Walker, et al. (2007). "Depletion of ovarian follicles with age in chimpanzees: similarities to humans." Biol Reprod 77(2): 247-251.

Keller, S. S., N. Roberts, et al. (2009). "A comparative magnetic resonance imaging study of the anatomy, variability, and asymmetry of Broca's area in the human and chimpanzee brain." J Neurosci 29(46): 14607-14616.

Kertesz, A., S. E. Black, et al. (1986). "Cerebral asymmetries on magnetic resonance imaging." Cortex 22(1): 117-127.

Koay, C. G. and P. J. Basser (2006). "Analytically exact correction scheme for signal extraction from noisy magnitude MR signals." J Magn Reson 179(2): 317-322.

Kochunov, P., P. M. Thompson, et al. (2007). "Relationship between white matter fractional anisotropy and other indices of cerebral health in normal aging: tract-based spatial statistics study of aging." Neuroimage 35(2): 478-487.

Kubicki, M., C. F. Westin, et al. (2002). "Uncinate fasciculus findings in schizophrenia: a magnetic resonance diffusion tensor imaging study." Am J Psychiatry 159(5): 813-820.

Lacreuse, A., L. Chennareddi, et al. (2008). "Menstrual cycles continue into advanced old age in the common chimpanzee (Pan troglodytes)." Biol Reprod 79(3): 407-412.

Lacreuse, A., M. M. Diehl, et al. (2005). "Sex differences in age-related motor slowing in the rhesus monkey: behavioral and neuroimaging data." Neurobiol Aging 26(4): 543-551.

Lacreuse, A. and J. G. Herndon (2003). "Effects of estradiol and aging on fine manual performance in female rhesus monkeys." Horm Behav 43(3): 359-366.

Lancaster, J. L., P. V. Kochunov, et al. (2003). "Asymmetry of the brain surface from deformation field analysis." Hum Brain Mapp 19(2): 79-89.

Le, T. H. and X. Hu (1996). "Retrospective estimation and correction of physiological artifacts in fMRI by direct extraction of physiological activity from MR data." Magn Reson Med 35(3): 290-298.

LeMay, M. (1976). "Morphological cerebral asymmetries of modern man, fossil man, and nonhuman primate." Ann N Y Acad Sci 280: 349-366.

Li, L., T. M. Preuss, et al. (2010). "Chimpanzee (Pan troglodytes) precentral corticospinal system asymmetry and handedness: a diffusion magnetic resonance imaging study." PLoS One 5(9): e12886.

Lyons, D. M., C. Yang, et al. (2004). "Cognitive correlates of white matter growth and stress hormones in female squirrel monkey adults." J Neurosci 24(14): 3655-3662.

Madden, D. J., I. J. Bennett, et al. (2009). "Cerebral white matter integrity and cognitive aging: contributions from diffusion tensor imaging." Neuropsychol Rev 19(4): 415-435.

Madden, D. J., W. L. Whiting, et al. (2004). "Diffusion tensor imaging of adult age differences in cerebral white matter: relation to response time." Neuroimage 21(3): 1174-1181.

Makris, N., G. M. Papadimitriou, et al. (2007). "Frontal connections and cognitive changes in normal aging rhesus monkeys: a DTI study." Neurobiol Aging 28(10): 1556-1567.

Matsui, H., K. Nishinaka, et al. (2007). "Dementia in Parkinson's disease: diffusion tensor imaging." Acta Neurol Scand 116(3): 177-181.

Moore, T. L., R. J. Killiany, et al. (2003). "Impairment in abstraction and set shifting in aged rhesus monkeys." Neurobiol Aging 24(1): 125-134.

Morgan, P. S., R. W. Bowtell, et al. (2004). "Correction of spatial distortion in EPI due to inhomogeneous static magnetic fields using the reversed gradient method." J Magn Reson Imaging 19(4): 499-507.

Mori, S. and P. B. Barker (1999). "Diffusion magnetic resonance imaging: its principle and applications." Anat Rec 257(3): 102-109.

Moscrip, T. D., D. K. Ingram, et al. (2000). "Locomotor activity in female rhesus monkeys: assessment of age and calorie restriction effects." J Gerontol A Biol Sci Med Sci 55(8): B373-380.

Moss, M. B., J. G. Herndon, et al. (1998). "Age-related cognitive impairment in the rhesus monkey: Successful and unsuccessful aging." Faseb Journal 12(5): A943-A943.

Nair, G., Y. Tanahashi, et al. (2005). "Myelination and long diffusion times alter diffusion-tensor-imaging contrast in myelin-deficient shiverer mice." Neuroimage 28(1): 165-174.

Nelson, P. T., K. Stefansson, et al. (1996). "Molecular evolution of tau protein: implications for Alzheimer's disease." J Neurochem 67(4): 1622-1632.

Oosterman, J. M., J. A. Sergeant, et al. (2004). "Timed executive functions and white matter in aging with and without cardiovascular risk factors." Rev Neurosci 15(6): 439-462.

Orban, G. A., K. Claeys, et al. (2006). "Mapping the parietal cortex of human and non-human primates." Neuropsychologia 44(13): 2647-2667.

Pakkenberg, B., D. Pelvig, et al. (2003). "Aging and the human neocortex." Exp Gerontol 38(1-2): 95-99.

Passingham, R. E. (1973). "Anatomical differences between the neocortex of man and other primates." Brain, Behavior and Evolution 7: 337-359.

Peters, A. (2002). "The effects of normal aging on myelin and nerve fibers: a review." J Neurocytol 31(8-9): 581-593.

Peters, A. (2002). "Structural changes in the normally aging cerebral cortex of primates." Prog Brain Res 136: 455-465.

Peters, A., M. B. Moss, et al. (2000). "Effects of aging on myelinated nerve fibers in monkey primary visual cortex." J Comp Neurol 419(3): 364-376.

Peters, A., M. B. Moss, et al. (2001). "The effects of aging on layer 1 of primary visual cortex in the rhesus monkey." Cereb Cortex 11(2): 93-103.

Peters, A. and C. Sethares (2004). "Oligodendrocytes, their progenitors and other neuroglial cells in the aging primate cerebral cortex." Cereb Cortex 14(9): 995-1007.

Pfefferbaum, A., E. Adalsteinsson, et al. (2010). "Diffusion tensor imaging of deep gray matter brain structures: effects of age and iron concentration." Neurobiol Aging 31(3): 482-493.

Pfefferbaum, A. and E. V. Sullivan (2003). "Increased brain white matter diffusivity in normal adult aging: relationship to anisotropy and partial voluming." Magn Reson Med 49(5): 953-961.

Pierpaoli, C., P. Jezzard, et al. (1996). "Diffusion tensor MR imaging of the human brain." Radiology 201(3): 637-648.

Pierre, P. J., W. D. Hopkins, et al. (2008). "Age-related neuroanatomical differences from the juvenile period to adulthood in mother-reared macaques (Macaca radiata)." Brain Res 1226: 56-60.

Pilcher, D. L., E. A. Hammock, et al. (2001). "Cerebral volumetric asymmetries in non-human primates: a magnetic resonance imaging study." Laterality 6(2): 165-179.

Powell, H. W., G. J. Parker, et al. (2006). "Hemispheric asymmetries in language-related pathways: a combined functional MRI and tractography study." Neuroimage 32(1): 388-399.

Preuss, T. M. (2004). What is it like to be a human? The Cognitive Neurosciences. M. S. Gazzaniga. Cambridge, MA, MIT Press: 5-22.

Raz, N., F. M. Gunning, et al. (1997). "Selective aging of the human cerebral cortex observed in vivo: differential vulnerability of the prefrontal gray matter." Cereb Cortex 7(3): 268-282.

Raz, N., U. Lindenberger, et al. (2005). "Regional brain changes in aging healthy adults: general trends, individual differences and modifiers." Cereb Cortex 15(11): 1676-1689.

Raz, N. and K. M. Rodrigue (2006). "Differential aging of the brain: patterns, cognitive correlates and modifiers." Neurosci Biobehav Rev 30(6): 730-748.

Rilling, J. K. (2006). "Human and non-human primate brains: are they allometrically scaled versions of the same design?" Evolutionary Anthropology 15: 65-77.

Rilling, J. K. and R. A. Seligman (2002). "A quantitative morphometric comparative analysis of the primate temporal lobe." J Hum Evol 42(5): 505-533.

Rodrigo, S., O. Naggara, et al. (2007). "Human subinsular asymmetry studied by diffusion tensor imaging and fiber tracking." AJNR Am J Neuroradiol 28(8): 1526-1531.

Rose, S. E., F. Chen, et al. (2000). "Loss of connectivity in Alzheimer's disease: an evaluation of white matter tract integrity with colour coded MR diffusion tensor imaging." J Neurol Neurosurg Psychiatry 69(4): 528-530.

Rosen, R. F., A. S. Farberg, et al. (2008). "Tauopathy with paired helical filaments in an aged chimpanzee." J Comp Neurol 509(3): 259-270.

Salat, D. H., R. L. Buckner, et al. (2004). "Thinning of the cerebral cortex in aging." Cereb Cortex 14(7): 721-730.

Salat, D. H., J. A. Kaye, et al. (1999). "Prefrontal gray and white matter volumes in healthy aging and Alzheimer disease." Arch Neurol 56(3): 338-344.

Salat, D. H., D. S. Tuch, et al. (2005). "Age-related alterations in white matter microstructure measured by diffusion tensor imaging." Neurobiol Aging 26(8): 1215-1227.

Schenker, N. M., A. M. Desgouttes, et al. (2005). "Neural connectivity and cortical substrates of cognition in hominoids." J Hum Evol 49(5): 547-569.

Schenker, N. M., W. D. Hopkins, et al. (2010). "Broca's area homologue in chimpanzees (Pan troglodytes): probabilistic mapping, asymmetry, and comparison to humans." Cereb Cortex 20(3): 730-742.

Schultz, C., F. Dehghani, et al. (2000). "Filamentous tau pathology in nerve cells, astrocytes, and oligodendrocytes of aged baboons." Journal of Neuropathology and Experimental Neurology 59(1): 39-52.

Semendeferi, K. and H. Damasio (2000). "The brain and its main anatomical subdivisions in living hominoids using magnetic resonance imaging." Journal of Human Evolution 38(2): 317-332.

Shenkin, S. D., M. E. Bastin, et al. (2003). "Childhood and current cognitive function in healthy 80-year-olds: a DT-MRI study." Neuroreport 14(3): 345-349.

Sherwood, C. C., D. C. Broadfield, et al. (2003). "Variability of Broca's area homologue in African great apes: implications for language evolution." Anat Rec A Discov Mol Cell Evol Biol 271(2): 276-285.

Sherwood, C. C., F. Subiaul, et al. (2008). "A natural history of the human mind: tracing evolutionary changes in brain and cognition." J Anat 212(4): 426-454.

Smith, S. M., M. Jenkinson, et al. (2006). "Tract-based spatial statistics: voxelwise analysis of multi-subject diffusion data." Neuroimage 31(4): 1487-1505.

Song, S. K., S. W. Sun, et al. (2003). "Diffusion tensor imaging detects and differentiates axon and myelin degeneration in mouse optic nerve after retinal ischemia." Neuroimage 20(3): 1714-1722.

Song, S. K., S. W. Sun, et al. (2002). "Dysmyelination revealed through MRI as increased radial (but unchanged axial) diffusion of water." Neuroimage 17(3): 1429-1436.

Stephan, H., H. Frahm, et al. (1981). "New and revised data on volumes of brain structures in insectivores and primates." Folia Primatologica. 35(1): 1-29.

Sullivan, E. V., E. Adalsteinsson, et al. (2001). "Equivalent disruption of regional white matter microstructure in ageing healthy men and women." Neuroreport 12(1): 99-104.

Sullivan, E. V. and A. Pfefferbaum (2006). "Diffusion tensor imaging and aging." Neurosci Biobehav Rev 30(6): 749-761.

Sullivan, E. V., T. Rohlfing, et al. (2010). "Longitudinal study of callosal microstructure in the normal adult aging brain using quantitative DTI fiber tracking." Dev Neuropsychol 35(3): 233-256.

Sullivan, E. V., T. Rohlfing, et al. (2010). "Quantitative fiber tracking of lateral and interhemispheric white matter systems in normal aging: relations to timed performance." Neurobiol Aging 31(3): 464-481.

Sullivan, E. V., M. Rosenbloom, et al. (2004). "Effects of age and sex on volumes of the thalamus, pons, and cortex." Neurobiol Aging 25(2): 185-192.

Thompson, M. E., J. H. Jones, et al. (2007). "Aging and fertility patterns in wild chimpanzees provide insights into the evolution of menopause." Current Biology 17(24): 2150-2156.

Toga, A. W. and P. M. Thompson (2003). "Mapping brain asymmetry." Nat Rev Neurosci 4(1): 37-48.

Tyszka, J. M., C. Readhead, et al. (2006). "Statistical diffusion tensor histology reveals regional dysmyelination effects in the shiverer mouse mutant." Neuroimage 29(4): 1058-1065.

Varki, N., D. Anderson, et al. (2009). "Heart disease is common in humans and chimpanzees, but is caused by different pathological processes." Evolutionary Applications 2(1): 101-112.

Voytko, M. L. (1998). "Nonhuman primates as models for aging and Alzheimer's disease." Lab Anim Sci 48(6): 611-617.

Voytko, M. L. (2000). "The effects of long-term ovariectomy and estrogen replacement therapy on learning and memory in monkeys (Macaca fascicularis)." Behav Neurosci 114(6): 1078-1087.

Voytko, M. L. (2002). "Estrogen and the cholinergic system modulate visuospatial attention in monkeys (Macaca fascicularis)." Behav Neurosci 116(2): 187-197.

Voytko, M. L. and G. P. Tinkler (2004). "Cognitive function and its neural mechanisms in nonhuman primate models of aging, Alzheimer disease, and menopause." Front Biosci 9: 1899-1914.

Walker, M. L. and J. G. Herndon (2008). "Menopause in nonhuman primates?" Biol Reprod 79(3): 398-406.

Watkins, K. E., T. Paus, et al. (2001). "Structural asymmetries in the human brain: a voxel-based statistical analysis of 142 MRI scans." Cereb Cortex 11(9): 868-877.

Westlye, L. T., K. B. Walhovd, et al. (2010). "Life-span changes of the human brain White matter: diffusion tensor imaging (DTI) and volumetry." Cereb Cortex 20(9): 2055-2068.

Witelson, S. F. (1989). "Hand and sex differences in the isthmus and genu of the human corpus callosum. A postmortem morphological study." Brain 112 (Pt 3): 799-835.

Zahr, N. M., T. Rohlfing, et al. (2009). "Problem solving, working memory, and motor correlates of association and commissural fiber bundles in normal aging: a quantitative fiber tracking study." Neuroimage 44(3): 1050-1062.

Zhang, Y., M. Brady, et al. (2001). "Segmentation of brain MR images through a hidden Markov random field model and the expectation-maximization algorithm." IEEE Trans Med Imaging 20(1): 45-57.

Zhang, Y., A. T. Du, et al. (2008). "Patterns of age-related water diffusion changes in human brain by concordance and discordance analysis." Neurobiol Aging.

Zhang, Z., A. Andersen, et al. (2000). "Motor slowing and parkinsonian signs in aging rhesus monkeys mirror human aging." J Gerontol A Biol Sci Med Sci 55(10): B473-480.

Zimmerman, M. E., A. M. Brickman, et al. (2006). "The relationship between frontal gray matter volume and cognition varies across the healthy adult lifespan." Am J Geriatr Psychiatry 14(10): 823-833.